1

AFML-TR-75-10

16

EXPERIMENTAL HYSTERETIC LOSS FOR A SERIES OF SUPERCONDUCTING FILAMENTARY NbTi WIRES AND A FIELD DEPENDENT CRITICAL STATE MODEL

SOLID STATE MATERIALS BRANCH
ELECTROMAGNETIC MATERIALS DIVISION

JULY 1975

TECHNICAL REPORT AFML-TR-75-10
FINAL REPORT FOR PERIOD 2 OCTOBER 1972-31 DECEMBER 1974

DDC
RECEIVED
DEC 9 1975
A

Approved for public release; distribution unlimited

AIR FORCE MATERIALS LABORATORY
AIR FORCE WRIGHT AERONAUTICAL LABORATORIES
Air Force Systems Command
Wright-Patterson Air Force Base, Ohio 45433

NOTICE

This report has been reviewed by the Information Office (IO) and is releasable to the National Technical Information Service (NTIS). At NTIS, it will be available to the general public, including the foreign nations.

This technical report has been reviewed and is approved for publication.

Melvin C. Ohmer
MELVIN C. OHMER
Project Monitor

FOR THE COMMANDER

W G D Frederick

WILLIAM G. D. FREDERICK
Chief
Laser and Optical Materials Branch
Electromagnetic Materials Division

A

UNCLASSIFIED

SECURITY CLASSIFICATION OF THIS PAGE (*When Data Entered*)

REPORT DOCUMENTATION PAGE		READ INSTRUCTIONS BEFORE COMPLETING FORM
1. ~~REPORT NUMBER~~ (14) AFML-~~T~~R-75-10	2. GOVT ACCESSION NO.	3. RECIPIENT'S CATALOG NUMBER
4. TITLE ~~(and Subtitle)~~ (6) Experimental Hysteretic Loss for a Series of Superconducting Filamentary NbTi Wires and a Field Dependent Critical State Model.		(9) 5. ~~TYPE OF REPORT & PERIOD COV~~ERED Final Technical Report. 2 Oct 72 ~~to~~ – 31 Dec 74,
		6. ~~PERFORMING ORG. REPORT NUMBER~~
7. AUTHOR(s) (10) Melvin C./Ohmer, John J./Wollan ~~and~~ Larry O./Lawson		8. ~~CONTRA~~CT OR GRANT NUMBER(s) (16) AF-73710226 67505.0(ACC)
9. PERFORMING ORGANIZATION NAME AND ADDRESS Air Force Materials Laboratory (LPE) Air Force Systems Command Wright-Patterson AFB, Ohio 45433		10. PROGRAM ELEMENT, PROJECT, TASK AREA & WORK UNIT NUMBERS 62102F (17) 73710226
11. CONTROLLING OFFICE NAME AND ADDRESS Air Force Materials Laboratory (LPE) Air Force Systems Command Wright-Patterson Air Force Base, Ohio 45433		12. ~~REPORT DATE~~ (11) July 1975
		13. ~~NUMBER~~ OF PAGES (12) 129 p.
14. MONITORING AGENCY NAME & ADDRESS(*if different from Controlling Office*)		15. ~~SECURITY~~ CLASS. (*of this report*) Unclassified
		15a. DECLASSIFICATION/DOWNGRADING SCHEDULE

16. DISTRIBUTION STATEMENT (*of this Report*)

Approved for public release; distribution unlimited.

17. DISTRIBUTION STATEMENT (*of the abstract entered in Block 20, if different from Report*)

18. SUPPLEMENTARY NOTES

19. KEY WORDS (*Continue on reverse side if necessary and identify by block number*)

Hysteretic loss
Superconducting wire
Niobium titanium wire
Multifilamentary wire
Critical state models
Magnetization
Superconductors

20. ABSTRACT (*Continue on reverse side if necessary and identify by block number*)

This report summarizes the Air Force superconducting wire applications, the goals of future superconducting materials development, the state of the art theories of ac loss in superconductors, and the results of hysteretic loss measurements on a series of niobium titanium multifilamentary wires. Expressions were developed for magnetization and hysteretic loss for half cycle and full cycle for rod geometries for a critical state model with critical current inversely proportional to field. Bulk effects with surface like character are

over

DD FORM 1 JAN 73 1473 EDITION OF 1 NOV 65 IS OBSOLETE

Unclassified

SECURITY CLASSIFICATION OF THIS PAGE (*When Data Entered*)

DN

012320

20. discussed along with surface shielding fields and the demagnetizing factor. The loss expressions of various models are compared to experimental loss. Universal loss curves constructed from experimental loss curves by appropriate normalization are obtained and used to predict loss accurately. Saturation fields for various diameter wires and hysteretic loss for wires used by AFAPL in generator construction are reported. The temperature dependence of the critical current for niobium titanium, niobium(sub 3)-tin, and niobium carbonitride was obtained from magnetization curves through the critical state model.

FOREWORD

This is the final technical report prepared by the Air Force Materials Laboratory under Inhouse Work Unit 73710226, Task 737102, Project 7371. Dr. Melvin C. Ohmer was the principal investigator and project engineer for 73710226. The report covers the period 2 October 1972 to 31 December 1974.

The work was performed in the Solid State Materials Branch (LPE) of the Electromagnetic Materials Division of the Air Force Materials Laboratory.

During 1973, Dr. John Wollan participated in the National Research Council Resident Research Associate program.

TABLE OF CONTENTS

LIST OF ILLUSTRATIONS

LIST OF ILLUSTRATIONS (CONTINUED)

LIST OF ILLUSTRATIONS (CONTINUED)

FIGURE PAGE

LIST OF ILLUSTRATIONS (CONTINUED)

LIST OF ILLUSTRATIONS (CONCLUDED)

LIST OF TABLES

LIST OF TABLES (CONCLUDED)

SECTION I

INTRODUCTION

It has been said that the technology of superconductivity shows great promise but all we have gotten is promises for the past 60 years. The successful operation of prototype superconducting dc and ac rotating machinery generators and large superconducting MHD magnets in the early 70's has stimulated new interest in large scale superconducting devices. Superconducting transmission lines and peak-shaving energy storage superconducting inductors are being developed by the power industry. In addition, superconducting materials research has been significantly increased because of energy related applications. The future of the technology of superconductivity depends critically upon the results obtained through the increased level of research and development funds in the decade of the 70's.

There are several superconducting materials properties of interest for wire applications. The superconducting transition temperature (T_c) is the temperature below which a material becomes superconducting ($T_c < 23K$). The critical current density ($J_c(H)$) is the current density (i.e.$\sim 10^5$ A/cm^2) that a superconductor will carry without ohmic loss in an applied dc magnetic field (H). The upper critical field (H_{c2}) is the largest magnetic field in which a material remains superconducting. Table 1 indicates the properties of several promising superconducting materials. At the present time, thousands of superconductors are known and B.W. Roberts has published several surveys of superconducting properties. Only a few are being considered for wire applications. Elemental Nb may be useful in transmission lines. The ductile alloys NbZr and NbTi are commercially available in round wire form. However at the present time, the brittle A15 compounds Nb_3Sn and V_3Ga are available only in tape form. There are many suppliers of superconducting wire and a partial listing is given by P.A. Battams. In a recent article on the abundance and sources of Nb, T. Takai summarized superconducting raw materials and wire costs. Nb ingots are 16-27$/lb, approximately 20 times the price of copper and ten times the price of titanium. NbTi ingots are

60$/kg and NbTi is twice that in wire form. Nb_3Sn wire is approximately four times the cost of NbTi and V_3Ga is even more expensive than Nb_3Sn. The strength of magnetic field required in an application and materials cost determine the wire used. Typically, below 80 kOe NbTi is used, from 80 to 120 kOe Nb_3Sn is superior and above 120 kOe V_3Ga has the best properties.

Since the transition temperature of NbTi is 9.5K and that of Nb_3Sn is 18K a low temperature refrigerator or liquid helium is required to operate a superconducting device. At the present time cooling a superconductor to temperatures near absolute zero is no more difficult than putting ice in scotch whiskey. In 1974 liquid helium costs were $3.00 per liter ($11.40 per gallon) which is approximately 30¢ over the cost of the helium gas. Liquid nitrogen costs were 12.6¢ per liter (47.7¢ per gallon). Because of the large high temperature specific heat ($C \propto T^3$) of all materials, it is more economical to pre-cool to 77K with nitrogen because of its larger latent heat of vaporization, 1.6×10^5J/l compared to 2.7×10^3J/l. Using the above cost figures the cooling power of nitrogen in Joules per dollar is 1.2×10^6 compared to helium at 893. It is a general feature of gases that the lower the boiling point, the lower their latent heat of vaporization. Helium is used to cool from 77K to 4.2K. In order to maintain the temperature at 4.2K in pool boiling helium the helium boils away at a nominal rate (1mW heat leak=1ml of liquid per hour). The cost of extracting energy in a refrigeration cycle is shown in Figure 1. The curve denotes the ideal Carnot efficiency. Typically, large refrigerators operate at 30% of Carnot and small refrigerators at 15% of Carnot. This results in a cost of from 200-500 watts of refrigeration per watt extracted from the cold end of the refrigerator. Obvious cost advantages can be obtained by operating at 8 or 12K where refrigeration costs have been reduced to respectively 1/2 and 1/3 of the cost at 4.2K. This is a real possibility for a superconductor like Nb_3Sn but not for NbTi. The present attitude is that refrigeration costs are low enough that existing superconducting materials are adequate for engineering applications. While it would be nice to have higher T_c materials they are not required for a practical superconducting technology.

Superconducting devices have two advantages over conventional copper devices, lower operating costs because of the elimination of ohmic loss and smaller size and weight because of increased current density. Unfortunately superconductors act irreversibly in changing magnetic fields resulting in energy loss in ac applications. This energy loss produces two problems in superconducting devices: 1) the energy cannot be extracted from the available surface area and the superconductor warms up to the point that its current carrying properties are so degraded that the device fails to operate; 2) the energy loss requires excessive refrigeration requirements outweighting any advantages obtained from utilizing superconductors. Both of these problems must be addressed in Air Force superconducting wire applications in the area of small lightweight megawatt ac generators and megajoule energy storage devices. The relevant superconducting materials problems are defined in terms of the following Air Force applications.

The Air Force Aero Propulsion Laboratory has been a pioneer in the area of superconducting machinery and there are several important recent reports describing results on inductors, a superconducting rotor and MHD magnets. Tables 2, 3, and 4 describe the type and amount of wire used in some of these applications and Figures 2 and 3 show metallurgical cross sections of the NbTi wire used in the rotor. These are multi-strand NbTi wires embedded in a copper matrix. In composite wires, the NbTi filaments are typically 5-500 microns in diameter and the resistivity ratio of the copper is approximately 80. The high magnetoresistance of high purity copper results in very little gain from using higher ratios. A rule of thumb for five micron filaments is ten filaments per ampere. The composite wire is usually twisted around its axis to decouple the filaments up to a maximum twist of about one twist per seven wire diameters.

The simplest Air Force application is magnetohydrodynamic power generation. A MHD generator consists of an ionized gas flowing through a channel which has a magnetic field perpendicular to the axis of the channel. A voltage is induced across the gas by the Hall effect and a series of electrodes along the channel are used to extract electrical power. MHD power is roughly given by

$$P \propto \sigma U^2 B^2 V \qquad (1)$$

in the region of interest where σ is the conductivity of the medium flowing in the channel, B is the magnetic field strength, V is the volume of the channel, and U is the velocity of the medium. The MHD generator has the advantage of instant on instant off operation, and it has many advantages in the regime of large energy per pulse short pulse time applications as shown in Figure 4. The magnetic field is generally produced by two racetrack or saddle coils. Conventional magnets are limited to about 20kOe, the saturation moment of iron, and ohmic power losses in the copper coil reduce the operating efficiency of the generator. In some instances 1/3 of the generated power is required to operate the magnet. Since the specific power density is proportional to the square of the magnetic field, superconducting coils capable of producing fields in the range of 40-80kOe which exhibit no ohmic loss offer a significant advantage over conventional coils. Three superconducting MHD magnets have been built by AFAPL. The first was built by Airco Temescal in 1969 and tested at NASA Lewis in Cleveland. It was designed to attain a 60kOe field but the actual field was 33kOe. The bore was 6 7/8 inches in diameter and the magnet weighed 5000 lbs. Due to internal shorting it required three days to energize the magnet. The stresses in the windings were supported by appropiately wound insulated stainless steel wire. Wire motion due to magnetic forces destroyed the insulation resulting in excessive turn to turn shorts. Magnet Corporation of America (MCA) constructed a magnet with a bore size of 6 7/8 inches weighing 1200 lbs designed for 50kOe. This magnet was tested in 1973 and it attained a field of 40 kOe after structural modifications. Failure to achieve design field was attributed to wire motion. However, the MCA magnet is an excellent lightweight MHD magnet. The MCA magnet is electrically segmented in quarters so that the outer windings may also be used for energy storage. The energy stored in the MCA magnet is one megajoule. A third MHD magnet was constructed by Ferranti-Packard

Electric Ltd. of Canada. The design included the use of composite materials in the cryogenic region. The bore size was 10 1/2 inches, the weight with a plastic dewar was 1000 lbs, and the design field was 45 kOe. The F-P magnet stores 1.5 MJ. Since the channel volume for this magnet is substantially larger than the MCA magnet the power density will be greater. Initial testing of this magnet indicated that structural changes are required because of excessive wire motion. The solution of the problem of wire motion while maintaining a low structural weight requires a better understanding of the magnetic forces on a conductor. This fact was recently stressed by Richard Stevenson. He constructed a large bore (41cm) solenoidal composite magnet which operated at a field level of 75kOe. The inner windings consisted of a Nb_3Sn coil containing 1.5 tons of material and the outer coil was NbTi. With the inner coil open circuited he charged the outer coil and the inner coil broke. Both coils were designed to withstand the maximum Lorentz force. It appears that the break was caused by the induced diamagnetism in the Nb_3Sn in regions of large field gradients. This indicates that the magnetic behavior of superconductors must be taken into account in force calculations. However, it is possible that turn to turn shorting caused the problem. Present multifilamentary NbTi is adequate for MHD magnets in the field range (40-70 kOe) of present designs, however, multifilamentary Nb_3Sn is desirable from the standpoint of reduced sensitivity to wire motion because of its higher T_c. Nb_3Sn tape cannot be used because large components of the field would be perpendicular to the large face of the tape particularily at the end turns.

Superconducting inductors are competitors of capacitors in the area of energy storage. Commercial energy storage capacitors have an overall energy density of about 2.5J/in^3 or a specific density of 40 J/lb. For comparison a superconducting coil with a 50 kOe central field has an energy density of 164.5 J/in^3. Generally speaking inductors are better than capacitors for large energy pulses at low frequency and worse for low energy pulses at high frequency. Figure 4 depicts the range of applicability of inductors vs capacitors although the line is not well defined because of present limitations in the theory of ac loss in superconductors. Maxwell Laboratories under contract to AFAPL is conducting a system study of pulse forming networks (PFN) considering both capacitors and inductors over the operating range described in Table 5. Because of the high pulse rate (100-1000pps) required, inductors represent the harshest ac environment in which superconducting materials are required to operate efficiently. Two superconducting inductive storage systems have been built by AFAPL. The programs started at the same time (one at Avco and one at MCA). Although the philosophy of each was different. MCA approached the problem from the standpoint of minimizing ac loss. Their conductor was braided and cabled with each strand insulated from each other and the coil was potted. Avco approached the problem from the standpoint of optimizing heat transfer. Their conductor was braided and cabled and potted in solder and the coil was wound with a single turn in an open structure. A summary of the coil properties is given in Table 2. The MCA coil stored 1kJ and the Avco coil stored 20kJ operating at 5Hz and 3Hz respectively. A follow-on contract was awarded to MCA to construct a 100kJ coil operating at 5Hz. A very dramatic experiment demonstrating the problem of ac loss in superconductors was reported by MCA. For discharge times from .1 to 4 milliseconds, the ac loss was measured to be approximately .3% of the stored energy. For the 1kJ coil this corresponds to a loss of 3J/pulse which means that approximately 900 pulses can be obtained for one liter of helium at an approximate cost of $3. However the operation of this coil was heat transfer limited. In pool boiling helium only about .4 watts/cm^2 of power can be transmitted across a surface. It is very difficult to extract energy dissipated in a coil potted with nonmetallic materials because of the small surface area and the poor thermal conductivity of the potting materials. Figure 30 of the MCA report shows a 16.4 sec pulse train at five pulsed per second. The trapezoidal pulse shape was a .155 sec charge time, a .2ms discharge time, and a dead time less than 55ms. The coil was charged at a constant voltage. A photograph of the pulse train indicates the charging current vs. time. After several seconds the charging current falls as the coil becomes resistive because of heating until finally the inductor fails to operate. In contrast the open structured Avco coil operated indefinitely at 3Hz.

Unfortunately extensive ac loss measurements were not made on the Avco coil Future inductive storage systems will probably be in the 10-15kJ range operating at 100-250 Hz. The substantially higher frequency of operation will require open-structured coils utilizing lower ac loss superconducting wire or wire which has acceptable current properties at temperatures well above 4.2K. The precise definition of the range of applicability of superconducting inductors and the best way of extracting energy from them awaits the development of a more accurate theory of ac loss.

Superconducting generators are smaller and lighter (by respectively an order of magnitude) than conventional generators in the high power region (greater than 1MVA). An MIT superconducting generator had a specific weight of 3.75 lbs/KVA and the present design goal of AFAPL is .2-1 lb/KVA. A superconducting four pole rotor operating at 40kOe for a rotating machinery generator was built by Westinghouse under contract to AFAPL. It was operated successfully in the fall of 1973. For an appropiately designed armature a generator using this rotor would have a rating of 5MVA operating steady state at a coil current of 250A. For 400 cycle output in a three phase synchronous machine the rotor will spin at 12,000 RPM. When operating the rotor at 12,000 RPM, the temperature of the outer turns of the coils rose to 6K and the coils had a quench current of 280A, substantially less than the 4.2K short sample critical current. There are two types of ac loss encountered in the rotor: 1) losses produced by low frequency large amplitude changes in the rotor current during charging or regulation (the rotor coils were charged in one minute) and 2) losses produced by high frequency low amplitude ripple from unbalanced phase loading. Typical ripple fields that are expected are in the range of 100 Oe at twice the frequency of the machine (i.e. 800Hz). The Westinghouse rotor has a copper eddy current shield maintained at a temperature of 80K to eliminate the ripple induced loss in the superconductor coils. The weight of the eddy current shield increases the strength requirements of the torque tube resulting in larger refrigeration loads from larger heat leaks by thermal conduction. It has not been definitely established that the eddy current shield is required. The superconductor coil's outer windings can provide self-shielding and in the case of small amplitude (approximately 500 Oe) ripple, the loss can be quite small. However following a conservative approach, because of the state of the theory of ac loss, a new rotor is being designed to operate with an eddy current shield.

In consideration of the AFAPL programs in superconductivity, several relevant objectives of superconducting materials research have been identified. The goals are: 1) to develop high T_c filamentary superconducting wire such as Nb_3Sn, V_3Ga, or NbCN, 2) to predict the energy loss in superconductors produced by ac fields and currents, 3) to develop short sample ac loss measurement techniques which may be used to predict long sample or coil performance from short sample data and, 4) to predict the optimum conductor configuration for each superconducting wire application. The goal of producing filamentary Nb_3Sn wire has been identified as the number one goal of further superconducting materials development by the Advanced Interagency Power Group (AIPG), an organization with representation from many DOD agencies, and the Interlaboratory Committee (ILC) comprised of many government agencies such as the AEC, DOT, NSF, NBS, DOT, and DOD. Hopefully, an AFML manufacturing technology program initiated in FY75 will result in a practical filamentary Nb_3Sn superconductor.

The Air Force, in the recent past, has played a significant role in the development of superconducting materials, particularly Nb_3Sn. Two agencies have had large contractual efforts in superconducting materials, the Air Force Materials Laboratory (AFML) and the Air Force Office of Scientific Research (AFOSR). Donald Evans of AFML directed contractual programs in superconductivity from 1960 to 1967. The total contractual dollars for this period was approximately 2000K. RCA under AFML contract was investigating the fundamental properties of Nb_3Sn when Kunzler in 1961 at Atomics International discovered that Nb_3Sn could carry practical current densities in high magnetic fields. After a very extensive effort by RCA, the brittle A15 compound superconductor Nb_3Sn was produced in tape form by chemical deposition of Nb_3Sn upon a stainless steel substrate. This wire was marketed under the trade name "Vapo-Dep". Max Swerdlow of AFOSR under Project 9764 has funded basic materials research in superconducting materials at an annual rate of 500-800K for the past decade. The work of Matthias and others directed toward increasing T_c has received major support from AFOSR. The work of Deis and Webb on the Nb_3Ga resulting in a T_c of 20.4K and the work of Gavaler on sputtered Nb_3Ge resulting in a T_c of 23K were funded by AFOSR. Besides the substantial contribution of the Air Force to superconducting materials development several fundamental studies of ac loss on superconductors were supported in the early 60's. The ac loss programs were initiated in support of an Air Force Avionics Laboratory (AFAL) superconducting gyro program. An AFML final report on ac loss authored by C. Bean et. al. of General Electric is still an excellent text on ac loss. The ac loss measurement program on high purity Nb by Beall and Meyerhoff resulted in a classic paper. These measurements demonstrated that ac losses can be reduced to acceptable levels and were the basis of present large scale superconducting transmission line programs. Historical funding charts are shown for the years 1960-1973 in the Appendix.

Present AFML superconducting materials programs are devoted to low ac loss high T_c filamentary wire. In 1973 The Carborundum Company and AFML were awarded an IR 100 award for their work on filamentary NbCN. Several hundred inquiries about NbCN wire were received as a result of the publicity resulting from the IR 100 award. In addition inhouse ac loss modeling and ac loss measurements have been directed toward attaining the objectives previously stated. Results of the inhouse studies on ac loss are presented in the following sections.

Kunzler's discovery in 1961 stimulated research in superconducting materials but the predicted large markets for wire failed to materialize resulting in a major decline in industrial support. The successful operation of superconducting devices such as the MIT 70 KVA 60 cycle generator in the early 70's and the energy crisis have produced a rebirth of interest in superconducting materials. Chronologically the late 50's and early 60's represented the golden age of superconductivity, the middle 60's through early 70's the dark ages, and the middle 70's mark the beginning of the renaissance of superconductivity.

SECTION II

COMMENTS ON AC LOSS IN SUPERCONDUCTORS

There are two types of superconductors (Type I and Type II) which are easily distinguished by their magnetic behavior as shown in Figure 5. Consider the curves for the case of zero demagnetizing factor. Type I is a perfect diamagnet for fields below H_c and normal above H_c. Type II is a perfect diamagnet until the lower critical field H_{c1} where magnetic flux begins to enter. For high-field high-current applications irreversible Type II superconductors are required and their magnetization curve is shown in Figure 14. Some Type I and weak Type II (H_c~H_{c1}) superconductors have been considered for ac transmission lines because ac loss for surface fields less than H_c or H_{c1} is small. However for Type I the surface field is limited to 540 G in the case of Pb at 4.2K the best Type I and for Nb at 4.2K a weak Type II the surface field is limited to approximately 1200G. The irreverible magnetic behavior of high-field high-current materials is produced by flux pinning, a necessary feature for practical supercurrent densities. Flux pinning centers are purposefully introduced to enhance J_c. Examples of flux pinning centers are second phase precipitates, dislocation networks, grain boundaries, vacancies, radiation induced defects, and surfaces. A crude consideration of the force balance between the Lorentz Force per unit volume (J_cB) and a constant pinning strength parameter yields a hyperbolic field dependence for $J_c(H)$. The ideally irreversible magnetization curve in Figure 14 was calculated from $J_c(H) = \alpha/H$ and the critical state model assumptions which will be described later. The area enclosed by the M-H curve corresponds to an energy loss. This hysteretic loss is produced by a zero frequency eddy current effect where the induced current density has a finite upper limit determined by J_c. As in the case of eddy currents in copper there are many geometrical tricks available to reduce ac loss in hard superconductors like NbTi or Nb_3Sn. Some of the geometrical variables determining the ac loss in multifilamentary wire are the diameter of the superconductor filament, the diameter of the composite wire, the separation between filaments, and the twist pitch. Some of the materials parameters are $J_c(H)$, dJ_c/dT, the resistivity of the copper matrix (ρ_c), and possibly a surface shielding field (H_s).

Superconducting ac loss can be determined experimentally utilizing various techniques. At the present time electrical techniques such as the Brookhaven bridge, the mutual inductance bridge of Sekula, the LRC circuitry of Haller, the integrating Hall circuitry and the digital-multiplier-integrator circuitry of Gilbert and Voelker, the integrating technique of Wilson, and magnetization measurements are favored over conventional calorimetric techniques. Figure 6 shows a typical result of magnetization measurements of filamentary NbTi (in this case Supercon 241E-13). The ac loss for a given field amplitude is obtained from the area of the corresponding M-H loop. An example of the ac loss for a constant ripple field superimposed on various bias fields is given in Figure 7, and an example of a fixed bias field with a varied ripple field is shown in Figure 8. Figure 9 shows a typical voltage waveform produced by a superconductor's nonlinear response to an ac field or current. Bridge techniques are used to obtain the loss voltage from total voltage waveforms such as those in Figure 9. While the situation of ac loss is very complex a nominal value of ten microwatts/cm^3-Oe-cycle is typical for 5-10 micron filament NbTi for large amplitude field changes. In composite wires the loss is not hysteretic (i.e. linearly dependent on frequency) because of coupling currents between the filaments and eddy currents in the copper matrix. The relative importance of the various losses is frequency dependent. At low frequencies hysteretic loss dominates, at intermediate frequencies coupling losses must be considered, at high frequencies eddy current losses in the copper can dominate. For the special case of a small solenoid (ID=2.4cm, OD=6.5cm, L=5.3cm) Brechna and Ries have compared the various losses for a B of 70kOe/sec. The loss due to hysteresis was 2.14 watts, the coupling loss was .96 watts, and the eddy current loss was negligible.

In 1962-63 Bean and London introduced the concept of a critical state model to explain the irreversible behavior of superconductors and to predict ac loss. The magnetic behavior of hard superconductors is produced by circulating supercurrents and not by intrinsic spin as in the case of permanent magnets. A composite J_c(H) vs H curve for NbTi is shown in Figure 10. The curve is generally hyperbolic. J_c(H) determines the magnitude of these supercurrents. The Bean-London model assumed that

$J_c(H)$ was independent of field, a very unrealistic assumption. However many important conclusions about geometry effects were drawn from the model. Since that time a considerable amount of effort has been devoted to developing the theory of ac loss. Unfortunately, accurately predicting the ac loss for a given situation is beyond the present state of the art. The following recent quotations demonstrate this point. In 1972 Haller stated:

> "In spite of a rather comprehensive application of the foregoing loss expressions, a considerable discrepancy exists between predicted and measured losses."

In 1973 Tinkham wrote an addendum to a paper on ripple loss in order to correct an "overly pessimistic earlier estimate." Technical Note 25 on the Brookhaven National Laboratory's Power Transmission Project released in 1974 stated:

> "Although it is not possible to calculate from a theoretical basis the losses as a function of excitation which yield complete agreement with the experimental data (except in a few cases), the theories of ac losses, especially that of Fournet and Mailfert (1970), generally appear to give a good qualitative description of the phenomena for many of the Nb_3Sn specimens. A weakness of present theories of loss prediction is a lack of theoretical and experimental understanding of the nature of surface currents. Although H_s is chosen to be independent of H when calculating $P(\sigma)$, it is known that H_s decreases rapidly with H in some cases. Hence, introduction of a H_s with magnetic field dependence may improve the theory. In addition, it is not clear whether the surface current in these situations is entirely irreversible."

It is interesting to note that Wipf in a review paper on ac losses in superconductors in 1968 concluded:

> "But we ought to increase our understanding of H_s. This may open the door towards reducing ac losses."

The parameter H_s mentioned above is a surface screening field which has been introduced to bring about better agreement between small field amplitude ac loss data and the theoretical fit. H_s is typically 100 G. In addition the concept of H_s has been utilized to construct voltage waveforms which are qualitatively similiar to experimental waveforms. The concept of surface superconductivity, the enhancement of the superconducting electron density at a superconductor insulator interface in ideal reversible superconductors, was probably the initial motivation for H_s. The Bean model, a one parameter theory, assumes a uniform current density throughout the sample. By assuming stronger pinning or a higher J_c at the surface a second parameter H_s is introduced. It has been noted that J_c, because of its field dependence, varies across the cross section of a superconductor because of self-shielding effects. Incorporation of this fact into a critical state model yields many surface like results which are produced by bulk pinning. In the following sections of this report the consequences of a field dependent critical-state model ($J_c=\alpha/H$) have been calculated analytically, and many effects attributed to surface currents or H_s are obtained without additional assumptions. In fact, it appears an assumption of a region of weaker pinning at the surface is required to incorporate an H_s for this model. Experiments on surface roughness indicate that this might be a more reasonable assumption. Rough surfaces have larger losses than smooth surfaces because the effective field at the surface is larger. However, the Bean London model underestimates dJ/dH and the alpha model overestimates dJ_c/dH. An exact calculation of the loss using the more realistic Kim-Hempstead expression for J_c ($J_c=J_oH_o/(H_o+H)$) would lie intermediate between the two and reduce the need to incorporate an H_s.

SECTION III

COMMENTS ON CRITICAL STATE MODELS

Bean and London introduced the critical-state model in an attempt to explain the magnetic behavior of hard superconductors. The model assumes that a superconductor has a critical current density J_c which is independent of magnetic field and that this full current density will flow in the regions of the superconductor where the magnetic field has penetrated. The direction of the circulation of the current is determined by the sense of the electromotive force associated with the last field change. From these assumptions hysteresis loops for superconductors can be calculated from Maxwell's equations and the definitions of magnetic induction (B), magnetic intensity (H), and magnetization (M) as outlined in Table 6. Practical units are employed, i.e. Oe, A/cm^2, and V, following the notation of Bean. All equations apply to the rod geometry and zero demagnetization factor unless otherwise specified.

Magnetization loops and the expressions for the hysteretic loss have been obtained for the Bean-London model only for the case of magnetic fields parallel to the face of infinite slabs and parallel to the axis of long cylinders. In practice the model is applied to situations where the fields are perpendicular to slab faces or cylinder axes. This practice amounts to ignoring the demagnetizing factor (n). It is worthwhile considering the effect this approximation may have on the calculated hysteretic loss. Figure 5 shows the magnetization curves for ideal Types I and II superconductors for the case of n=0 (slab with field parallel to face) and n=1/3 (sphere). In both cases for non-zero n, the low field magnetization is higher and the high field magnetization is lower than the corresponding zero n magnetization. However, the area under the M-H curve is independent of n. Note, that the expression for the high field magnetization obtained by Cape and Zimmerman for Type II superconductors is essentially independent of n since K's are typically 50. For the Bean critical state model the ratio of the perpendicular to the parallel field magnetization for a cylinder is two at large fields. This result indicates that applying the Bean model loss expression to a cylinder for large field sweeps and a perpendicular field underestimates the loss by a factor of two. However, considering the field dependence of J_c, the perpendicular geometry with larger internal fields will reduce J_c below that of the corresponding parallel geometry tending to reduce the influence of the demagnetizing factor. In one instance the ratio of the measured hysteretic losses $(Q_{\parallel}/Q_{\perp})$ was 1.02 for seven micron diameter NbTi wire and a 18 kOe full cycle sweep. So ignoring the demagnetizing factor for large field sweeps can introduce an error of a factor of two in the hysteretic loss for the worst case $(dJ_c/dH=0)$ and in many instances, particularly field sweeps centered about the origin the error can be much less. The hysteretic loss per unit volume of the superconductor, obtained from the Bean-London model for a cylindrical wire of radius (R) and with the magnetic field parallel to its axis is given by

$$Q=(H_B^{*2}/4\pi)\ (4h_m^3/3-2h_m^4/3),\ h_m=\frac{H}{H_m}\leq 1 \tag{2}$$

$$Q=(H_B^{*2}/4\pi)(4h_m/3-2/3),\ h_m\geq 1,\ H_B^{*}=\frac{4\pi J_c R}{10} \tag{3}$$

Equation (2) for partial penetration is the corrected form of Equation (7) of Bean's (Reference 116) article. Generally slab expressions are applied in loss analysis. The partial penetration slab loss expression can fit loss data of any magnitude, however, because of the second term in Equation (2) the cylinder loss expressions are limited to be below a certain region of loss independent of the fitting parameter J_c. Equation (2) and Equation (3) indicate that for partial penetration the loss is proportional to $1/J_cR$, the transmission line limit, and for full penetration the loss is proportional to J_cR, the high field magnet limit. This result has aided substantially superconducting wire development for ac applications. The Bean-London model assumption of a field independent J_c is extremely unrealistic. As a result the model is limited to small amplitude field oscillations or field regions where $dJ_c/dH\sim 0$. Various techniques have been utilized to incorporate a field dependent J_c into the Bean model. Typical expressions for $J_c(H)$ are given in Table 7. One approach is to insert an analytical form for J_c, usually the Kim expression, in the Bean-London expression for the loss. Another approach is to insert the expression for J_c into the Bean-London expression for the magnetization prior to integration to obtain the hysteretic loss. These approaches ignore the self-shielding of the induced currents which cause a variation of J_c across the cross section of the superconductor so their results apply only to "very thin" wires. Exact models have been investigated in varying degrees by Watson, Karasik et.al., and others. In the following sections the consequences of an exact critical state model calculation for the relationship $J_c = \alpha/H$, a special case of the generalized pinning model of Ire and Yamafuji will be presented and be compared to other models. In particular, the bulk pinning effects which have surface like consequences will be stressed in order to distinguish them from the concept of H_s. The self-shielding field for this model is of the order of $H^* = (8\pi\alpha R/10)^{1/2}$. The parameter α is of the order of 5×10^9 A-Oe/cm^2 for NbTi, demonstrating that H* has a relatively large value for typical wire diameters and that self-shielding effects are important.

The curl equation in Table 6 for a cylindrical geometry of radius R and zero demagnetizing factor has a solution for the alpha model of

$$H^2(r)/2=\pm\, 4\pi\alpha r/10 + C \quad 0\le r\le R \tag{4}$$

where the sign of the first term depends on the sense of the electromotive force associated with the last local field change and C is a constant determined by the boundary conditions. The internal field profile upon initial magnetization is

$$H(r) = \left[\frac{8\pi\alpha}{10}\left(r-R+\Delta\right)\right]^{1/2} \quad 0\le r\le R \tag{5}$$

where the penetration depth Δ is given by $\Delta = 10\,H_e^2/8\pi\,\alpha$. Figure 11 shows the internal field profile for a complete field cycle. Sequence (a) and (e) should be noted carefully keeping in mind that J_c is high where H is small. In (a), bulk pinning produces a surface current sheath and in (e), there is a current sheath at large R approximately twice as thick (a). Since the moment of a current loop is proportional to the square of the radius of the loop, large current sheaths which look like surface currents at large R as in (a) and (e) contribute significantly to the total moment.

The field required to completely penetrate the superconductor, (H*), is defined as the field at which the penetration depth is equal to R. H* is a very important model parameter. For example, the field dependence of the ac loss for field amplitudes small compared to H* (for Bean $Q \sim H^3$) is different than for those large compared to H* (for Bean $Q \sim H$). Table 8 lists various expressions which may be used to calculate H*. The parameters involved are obtained by least square fitting (LSF) the J_c vs H data with an appropiate analytical expression.

In the Bean model J_c is the average value of $J_c(H)$ and the parameter of the alpha model is given by

$$\alpha = (\Sigma_i J_i/H_i)/\Sigma_i 1/H_i \tag{6}$$

Certain problems are encountered in fitting the Kim expression. Two approaches were used. The simplest approach was a LSF to the inverted expression

$$\frac{1}{J_c} = H/\left(J_o H_o\right) + 1/J_o \tag{7}$$

but occasionally the data will yield a negative unphysical H_o. The expressions for J_o and H_o obtained from the LSF procedure are complicated. The function $g(H_o)$ of Equation (8) was formed to obtain H_o. H_o is found by looking for the roots

$$g(H_o) = \left(\Sigma_i \left(\frac{J_i}{H_o + H_i}\right)\right)\left(\Sigma_i 1/(H_o + H_i)^3\right) - \left(\Sigma_i \frac{J_i}{(H_o + H_i)^2}\right)\left(\Sigma_i 1/(H_o + H_i)^2\right) \tag{8}$$

of $g(H_0)$. Unfortunately sometimes the only positive root of $g(H_0)$ is infinity. If a reasonable H_0 is obtained from Equation 7 then J_0 is obtained from Equation (8).

$$J_o = \left(\Sigma\left(J_i/(H_o+H_i)\right)\right) \tag{9}$$

A composite J_c-H curve was obtained for NbTi wires whose diameters varied from ten microns to 245 microns. The surface to volume ratio did not seem to affect the current density indicating that surface pinning was not a significant factor. In order to obtain a general expression for J_c-H for ac loss modeling NbTi a LSF of the composite curve of Figure 10 was made for the Kim and the alpha models yielding

$$J_c = 7 \times 10^9/H \quad (\text{A/cm}^2 \text{ for H in Oe}) \tag{10}$$

$$J_c = 9.91 \times 10^9/(12550+H) \quad (\text{A/cm}^2 \text{ for H in Oe}). \tag{11}$$

These fits are compared to the data in Figure 10.

The calculated values of H* from the expressions in Table 8 can be substantially different. Consider the results for a piece of Niomax-S 20-40 given in Table 9. H* varies from 2100 G for the Bean model to 11,700 G for the alpha model. Generally, the stronger the field dependence of the expressions for J_c the higher the value of H*. Experimentally a saturation field (H_{sat}), the field required to produce the maximum remanent moment at zero field ($-4\pi M_R$) is easily determined. H* obtained from relationships between H_{sat} and H* is the least model dependent determination of H*. Figure 12 shows a typical plot of the remanent moment versus the maximum field amplitude and H_{sat} is defined as the minimum field at which saturation occurs. The saturation field for the Bean model is 2H*, for the alpha model it is ($\sqrt{2}$)H*, and for the Kim model it is*

$$H_{sat} = \left(2(H^*+H_o)^2 - H_o^2\right)^{1/2} - H_o \tag{12}$$

Experimentally determined saturation fields are compared to those calculated from the Bean, Kim, and alpha models in Table 10 for Supercon 217E-19 and Supercon 241E-13. Agreement is not very good but it appears that the Kim result is best followed by the alpha model. In addition the smaller the wire diameter, the worse the agreement. The Kim and the alpha models overestimate H_{sat}. For the Bean and alpha models H* has also been obtained from the experimental hysteretic loss and the theoretical loss expressions and compared in Table 10.

The field change ΔH required to reverse the sense of the circulating current after full penetration has been attained is obtained from Equation (6) in Table 8 for the alpha model and Equation (7) for the Kim model. Using the parameters of the composite J-H curve the curve for the α model is plotted in Figure 13 and the result is compared to magnetization data. These curves are reminiscent of the surface screening field results of Ullmaier and Gauster. The feature that dB/dH is zero at the end points of the hysteresis loop and that the field range over which dB/dH is approximately zero is larger the lower the maximum field can be explained by bulk pinning. Therefore, the distinction of bulk and surface currents must be reconsidered.

*or $H^* = \left(\frac{(H_s+H_o)^2}{2} + \frac{H_o^2}{2} \right)^{1/2} - H_o$

SECTION IV

EXACT CALCULATION OF THE MAGNETIZATION CURVES, VOLTAGE WAVEFORMS, AND LOSS EXPRESSIONS FOR THE ALPHA MODEL AND LOSS EXPRESSIONS FOR OTHER MODELS

For the alpha model there are three different types of full cycle hysteresis loops determined by the maximum reduced field ($h_m = H/H_m$). There are magnetization loops for h_m less than 1, for h_m greater than 1 but less than the $\sqrt{2}$, and for h_m greater than the $\sqrt{2}$. The intermediate range corresponds to full penetration but with a remanent moment less than the saturation value. A corresponding situation exists for half cycle loops. The analytical expressions for the magnetization M for full and half cycle loops are given for various h_m's. The subscripts on M indicate the direction of the external field sweep.

The expressions for the magnetization in reduced units for a full cycle sweep and $H_m \leq 1$ are,

$$\frac{-4\pi M_-}{H^*} = h - \frac{4}{3}\left(1 - \frac{h_m^2}{2} + \frac{h^2}{2}\right)\left(\frac{h^2}{2} + \frac{h_m^2}{2}\right)^{3/2} + \frac{8}{15}\left(\frac{h^2}{2} + \frac{h_m^2}{2}\right)^{5/2}$$

$$+ \frac{4}{15}\left[2h^5 + 5h^3 - \left(\frac{7}{2}h^2 + 5 - \frac{3}{2}h_m^2\right)\left(\frac{h^2}{2} + \frac{h_m^2}{2}\right)^{3/2}\right], \quad 0 \leq h \leq h_m \qquad (13)$$

$$\frac{-4\pi M_-}{H^*} = h - \frac{4}{15}\left(5h^3 - 2h^5\right) - \frac{2}{3}^{1/2}\left(1-h^2\right)\left(h_m^2 - h^2\right)^{3/2} + \frac{7\cdot 2^{1/2}}{30}\left(h_m^2 - h^2\right)^{5/2}$$

$$+ \frac{2}{15}^{1/2}\left[\frac{3}{2}\left(h_m^2 - h^2\right)^{5/2} - 5\left(h_m^2 - h^2\right)^{3/2}\left(1 - h^2\right)\right] \cdot 0 \geq h \geq -h_m \qquad (14)$$

The other half of the cycle from $-h_m$ to h_m may be obtained from Equations (13) and (14) since the hysteresis loop is anti-symmetric in h. Several reduced magnetization curves are shown in Figure 14 for the case of full cycle partial penetration.

The expressions for the magnetization for a half cycle sweep and $h_m < 1$ are

$$\frac{-4\pi M+}{H^*} = h - {\frac{2}{3}}^{1/2}\left(1 - \frac{h_m^2}{2}\right)h_m^3 + {\frac{2}{15}}^{1/2} h_m^5 + {\frac{2}{15}}^{1/2}\left[h^5 + 5h^3\left(1 - \frac{h^2}{2}\right)\right.$$

$$\left. - \left\{\frac{7}{4}h^2 + 5\left(1 - \frac{h^2}{2}\right) - \frac{3}{2}\left(h_m^2 - \frac{h^2}{2}\right)\right\} h_m^3\right] \tag{15}$$

$$+ \frac{4}{15}\left[\left(2 - \frac{7}{4}{\left(\frac{1}{2}\right)}^{1/2}\right)h^5 + \left(5\,{\left(\frac{1}{2}\right)}^{3/2} - 5\right)h^3\right], \quad 0 \le h \le h_m$$

and Equation (13) for decreasing from h_m. Magnetization curves obtained from Equations (13) and (15) are shown in Figure 15.

The expressions for the magnetization for a full cycle sweep and h_m between 1 and $\sqrt{2}$ are

$$\frac{4\pi M+}{H^*} = h + \frac{4}{15}\left[2h^5 - 5h^3 - 2\,(h^2-1)^{5/2}\right], \quad 1 \le h \le h_m \tag{16}$$

$$\frac{-4\pi M-}{H^*} = h + \frac{4}{15}\left[2\left(\frac{h^2}{2} + \frac{h_m^2}{2}\right)^{5/2} - 5\left(1 - \frac{h_m^2}{2} + \frac{h^2}{2}\right)\left(\frac{h^2}{2} + \frac{h_m^2}{2}\right)^{3/2}\right.$$

$$\left. - 2\left(h_m^2 - 1\right)^{5/2}\right] + \frac{4}{15}\left[2h^5 + 5h^3 - \left(\frac{7}{2}h^2 + 5 - \frac{3}{2}h_m^2\right)\right. \tag{17}$$

$$\left.\left(\frac{h^2}{2} + \frac{h_m^2}{2}\right)^{3/2}\right], \quad 0 \le h \le h_m$$

$$\frac{-4\pi M-}{H^*} = h - \frac{4}{3}h^3 + \frac{8}{15}h^5 + {\frac{2}{15}}^{1/2}\left[5\left(h_m^2 - h^2\right)^{5/2} - 10\left(1 - h^2\right)\right.$$
$$\left.\left(h_m^2 - h^2\right)^{3/2} - 2^{5/2}\left(h_m^2 - 1\right)^{5/2}\right], 0 \geq h_m \geq -\left(2 - h_m^2\right)^{1/2} \quad (18)$$

$$\frac{-4\pi M}{H^*} = h - \frac{8}{15}\left(1 - h^2\right)^{5/2} - \frac{4}{15}\left(5h^3 - 2h^5\right). \quad -\left(2 - h_m^2\right)^{1/2}_{\geq h \geq -1} \quad (19)$$

Equations (16) through (19) produce one half of the hysteresis loop and the rest of the cycle is obtained from the anti-symmetric character of the loop. Figure 14 shows several magnetization curves for h_m between 1 and $\sqrt{2}$.

For a half cycle sweep and $1 \leq h_m \leq \sqrt{2}$ the magnetizations are,

$$\frac{-4\pi M+}{H^*} = \frac{-4\pi M+}{H^*}\left(\text{of Eq. (5)}\right) - \frac{8}{15}\left(h_m^2 - 1\right)^{5/2}, \quad 0 \leq h \leq h_m \quad (20)$$

and Equation (17) for decreasing h from h_m to 0. Figures 16 and 17 show magnetic induction, B, versus H loops for both full and half cycle for various h_m's.

For partial penetration, the magnetic induction B_m at H_m is related to the remanent magnetization B_r by

$$B_m = \frac{2^{1/2}\left(\frac{4}{3}h_m^2 - \frac{8}{15}h_m^5\right)B_r}{\frac{4}{3}h_m^2 - \frac{2}{3}h_m^5} \qquad 0 \leq h_m \leq 1 \qquad (21)$$

which is similar to the result of Malseed and Rachinger. The theoretical relationship between B_m and B_r for all h_m is shown in Figure 18. B_r becomes independent of B_m for $H_m > \sqrt{2}\, H^*$ and the initial slope is $2^{1/2}$. For the general model of Irie and Yamafuji B_r becomes independent of B_m for

$$H_m = \left(2^{\frac{1}{n+1}}\right) H^* .$$

The magnetization curves for $h_m > \sqrt{2}$ for full and half cycle have been previously obtained. Using these expressions for the magnetizations, the areas of the reduced hysteresis loops have been calculated for both full and half cycle for all h_m's.

The energy loss per unit volume Q for a half cycle sweep with $h_m \le \sqrt{2}$ is

$$Q = \frac{H^{*2}}{4\pi} \left(.1045 h_m^4 - .0250 h_m^6\right) . \qquad h_m \le \sqrt{2} \tag{22}$$

For a full cycle sweep and $h_m \le 1$ it is

$$Q = \frac{H^{*2}}{4\pi} \left(2.7339 h_m^4 - 1.4837 h_m^6\right) . \qquad h_m \le 1 \tag{23}$$

For a full cycle sweep and $1 \le h_m \le \sqrt{2}$ it is

$$\begin{aligned} Q = \frac{H^{*2}}{4\pi} \Bigg[& \left(1 + \frac{\sqrt{2}}{2} \log\left(1 + \sqrt{2}\right) + \frac{\sqrt{2}}{2} \sin^{-1} \frac{(2 - h_m^2)^{1/2}}{h_m}\right) h_m^4 \\ & - \left(\frac{7\sqrt{2}}{24} \sin^{-1} \frac{(2 - h_m^2)^{1/2}}{h_m} + \frac{17}{36} + \frac{7\sqrt{2}}{24} \log\left(1 + \sqrt{2}\right)\right) h_m^6 + \frac{\pi}{6} \\ & - \frac{1}{3} \sin^{-1} (2 - h_m^2)^{1/2} + \frac{1}{3} \log\left(h_m + (h_m^2 - 1)^{1/2}\right) \end{aligned} \tag{24}$$

$$
\begin{aligned}
&+ h_m (h_m^2 - 1)^{3/2} \left\{ \frac{8}{9} h_m^2 - \frac{2}{3} \right\} - \frac{h_m}{3} (h_m^2 - 1)^{1/2} \\
&+ (2 - h_m^2)^{1/2} (h_m^2 - 1)^{1/2} \left(\frac{5}{12} h_m^4 - \frac{2h_m^2}{3} + \frac{1}{3} \right) \Bigg]
\end{aligned}
$$

For a half cycle sweep and $h_m > \sqrt{2}$ it is

$$
\begin{aligned}
Q = \frac{H^{*2}}{4\pi} \Bigg[&\Bigg\{ \frac{1}{2} + \frac{\sqrt{2}}{4} \log (h_m + \sqrt{2}\, h_m) - \frac{\sqrt{2}}{4} \log \Big((h_m^2 - 2)^{1/2} \\
&+ \sqrt{2}\, (h_m^2 - 1)^{1/2} \Big) \Bigg\} h_m^4 + \Bigg\{ - \frac{17}{72} - \frac{7\sqrt{2}}{48} \log (h_m + \sqrt{2}\, h_m) \\
&+ \frac{7\sqrt{2}}{48} \log \Big((h_m^2 - 2)^{1/2} + \sqrt{2}\, (h_m^2 - 1)^{1/2} \Big) \Bigg\} h_m^6 \qquad (25) \\
&+ (h_m^2 - 2)^{1/2} (h_m^2 - 1)^{1/2} \left\{ - \frac{5}{24} h_m^4 + \frac{1}{3} h_m^2 - \frac{1}{6} \right\} \\
&+ (h_m^2 - 1)^{3/2} h_m \left(\frac{4}{9} h_m^2 - \frac{1}{3} \right) - \frac{1}{6} (h_m^2 - 1)^{1/2} h_m \\
&+ \frac{1}{6} \log \Big((h_m^2 - 1)^{1/2} + (h_m^2 - 2)^{1/2} \Big) + \frac{1}{6} \log \Big(h_m + (h_m^2 - 1)^{1/2} \Big) \\
&- \frac{\sqrt{2}}{6} - \frac{1}{6} \log (1 + \sqrt{2}\,) \Bigg] .
\end{aligned}
$$

For a full cycle sweep and $h_m > \sqrt{2}$ it is

$$
\begin{aligned}
Q = \frac{H^{*2}}{4\pi}\Bigg[& \left\{1 + \frac{\sqrt{2}}{2}\log\left(h_m + \sqrt{2}\, h_m\right) - \frac{\sqrt{2}}{2}\log\left((h_m^2 - 2)^{1/2} + \sqrt{2}\,(h_m^2 - 1)^{1/2}\right)\right\} h_m^4 - \left\{\frac{17}{36} + \frac{7\sqrt{2}}{24}\log\left(h_m + \sqrt{2}\, h_m\right)\right. \\
& \left. - \frac{7\sqrt{2}}{24}\log\left((h_m^2 - 2)^{1/2} + \sqrt{2}\,(h_m^2 - 1)^{1/2}\right)\right\} h_m^6 + \frac{\pi}{6} \\
& + \frac{1}{3}\log\left(h_m + (h_m^2 - 1)^{1/2}\right) + \frac{1}{3}\log\left((h_m^2 - 1)^{1/2} + (h_m^2 - 2)^{1/2}\right) \\
& + h_m (h_m^2 - 1)^{3/2}\left(\frac{8}{9}h_m^2 - \frac{2}{3}\right) - \frac{1}{3}(h_m^2 - 1)^{1/2} h_m \\
& + (h_m^2 - 2)^{1/2}(h_m^2 - 1)^{1/2}\left(-\frac{5}{12}h_m^4 + \frac{2}{3}h_m^2 - \frac{1}{3}\right)\Bigg] .
\end{aligned}
\qquad (26)
$$

Figure 19 compares the reduced short sample loss obtained from the previous expressions to the Bean-London model. The log-log plot demonstrates that the magnetic field dependence, H^n, in the partial penetration region is approximately four for the field dependent model. For the full penetration region the field dependent model has a field dependence which is much less than linear.

For comparison the Bean hysteresis loops are shown in Figure 20 and 21. Since J_c is independent of field, full and half cycle loops look the same. In Figure 22 full penetration using the Bean magnetization and the Kim expression for J_c is shown. Notice that the peak in the M-H curve is at zero field, a consequence of ignoring self-shielding effects. In Figure 17 the B-H loops resemble the loop of Dunn and Hlawiczka although they assumed a surface field and a material with an H_{c1}. Their loop has dB/dH equal to zero for a field change of ΔH at the end points and dB/dH equal to zero for a field change of $2H_{c1}$ at the midsection of the loop. The loop for a h_m of 1.4 in Figure 17 has all of these properties except there are no assumptions about surface fields or H_{c1}. dB/dH=0 is a consequence of creating reversing currents traveling in large loops which contribute significantly to the moment and the flat portion at the midsection is a consequence of J_c increasing sharply with decreasing H.

It is standard practice to measure ac loss in a superconductor by looking at the voltage induced across an inductor or a mutual inductor with a superconductor core or by a standard four probe technique resulting in voltage traces like those shown in Figure 23. These traces were obtained by W.C.H. Joiner at the University of Cincinnati. The voltage waveforms contain a large inductive component typically 100 times the voltage produced by the superconductor. This inductive voltage must be subtracted out to obtain the superconductor voltage calculated from the alpha model for full cycle and half cycle ac fields. These voltages were added to inductive voltages to obtain typical total waveforms. The superconductor voltage is sometimes called the loss voltage, however only the component of the fundamental in phase with the drive current contributes to the loss if the drive current is sinusoidal. Figure 24 was obtained from the B-H curve and a sinusoidal field $H=H_m \cos(\omega t)$ at a frequency of 60 Hz, and the expression for the voltage

$$V \propto \frac{dB}{dt} \propto \frac{\partial B}{\partial H}\frac{dH}{dt} \tag{27}$$

for the full cycle case starting at t=0. There is a diamagnetic region because both $\partial B/\partial H$ and dH/dt are zero. However, the dip to zero is produced because J_c increases to the point where it is difficult to change the internal field and again $\partial B/\partial H$ is small. Experimentally the dip does not extend to zero voltage but the alpha curve which overestimates low field J_c's does. The biased field case shown in Figure 25 for $H=H_m/2 + (H_m/2)\cos(\omega t)$ has an interesting property. The length of the diamagnetic region is longer at the low field end than in the high field end. This results because the hysteresis loop for the biased case is not symmetric through its center. This may cause a rectification effect although no analytical calculation has yet been made. DC voltages have been previously observed in superconductors in the presence of superimposed ac and dc magnetic fields when no current was flowing. This rectification is one possible source of the dc voltage. It has become a practice when balancing loss measuring circuits to use the diamagnetic region to judge the proper balance point.

It is difficult to measure the loss from the amplitude of the in phase component of the first harmonic. It is easier to measure the amplitude of the higher harmonics and Bean has related ac loss to the amplitude of the third harmonic. The ratio of the amplitudes of the harmonics have been recalculated. The ratio of $|V_3/V_1| = 4.266$ differs from Bean's result (Reference 116). Analytical expressions for the amplitude of the harmonics have not been correctly calculated for the more complex alpha model. Preliminary calculations indicate that the value of the ratio of the harmonics is field dependent. However the waveforms have been analyzed with a computer program which Fourier analyzes a tabulated function. The program was FORTAB available from Com-Share. The results for several cases are shown in Table 11. The amplitude V_i and the phase angle P_i can be obtained from the cosine amplitude (C_i) and the sine (S_i) amplitude from the following expressions.

$$V_i = (S_i^2 + C_i^2)^{1/2} \; ; \; P_i = \tan^{-1} (S_i/C_i) \tag{28}$$

Table 11 indicates that for the full cycle case the odd harmonics are much larger than the even harmonics but for half cycle the even harmonics are nearly as large as the odd. Bean deleted the cubic terms in his Equation (5) and calculated ratios of the amplitudes. The total expression for B in his Equation (5) was used to obtain the amplitude ratio from FORTAB and the results are compared to the alpha and Bean results in Table 12. Note the ratio for the exact Bean and the alpha model are slightly field dependent. The approximate Bean was also calculated showing again that V_1 of Bean's calculation is incorrect. The modified Bean model which incorporates the Kim expression yields the following loss expression for large field sweeps.

$$Q= \frac{4\pi r J_o H_o}{5} \left\{ \ln\left(1+\frac{H_m}{H_o} - \frac{2}{3}\frac{H_s^*}{H_m}\right) \right\} \tag{29}$$

Where $H_m >> H^*$ from the Kim model and $H_m >> H_s^* = \frac{4\pi R}{10}\left(\frac{J_o H_o}{H_o+H_m}\right)$. For partial penetration the modified Bean model merely incorporates the Kim expression into the Bean loss expression of Equation 2. Dunn and Hlawiczka have modified the Bean model by incorporating a surface shielding field ΔH and H_{c1}. Their loss expression is

$$Q = \frac{10}{12\pi^2 J_c d} \left\{ \left(H_m^1\right)^2 (1.5H_{c1}+3\,\Delta H+H_m^1) \right\}, \quad H_m^1= (H_m - \Delta H-H_{c1}) \tag{30}$$

for the slab geometry of thickness d and partial penetration. To convert loss per unit volume to loss per unit surface the loss per unit volume should be multiplied by R/2 for a cylinder and d/2 for a slab. So Equation (30) can be applied to a cylinder when it has been converted to loss per unit surface for small field changes.

The screening field ΔH, typically 100 Oe., is varied to obtain agreement with low field loss and J_c is varied to obtain agreement at high fields. Basically, ΔH is used to steepen the slope of the low field region and it has very little effect on the high field region because ΔH becomes small compared to H_m. For commercial superconductors H_{c1} is approximately zero.

Ire and Yamafuji have obtained a loss expression for partial penetration for the generalized expression from an exact critical state model calculation for a slab.

$$Q=.054\ (2-\gamma)h^{4-\gamma}\, {H^*}^2, \quad 0\leq \gamma\leq 1 \quad H^*= \left\{(2-\gamma)\ 4\pi\alpha\ \gamma/10\right\}^{1/(2-\gamma)} \tag{31}$$

For γ = 0 the result of Equation (31) should be compared to Equation (23) of the alpha model. As in the Bean case the cylinder loss is twice the slab loss. Finally, for partial penetration an exact calculation for the energy loss using the Kim expression is given in Fournet and Mailfert. However, the only complete set of analytical expressions for the loss for all field ranges for a field dependent model are those calculated in this report.

There are several interesting results of the general critical state model for $J_c = \alpha/H^n$. The general expression for H* is

$$H^* = \left[\frac{4\pi}{10} (n+1)\ \alpha r\right]^{1/(n+1)} \qquad n \geq 0 \tag{32}$$

The general expression for the saturation remanent is

$$b_R = 2(n+1)^2 / (n+2)\ (2n+3) \tag{33}$$

The minimum field required to obtain full reversal or produce maximum B_r is

$$H_m = 2^{(1/(n+1))} H^* \tag{34}$$

The field change required to reverse the circulating current at field is given by

$$\Delta H = H_m - (H_m^{n+1} - 2H^{*n+1})^{1/(n+1)} \tag{35}$$

where H* is for the appropiate n.

Finally, it is of some interest to relate partial penetration ac loss to the remanent moment in order to reduce the time required to obtain data as did Meyerhoff and Beall. For the Bean model Q is given by

$$Q = \frac{H^{*2}}{4\pi} \left\{ \frac{8\sqrt{2}}{3} b_r^{3/2} \right\} = H^{*2}/_{4\pi} \left\{ \frac{8}{3} b_r\ h_m \right\}, \quad h_m << 1 \tag{36}$$

where $b_r = B_r/H^*$ and for the alpha model

$$Q = \frac{H^{*2}}{4\pi} \left\{ 2.957 b_r^{4/3} \right\} = \frac{H^{*2}}{4\pi} \left\{ 2.9\ b_r h_m \right\}, \quad h_m << 1 \tag{37}$$

A plot of Q vs b_r for the alpha model indicates a slope of 4/3 on a log-log plot up to $b_r = .4$.

In the following sections the loss expressions for Bean, modified Bean and the alpha model are compared to experimental loss measurements.

SECTION V

HYSTERETIC LOSS IN SOLENOIDS FOR BEAN AND ALPHA MODELS

The ac loss for small standard solenoids and inductive storage systems has been measured calorimetrically and by electrical techniques by various experimenters and modeled using the Bean-London model. For a long solenoid and $h_m << 1$ the loss per unit length Q' for a full cycle sweep for the Bean-London model from Equation (2) is

$$Q' = \frac{5(a_2 - a_1)}{3\pi J_c R\lambda} \left(\frac{a_2}{20} + \frac{a_1}{5} \right) H_m^3, \tag{38}$$

where a_2 and a_1 are respectively the outer and the inner radius of the windings, and λ is the copper to superconductor ratio. For $h_m >> 1$ it is

$$Q' = \frac{2\pi R J_c}{45\lambda(a_2 - a_1)} (a_2^3 - 3a_2 a_1^2 + 2a_1^3)\ H_m \ . \tag{39}$$

Equations (38) and (39) indicate that the field dependence of the coil loss for the Bean-London model can vary from cubic (n=3) to linear (n=1).

For the field dependent model for $h_m << 1$ the corresponding loss per unit length from Equation (23) is

$$Q' = \frac{5}{8\pi\lambda\alpha R} (a_2 - a_1) \left(\frac{a_2}{30} + \frac{a_1}{6} \right) H_m^4 \ . \tag{40}$$

The field dependence of the solenoidal loss for the field dependent model for a wide range of h_m is shown in Figure 26 for the coil geometry of Haller in Reference 41. Equation (39) and Figure 26 indicate that for the field dependent model n varies from four to less than one. Curve A in Figure 7 was obtained for a 64 strand wire having 27.6 micron filaments and the same superconductor cross section at Haller's single core wire. The filaments were assumed to be totally decoupled by twisting. For fields less than 10kOe Figure 26 indicates that the single core wire (curve B) performs better than the multifilamentary wire (a reflection of the size dependence of the loss given by Equation (39).

Experimental results similar to Figure 26 are given in Dahl, Morgan, and Sampson and in Hunt.

The magnitude of the ac loss aside from geometrical factors is determined theoretically by the Bean-London parameter J_c or the parameter α. The Haller coil loss determined by using the reported values of J_o and H_o to calculate α is shown as curve B in Figure 27. This procedure yields loss values higher than the measured values above 4kOe. Varying α to minimize the standard deviation between the theoretical and experimental curve produces curve C in Figure 27 which agrees better at high field. For curve B α is 5.7 X 10^9 A-Oe/cm^2 and H* is 17,787G, and for curve C α is 2.4 X 10^9 A-Oe/cm^2 and H* is 36,650G. Since the range of Haller's data is less the H*, the theory predicts a slope of four which disagrees with the data, curve A in Figure 27 which has a slope of 2.25. For this model and the Bean-London model overestimating H* underestimates the hysteretic loss which may explain the position of Haller's theoretical curve, E of Figure 27. Figure 28 shows the loss for full-cycle for a fixed geometry (Haller's) for two maximum fields, 8,000 Oe and 12,000 Oe for various α's and for a frequency of 9.9Hz. Figure 28 indicates that for a given maximum field there is a critical current density which maximizes the loss. The model indicates that very high critical current round wire such as multifilamentary Nb_3Sn UNTWISTED could greatly reduce the hysteretic loss in inductors operated to fields less than H* or for the same loss yield higher energy densities.

SECTION VI

EXPERIMENTAL RESULTS FOR NbTi COPPER STABILIZED WIRE

Magnetization measurements were made on a number of commercially available NbTi filamentary wires and on short lengths of the two types of NbTi wire used to construct the experimental rotor by Westinghouse under contract to AFAPL. Dr. Charles Oberly of AFAPL/POD-1 obtained the rotor measurements in the H. Kamerlingh Onnes Memorial Laboratory of AFML/LPE. The experimental hysteretic loss curves are compared to theoretical predictions and a set of reduced curves from which loss can be predicted are constructed from the loss data. The size dependence of the loss, the saturation field as a function of size, and the dependence of the reversal field on bias field were experimentally determined.

All magnetization measurements were taken on a PAR model 155 vibrating sample magnetometer used in conjunction with a Varian 12 inch electromagnet. The field is uniform to better than 0.01% in a 1/2 inch diameter spherical volume at 19kOe, the peak field. A picture of the apparatus is shown in Figure 29. The amplitude of the sample vibration is approximately 1mm ensuring that the sample is in a uniform external field. The frequency of vibration is 81 Hz. The temperature of the sample was measured with a calibrated GaAs diode. The magnetometer was calibrated with a standard nickel sphere from the NBS. The sampleholder was constructed from Kel-F and the samples were mounted in paraffin. The samples consisted of an appropriate number of approximately 1/4-inch wires mounted parallel to the sampleholder axis. The ends of the wires were polished and examined metallographically to ensure that the individual filaments were isolated from each other. The copper to superconductor ratios were determined by planimeter measurements and the average filament diameter was determined from the filament area. The magnetic field was always perpendicular to the wire axis. Due to zero field switching problems Q vs H was obtained only for half cycle loops. Double precision was utilized in evaluating the theoretical expressions for the magnetization. Short sample values for J_c were taken from manfacturer's data and from measurements by Canadian Superconductor and Cryogenics Company Ltd. (CSCC), an AFML contractor. Other types of ac loss measurements will be reported later on these same samples by CSCC. The data was analyzed in terms of the alpha model. There is a very good qualitative agreement between the theoretical alpha model (Figure 14) and the experimental hysteresis loops. An example is given in Figure 6. The relative position and amplitude of the low field peaks are predicted. Theoretically the maximum in the initial magnetization occurs at $h = .563$ and the other maxima occur at $h = \pm.291$. Theoretically, the initial magnetization has a maximum value given by $-4\pi\ M_1 = 0.355H^*$, and the maximum value of the magnetization is given by $|-4\pi M| = 0.686H^*$. Their ratio is 1.93. Experimentally the initial magnetization peak occurs at a higher field than the larger peak. For the Supercon rotor sample, the initial magnetization peak occurred at 1830 Oe and the large peak occurred at 763 Oe. These field values differ by a factor of 2.39 compared to the theoretical factor of 1.93. Note that the large peak is not centered about zero field. The ratio of the magnetizations for the Supercon wire was 1.34 compared to the predicted value of 1.93. The Bean model does not predict either peak. The alpha model predicts that the absolute magnetization at a given field is larger when that field was attained by decreasing the field to H. For the Supercon rotor wire and a field of 6 kOe, the ratio of $|-4\pi M_+/-4\pi M_-|=1.17$. The Bean model predicts that there would be no difference between $|-4\pi M_+|$ and $|-4\pi M_-|$ at H for large field sweeps. The alpha model predicts that the field change to totally reverse the direction of the circulating supercurrent is bias field dependent. Figure 13 shows a reduced plot of the field change ΔH vs the bias field H_m for Supercon 217E-19 and Supercon 241E-13. In addition the theoretical prediction of Equation 6 of Table 8 for the alpha model has been plotted for the appropriate parameters obtained from the universal J_c-H curve of Figure 10 in Figure 13. As expected ΔH for the alpha model falls off much more rapidly with H_m than the experimental curves. The Kim model predicts that ΔH falls more rapidly for larger R. The data shows this trend. The Bean model would predict that ΔH is independent of bias. Plots of ΔH for both rotor wires fall below the data Supercon 217E-19 with the Supercon wire lying lowest. The trend is the larger the wire diameter, the faster ΔH falls off with bias field. A plot of ΔH vs R for various bias fields is given in Figure 30. It is very important to know ΔH because in the case of ripple fields it divides the loss regions of full and partial penetration. Ripple loss will be discussed more completely later in this report.

The saturation field H_{SAT} is the field which will just produce the remanent maximum moment. Figure 12 shows a typical plot of remanent vs. H. H_{SAT} is also equal to ΔH of B_r (max). H_{SAT} for various wires is listed in Table 13 and a plot of H_{SAT} vs R is given in Figure 31. Figure 31 is very useful for estimating H_{SAT}. The alpha model predicts that $H_{SAT} \propto R^{1/2}$. For the generalized Irie-Yamafuji model one can relate the field dependence of the loss to the functional dependence of H_{SAT} on R. For $Q \propto H^{3.5}$, $H_{SAT} \propto R^{2/3}$ corresponding to $J_c = \alpha/H^{.5}$. The equation of the line shown in Figure 31 is Equation (41) where H is in Oe.

$$H_{SAT} = 427\ R^{2/3} \tag{41}$$

and R is in microns. The experimental hysteretic loss curves for several wires is shown in Figure 32. Note that at low fields the smaller the wire the larger the loss and at high fields the smaller the wire the smaller the loss. For any two wires there is a cross-over point but the field value at which cross-over occurs is not theoretically predictable so a plot such as Figure 32 is required to select the lower loss wire in the intermediate region. The loss for a half cycle sweep to 20kOe for various filament diameters from the experimental data is

$$Q = 1.72R^{3/4} \times 10^6 \qquad 5 \leq R \leq 120\mu \tag{42}$$

where Q is in ergs/cm^3-cycle and R is in microns. For the partial penetration case the loss is given by

$$Q = (4.3 \times 10^4)\ /\ R^{.9} \qquad 5 \leq R \leq 120\mu \tag{43}$$

for an 800 Oe field sweep. The size dependence of the loss is slightly different from the predicted Bean model dependence of R and 1/R. The theoretical dependence for the Bean and alpha model are the same for the limiting cases of $H_m << H^*$ and $H_m >> H^*$. Consider the full penetration situation. Reducing the radius of the filament does not reduce the loss as much as theoretically predicted, however it does reduce the loss significantly. Figures 33 and 34 depict the size dependence of the loss.

The theoretical loss is compared to the measured loss for Niomax S 20/40 with a filament diameter of 188μ in Figure 35 and for Supercon 241E-13 with a filament diameter of 10μ in Figure 36. The dashed line is the Bean model and the solid line is the alpha model. They were obtained from parameters calculated from short sample critical current curves. The Bean model overestimates the partial penetration loss at low fields and as previously stated incorporation of a surface field H_s and adjustment of the parameter could yield a better fit. The alpha model underestimates the loss at low field and one can compensate by adding a surface field instead of subtracting as in the Bean model. For zero surface field there is a region of the Q vs H plot that cannot be reached by varying J_c or alpha because of the second term in the round filament loss expressions. Figure 37 shows the limiting line for the alpha model. It has a slope of two as does the corresponding line for the Bean model. Figure 38 shows the loss for the Supercon 241E-13 and Niomax S 20/40 compared to the exact calculation of Fournet and Malfert (their equation Eq.(62)) for 0 and 500 Oe surface fields. The parameters of the theoretical curve were taken from Equation (11). The Fournet and Malfert result applies only to the full cycle partial penetration region. The zero surface field case corresponds to a field dependent loss of the form $Q \alpha H^{3.2}$. Various observed field dependences are listed in Table 13. So the F-M field dependence is closest to the measured dependence but the magnitude of the loss is still off. The point of Figures 35, 36, and 38 is that it is not possible to predict quantitatively the hysteretic loss from J_c vs H data. And even in curve fitting theories it is standard practive to make log-log plots which can give the appearance of a good fit while missing portions of the data by factors of two to ten.

An alternative approach to critical state models for predicting loss is to construct a set of universal loss curves based on a few representative samples. This method assumes that the J_c vs H curves for various filament diameters and for standard alloys are in reasonable agreement. Figure 10 shows that this is a valid assumption. In fact, if a good universal definition of J_c were agreed upon and applied, the scatter might be improved*. As will be seen, this empirical expression shows significant improvement in quantitative agreement between measurements and predictions. The half cycle universal loss curves generated here are only for Nb-Ti superconductors in a perpendicular applied field. Of course other curves would have to be generated for different materials and configurations. This method eliminates the need to consider the demagnetizing factor. The approach is as follows, a number of experimental hysteretic loss curves were normalized to H_{SAT} and $Q(H_{SAT})$. The result is a fairly well defined universal loss curve as shown in Figure 40. H_{SAT} was chosen as the normalizing parameter because it was easily determined experimentally, and also because it corresponds to the same relative point on each loss curve. For modeling purposes the equations for the two linear portions are

$$Q = 1.4\ Q_{SAT} \left(\frac{H}{H_{SAT}}\right)^{3.15} \qquad \frac{H}{H_{SAT}} < 1.25 \tag{44}$$

$$Q = 2.2\ Q_{SAT} \left(\frac{H}{H_{SAT}}\right)^{2/3} \qquad \frac{H}{H_{SAT}} > 1.25 \tag{45}$$

where Q_{SAT} is in ergs/cm^3-cycle. This procedure overestimates the loss in the intermediate region. If greater accuracy is desired the digital listing of Table 14 may be used.

---

*The inability of the superconducting community to agree upon a good quantitative definition of J_c is nowhere better illustrated than in the minutes of the committee on Cryoelectrical Engineering of the IEEE, August 10, 1973 where critical current is defined as the "DC current which just causes a detectable voltage to appear in a superconductor."

For predictive purposes, it is necessary to denormalize the universal loss curve using only geometrical parameters of the wire whose loss is to be estimated. This is done in Figures 39 and 31. Fortunately, the plot of $Q(H_{SAT})$ vs H_{SAT} is a simple power law

$$Q_{SAT} = Q(H_{SAT}) = 0.02\ H_{SAT}^{2} \tag{46}$$

which happens to agree with the theoretical value of the Bean and alpha models as discussed with Figure 37. Figure 31 can be used to obtain the value of H_{SAT} for any filament radius R. The equation relating H_{SAT} to R for modeling purposes is given by Equation (41). Combining the analytical expressions in Equations (41), (44), (45) and (46) yields

$$Q = (2.6 \times 10^{-5})\frac{H^{3.15}}{R^{.77}} \qquad \frac{H}{H_{SAT}} < 1.25 \tag{47}$$

$$Q = 141\ R^{8/9}\ \ H^{2/3} \qquad \frac{H}{H_{SAT}} > 1.25 \tag{48}$$

These universal loss equations can be used to predict hysteretic loss. This will be demonstrated for the two rotor wire samples which were not used to construct the composite curves. H_{SAT} for the MCA sample was experimentally determined to be 2300 Oe and predicted by Equation (41) to be 1981 Oe. For the Supercon sample H_{SAT} was respectively 4400 Oe and 3438 Oe. Then Q_{SAT} for the MCA wire is 7.87×10^{4} ergs/cm^{3}-cycle, and for the Norton wire it is 2.36×10^{5} ergs/cm^{3}-cycle. The calculated values of Q_{SAT} and H_{SAT} were used to denormalize the universal loss curve, Figure 40. The resulting calculated loss curve is compared to the MCA and the Supercon wires in Figures 41 and 42 which show substantially better agreement between predicted loss and measured loss than can be obtained from critical state model theory. An even better fit could be obtained by using the Q/Q_s vs H/H_s curve as a tabulated function (Table 14) for computer loss model calculations.

Note that the H and R dependence of Q in Equations (47) and (48) is different than that of the Bean or alpha model. The field dependence of Q is nearly equal to that predicted by Equation (62) of Fournet and Malfert ($Q \propto H^{3.2}$) with no surface field. Unfortunately full cycle universal curves were not obtained because of equipment and time constraints. As an approximation the half cycle loss may be multiplied by three to get the corresponding full cycle loss. The full cycle loss is more than twice the half cycle loss because the field sweep doubles and the low field magnetization increases.

The effect of bias field upon hysteretic loss produced by a superimposed varying field has been studied extensively. This situation simulates the type of loss encountered during unbalanced phase loading of a superconducting generator. A typical set of minor hysteresis loops are shown in Figure 7 for sample 217E-19. The amplitude of the loop is 500 Oe. A similar set of loops was also generated for sample 241E-13 with the same ripple amplitude. For each loop the bias field was set, the sample was warmed above T_c, and then cooled in field. The sweep rate for the loops was 500 Oe/min. Slower sweeps showed no changes in the loops.

The loop areas have been converted to losses and these are shown in Figure 43. Note the peak in the loss for the smaller wire at low field and the very broad maximum at high field. Generally, the maximum hysteretic loss for a given field sweep occurs for the case of the amplitude of the field change (in this case H_{RIP}) equal approximately to H* or for the bias field case the analogous field $\Delta H/2$. Also the loss for amplitudes of ac field equal to H* is given approximately by

$$Q(H^*) = \frac{H^{*2}}{4\pi} f(h=1) \approx \frac{H^{*2}}{4\pi} \tag{49}$$

The function f(h) is nearly one for all models for h = 1. For the case of H* = 500 Oe the loss predicted by Equation (49) is $Q = 1.98 \times 10^3$ $\mu J/cm^3$-cycle. This value agrees very well with the maximum ripple loss. Equation (49) provides a rule of thumb for estimating ripple loss in the worst possible case. The field position of the peak should be obtainable from ΔH vs H_m in Figure 13. The value of H_m for which ΔH = 1000 Oe (maximum loss) is respectively 1900 Oe for 241E-13 and 18400 Oe for 217E-19. These values correspond quite well to the bias field at which maximum loss occurs in Figure 43. Note that for the small wire the peak is sharp but for the large wire it is quite broad. By normalizing to the field at which Q_{MAX} occurs a universal curve similar to the theoretical curve Q vs R or α for fixed sweep can be obtained. This is shown in Figure 44. Then for a given ripple field and Figure 44 and Figure 30 the ripple loss for any two wires can be compared. That is, the field at which maximum loss occurs can be obtained from Figure 30 and this value can be used to denormalize Figure 44.

Besides predicting loss critical state models relate material parameters to magnetization. The temperature dependence of J_c for NbTi, NbCN, and Nb_3Sn have been obtained from magnetization data through the alpha model and the results are shown in Figure 45. The highest T_c material obviously has higher J_c's at elevated temperatures. This is the motivation for developing filamentary Nb_3Sn.

All of the results of this report apply to low frequency ac loss in which hysteretic loss is the dominant factor. However, coupling losses for multifilamentary wires may be included by incorporating an effective change in size. This can be seen from Figure 46 which simulates the full cycle high sweep rate loops of the Rutherford report. Note that the larger radius wire has a higher low field peak and it occurs at a higher field value. This same behavior is produced by sweep rate in the Rutherford report. This same situation occurs in experimental partial penetration loops. These loops change shape as though the wire diameter was varying as the frequency varies.

While one could obtain an expression for R(f) and use it to denormalize a theoretical expression for Q for qualitative modeling purposes, the procedure of reduced curves should be applied. There are several papers on coupling loss that will be useful for constructing an experimental expression for R(f) or Q(f) where Q_o is obtained from the universal curves in this report.

For two samples, one a NbCN sample and the other NbTi, the low field peaks had structure which may be referred to as flux floods. These flux floods may be attributed to a position dependent pinning potential (ie. surface pinning). However many other surface-like features cannot be separated from bulk effects.

SECTION VII

CONCLUSIONS

The various critical state models including the alpha model cannot accurately predict the hysteretic loss from the J_c vs H curve. However for modeling purposes they do give approximate functional dependences of various quantities of interest. The qualitative features of the magnetization curves predicted by the alpha model are very numerous and accurately reflect the experimental curves. The incorporation of the field dependent surface pinning parameter (α_2) into the alpha model would provide important information on the concept of surface pinning.

The ultimate goal from an engineering point of view is the ability to accurately predict surperconducting ac loss. It appears that the best way to achieve this goal is to create a complete set of universal curves describing ac loss for each type of superconductor. A set of such curves for the hysteretic loss were obtained in this report. The ability to compare ripple loss for two different wire sizes by universal curves was demonstrated. The ripple loss for the worst possible case may be estimated by $(H^2_{RIP})/4\pi$ (ergs/cm^3-cycle).

While there are hundreds of papers on superconducting loss more work is required for adequate quantitative prediction capability.

REFERENCES

AIR FORCE TECHNICAL REPORTS

1. Z.J.J. Stekly, E.J. Lucas, R.J. Thome and T.A. de Winter, Inductive Energy Storage System Study, AFAPL-TR-69-101.
2. E.J. Lucas, W.F.B. Punchard and R.J. Thome, Development of Pulsed High Energy Inductive Energy Storage System, AFAPL-TR-72-38.
3. J. Teno, O.K. Sonju and L.M. Lontai, et.al., Development of a Pulsed High Energy Inductive Energy Storage System, AFAPL-TR-73-49.
4. Z.J.J. Stekly and R.J. Thome, Lightweight Superconducting MHD Magnets, AFAPL-72-32.
5. Z.J.J. Stekly and R.J. Thome, Superconducting Magnetohydrodynamic Magnet Comprehensive Testing, AFAPL-TR-73-44.
6. David Atherton, Effects of Design Parameters for Lightweight Superconducting MHD Magnets, AFAPL-TR-70-68
7. D.L. Atherton and D. Gluck, Mechanical Structure, Magnet Geometry and Fabrication Techniques for Lightweight Superconducting MHD Magnets, AFAPL-TR-70-78.
8. D.L. Atherton, D. Gluck, J.M. Canty and E.S. Kordyban, Dewar Design and Vibrational Characteristics for Lightweight Superconducting MHD Magnets, AFAPL-TR-70-90.
9. D.L. Atherton, Energization and Protection Considerations for Lightweight Superconducting MHD Magnets, AFAPL-TR-71-19.
10. D. Gluck and D.L. Atherton, Fabrication of a Lightweight Superconducting MHD Magnet, AFAPL-TR-73-63.
11. R.W. Meyerhoff and W.T. Beall Jr., Magnetodynamics of Superconductors, AFML-TR-67-384.
12. C.P. Bean et.al., A Research Investigation of the Factors that Affect the Superconducting Properties of Materials, AFML-TR-65-431.
13. D.A. Haid and W.A. Fietz, Development of Manufacturing Methods for the Production of Superconductive Devices, AFML-TR-69-170.
14. N. Pessall, J.K. Hulm and M.S. Walker, A Study of the Superconducting Behavior of Alloyed Interstitial Compounds with the NaCl Crystal Structure, AFML-TR-67-168.

REFERENCES (CONTINUED)

AIR FORCE TECHNICAL REPORTS (CONTINUED)

15. James Economy, Ruey Yuan Lin, William D. Smith and C.K. Jun, Development of Process for Producing Continuous Fine Diameter Filaments of Superconductors, AFML-TR-72-189.

16. Ruey Y. Lin, William D. Smith, John Coppola and James Economy, Preparation and Properties of Fine Diameter Multifilament Niobium Carbonitride Superconducting Fibers, AFML-TR-74-113.

NAVY REPORTS

17. M. Superczynski, Superconducting Magnet Development, NSRDC Rept. 27-581.

18. T.J. Doyle and M.J. Cannell, Development of the Shaped Field Superconductive Motor, Report 4178.

19. H.O. Stevens, Acyclic Superconductive Generator Design, NSRDC Rept. 27-579.

20. S.T.W. Liang and L.F. Martin, Superconducting Machinery for Ship Propulsion Systems, NSRDC Rept. 3787.

COLLECTED PROPERTIES OF SUPERCONDUCTORS

Handbook of Electronic Materials
Electronis Properties Information Center
Hughes Aircraft Company
Culver City, California
Sponsored by AFML

21. D.L. Grigsby, DATA SHEET DS-152 (1966), Niobium-Zirconium

22. D.L. Grigsby, DS-154 (1967), Vanadium Silicide

23. D.L. Grigsby, DS-159 Part I, Niobium Tin

24. D.L. Grigsby, DS-160 Part II, Niobium Tin

25. M. Neuberger, D.L. Grigsby, and W. H. Vlazie, Jr., Niobium Alloys and Compounds, Plenum Press (1972).

26. "Superconductive Materials and Some of Their Properties," Progress in Cryogenics 4, 161 (1964).

REFERENCES (CONTINUED)

COLLECTED PROPERTIES OF SUPERCONDUCTORS (CONTINUED)

27. B.W. Roberts, Superconductive Materials and Some of Their Properties, NBS Technical Note 482 (1969).

28. B.W. Roberts, Properties of Selected Superconductive Materials, NBS Technical Note 724 (1972).

29. P.A. Battams, Cryogenics 5, 356 (1972).

29.1 T. Takai, Cryogenics 14, 304 (1974).

COLLECTED PAPERS

30. Superconductivity (Selected Reprints) & Superconductivity Book 2 (Selected Reprints) Dept. BN, AIP 335 East 45 Street, N.Y., N.Y. 10017.

CONFERENCES

31. 1963 International Conference on the Science of Superconductivity, Rev. of Mod. Physics, 36 (1964).

32. 1966 National Superconductivity Information Meeting BNL 50038 (C-49) 1966 (Abstracts Only).

33. 1967 Applied Superconductivity Conference, Journal of Applied Physics 39, 1968.

34. Proceedings of the 1968 Summer Study on Superconducting Devices and Accelerators, Parts I, II & III, BNL 50155(C-55).

35. 1968 Applied Superconductivity Conference, Journal of Applied Physics, 40 (1969).

36. Fluctuations in Superconductors, Edited by William S. Goree and Frank Chilton, ONR Contract # N00014-67-C-0393 (1968).

37. 1969 Proceedings of the International Conference on the Science of Superconductivity, Edited by Frank Chilton, Physica 55 (1971).

38. Proceedings of the International Conference on Organic Superconductors, J. Polymer Science, Part C (1970).

REFERENCES (CONTINUED)

CONFERENCES (CONTINUED)

39. 1970 Applied Superconductivity Conference, Journal of Applied Physics 42 (1971).

40. Superconductivity in d- and f- Band Metals, AIP Conference Proceedings No. 4, Edited by D.H. Douglass (1972).

41. 1972 Applied Superconductivity Conference, IEEE Pub. No. 72CH0682-5-TABSC.

42. 1974 Applied Superconductivity Conference, IEEE Transactions on Magnetics, March (1975).

CRITICAL STATE MODELS

43. C.P. Bean, Phys, Rev. Letters 8, 250 (1962).

44. Charles P. Bean, Rev. of Modern Physics, 36, 31 (1964).

45. Charles P. Bean, J. Appl. Physics, 41, 2482 (1970).

46. H. London, Phys. Letters, 6, 162 (1963).

47. J.H.P. Watson, J. Appl. Physics, 39, 3406 (1968).

48. Fujio Irie and Kaoru Yamafuji, J. Phys, Soc. Japan, 23, 255 (1967).

49. V.R. Karasik, N.G. Vasil'eu, and V.G. Ershov, Sov. Phys.-JETP 32,433 (1971).

50. R. Hancox, Proc. IEE, 113 1221 (1966).

51. W.I. Dunn and P. Hlawiczka, J. Phys. D, I, 1469 (1968).

52. P. H. Melville, Advances in Physics, 21, 647 (1972).

53. H. Inhaber, Cryogenics, 13,261 (1973).

54. Melvin C. Ohmer and J.P. Heinrich, Phys. Rev. 44, 1804 (1974).

55. Y.B. Kim, C.F. Hempstead, and A.R. Strnad, Phys. Rev. 129, 528 (1963).

56. Masanori Sugahara, J. Appl. Phys. 41, 3668 (1970).

57. G. Fournet and A. Mailfert, J. de Physique 31, 357 (1970).

REFERENCES (CONTINUED)

HYSTERESIS OR AC LOSS

58. M.N. Wilson, C.R. Walters, J.D. Lewin, P.F. Smith and A.H. Spurway, Journal of Physics D, 3, 1517 (1970).

59. W.T. Beall, Jr. and R.W. Meyerhoff, J. Appl. Phys. 40, 2052 (1969).

60. Power Transmission Project Technical Note PTP25, Brookhaven National Laboratory (1974).

61. C. Malseed and W. A. Rachinger, Scripta Metallurgica 2, 121 (1968).

62. Henry F. Taylor, Phys. Rev. 165, 517 (1968).

63. P.H. Melville, J. Phys. D, 5, 613 (1972).

64. A.M. Campbell, J. Phys. C, 2, 1492 (1969).

65. R.M. Easson and P. Hlawiczka, J. Phys. D, I, 1477 (1968).

66. L.N.J. De Jong and B.S. Blaisse, Phys, Letters, 9, 309 (1964).

67. P.F. Dahl, G.H. Morgan and W.B. Sampson, J. Appl. Physics, 40, 2083 (1969).

68. M.J. Chant, M.R. Halse and H.O. Lorch, Proc. IEE, 117, 1441 (1970).

69. P.H. Melville, J. Phys. C, 5, 147 (1972).

70. Donald G. Schwertzer and M. Garber, Phys. Rev. 160, 348 (1967).

71. Ko Yasukochi, Takeshi Ogasawara, Nobumitsu Usui and Shintaro Ushio, 19, 1649 (1964).

72. M.A.R. Le Blanc, B.C. Belanger, and R.M. Fielding, 14, 704 (1965).

73. Ko Yasukochi, Takeshi Ogasawara, Nobumitsu Usui and Hisayasu Kobayaski, J. Phys. Soc. of Japan, 21, 89 (1966).

74. M.A.R. Le Blanc, Phys. Rev. Letters, 11, 149 (1963).

75. M.A.R. Le Blanc, Phys. Letters 6, 140 (1963).

76. Ko Yasukochi, Takeshi Ogasahara and Nobumitsu Usui, J. Phys. Soc. Japan, 19, 137 (1964).

77. D. Ward and J. Sutton, J. Phys. C, 4, 1837 (1971).

78. Mananori Sugahara, Japan J. Appl. Phys. 9,625 (1970).

REFERENCES (CONTINUED)

HYSTERESIS OR AC LOSS (CONTINUED)

79. W.T. Norris, J. Phys. D, 3, 489 (1970).

80. Donald G. Schweitzer, M. Garber and B. Bertman, Phys. Rev. 159, 296 (1967).

81. J. Sutton and D.A. Ward, J. Phys. D, 5, 628 (1972).

82. A.D. McInturff and Arther Paskin, J. Appl. Phys. 40, 2431 (1969).

83. M. Tinkham, ARPA Materials Research Council Summer Conf. 128, (1973).

84. Donald J. Hanrahan, IEEE Trans. MAG-6, 833(1970).

85. R.M. Easson and P. Hlawiczka, Brit. J. Appl. Phys. 18, 1237 (1967).

86. William S. Gilbert, Ronald E. Hintz, and Ferd Voelker, Lawrence Radiation Laboratory Report UCRL-18176, April 1968.

87. W. Gilbert, F. Voelker, R. Acker and J. Kougerts, Proceedings 1972 Applied Superconductivity Conf. 486 (1972).

88. M. Tinkham, J. Appl. Phys. 44, 2385 (1973).

89. D.M. Kroeger, C.C. Koch and W.A. Coghlan, J. Appl. Phys. 44, 2391 (1973).

90. H. Brechna and G. Ries, IEEE Trans. Nuclear Science, 639, 18 (1971).

91. R.V. Harrowell, J. Phys. D, 4, 1769 (1971).

92. K.A.M. Arton and P. Hlawiczka, J. Phys. D. 4, 1762 (1971).

93. D.W. Deis, J.R. Gavaler and C.K. Jones, J. of Applied Phys. 42, 5710 (1971).

94. C. Dammann, E. Santamaria, J. Maldyet and L. Donadieu, Phys. Letters 24A, 574 (1967).

95. R. Hancox, Phys. Letters 16, 208 (1965).

96. G. Morgan, J. Appl. Phys. 41, 3673 (1970).

97. G.H. Morgan, P.F. Dahl, W.B. Sampson and R.B. Britton, J. Appl. Phys. 40, 1821 (1969).

98. T.K. Hunt, J. Appl. Phys. 45, 907 (1974).

REFERENCES (CONTINUED)

HYSTERESIS OR AC LOSS (CONTINUED)

99. G.H. Morgan, P.F. Dahl, W.B. Sampson and R.B. Britton, J. Appl. Phys. 40, 1821 (1969).

COUPLING LOSSES

100. Kazuo Shiiki, Katsuzo Aihara, and Mitsuhiro Kudo, Japan J. Appl. Phys. 13, 345 (1974).

101. K. Kwasnitza and I. Horvath, Cryogenics, 14, 71 (1974).

102. M.P. Mathur, M.S. Walker, D.W. Deis and D.K. Jones, J. Appl. Physics, 43, 3831 (1972).

103. P.R. Critchlow, B. Zeitlin and E. Gregory, Applied Physics Letters, 15, 225 (1969).

104. P.R. Critchlow, J. Appl. Physics, 42, 4506 (1971).

105. P.R. Critchlow and B. Zeitlin, J. Appl. Physics 41, 4860 (1970).

106. A.D. McInturff, P.F. Dahl and W.B. Sampson, J. Appl. Phys. 43, 3546 (1972).

107. K. Kwasnitza and I. Horvath, Cryogenics 14, 77 (1974).

MISCELLANEOUS

108. W.C.H. Joiner and Melvin C. Ohmer, Solid State Communications, 8, 1811 (1970).

109. Melvin C. Ohmer and John P. Heinrich, J. Appl. Phys. 44, 1804 (1973).

110. Melvin C. Ohmer and William G.D. Frederick, J. Appl. Phys. 45, 1382 (1974).

SURFACE SUPERCONDUCTIVITY

111. H.A. Ullmaier and W.F. Gauster, J. Applied Phys. 37, 4519 (1966).

112. R.W. Rollins and J. Silcox, Phys. Rev. 155, 404 (1967).

REFERENCES (CONTINUED)

SURFACE SUPERCONDUCTIVITY

113. H.J. Fink, Phys. Rev. 161, 417 (1967).

114. D.S. McLachlan, Physikkondens Materie, 7, 226 (1968).

115. H.J. Fink, Phys. Rev. Letters, 16, 447 (1966).

116. Several other errors exist in Bean's article (Rev. of Modern Physics, 36, 31 (1964). The correct equation for the cylinder is

$$B = \frac{HH_\circ}{H^*} \pm \frac{(H^2 - H_\circ^2)}{2H^*} \pm (H_\circ^3 \mp HH_\circ^2 - H^2H_\circ \mp H^3/3)/4H^{*2} \quad , \quad H_\circ \leq H^*$$

where the top (bottom) signs apply for H increasing (decreasing). In addition the correct ratio of V_3/V_1 is -4.266.

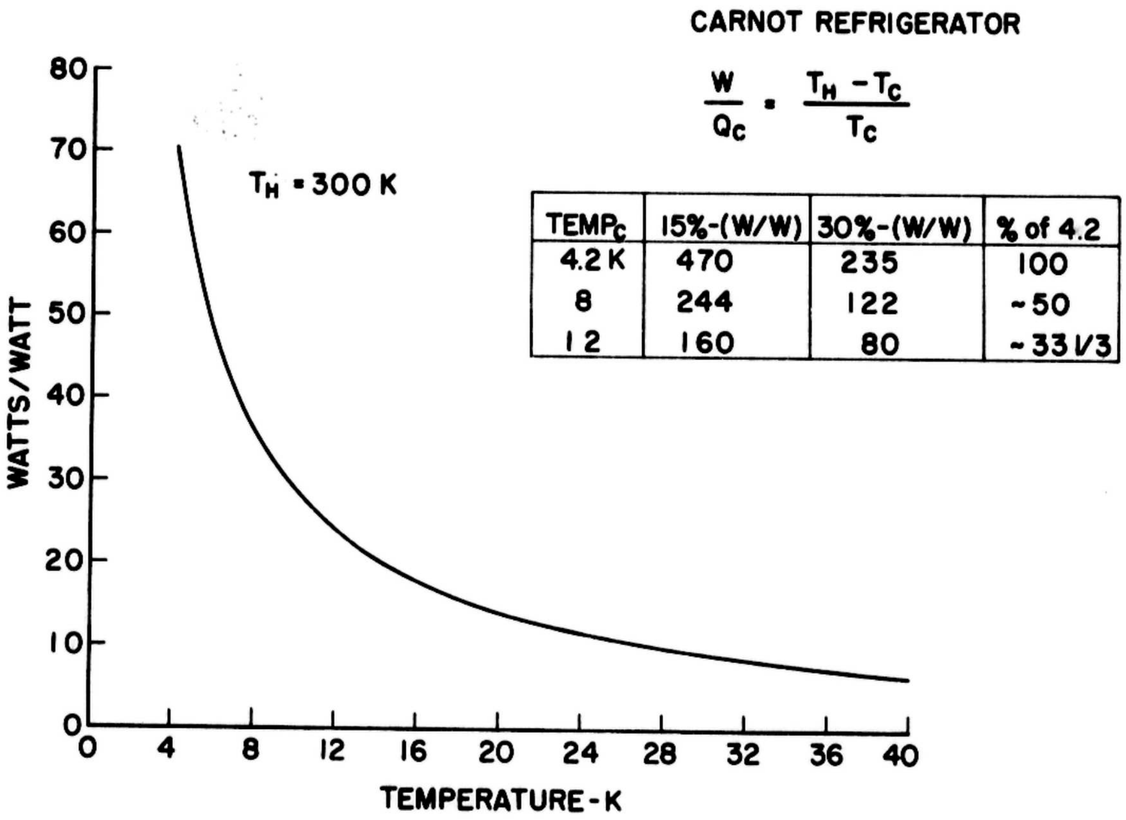

CARNOT REFRIGERATOR

$$\frac{W}{Q_C} = \frac{T_H - T_C}{T_C}$$

$TEMP_C$	15%-(W/W)	30%-(W/W)	% of 4.2
4.2 K	470	235	100
8	244	122	~50
12	160	80	~33 1/3

Figure 1. Efficiency of Carnot Refrigerator vs Refrigerator Temperature Referenced to 300K.

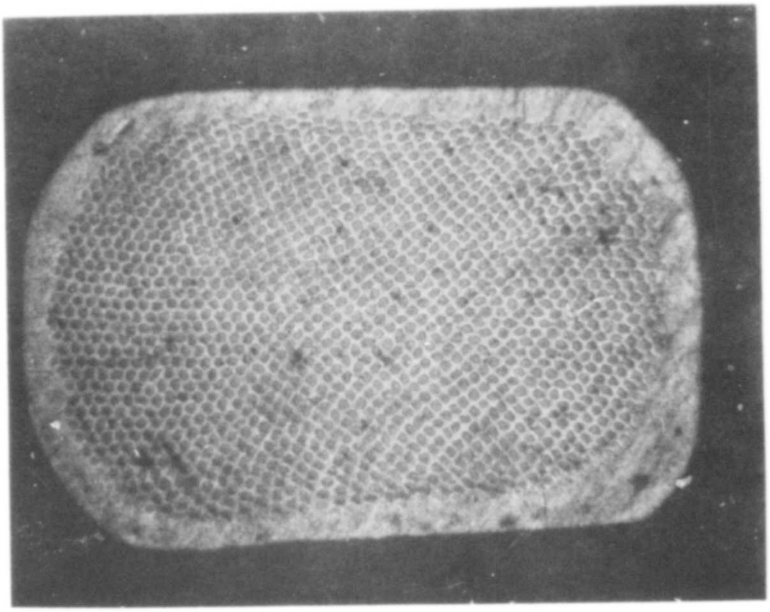

Figure 2. Cross Section of NbTi Copper Stablized Wire Supplied by MCA for 3/4 of the Protctype Rotor Windings Constructed by Westinghouse for AFAPL.

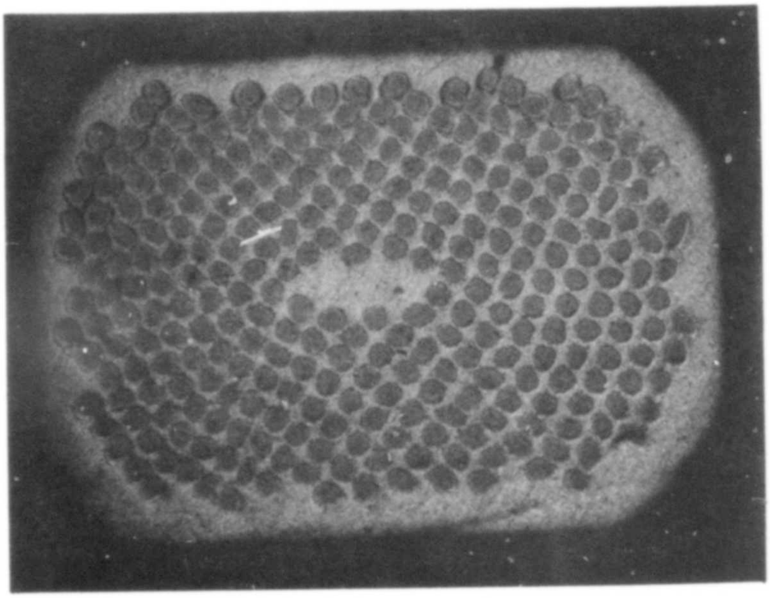

Figure 3. Cross Section of NbTi Wire Supplied by Supercon for 1/4 of the Rotor Winding.

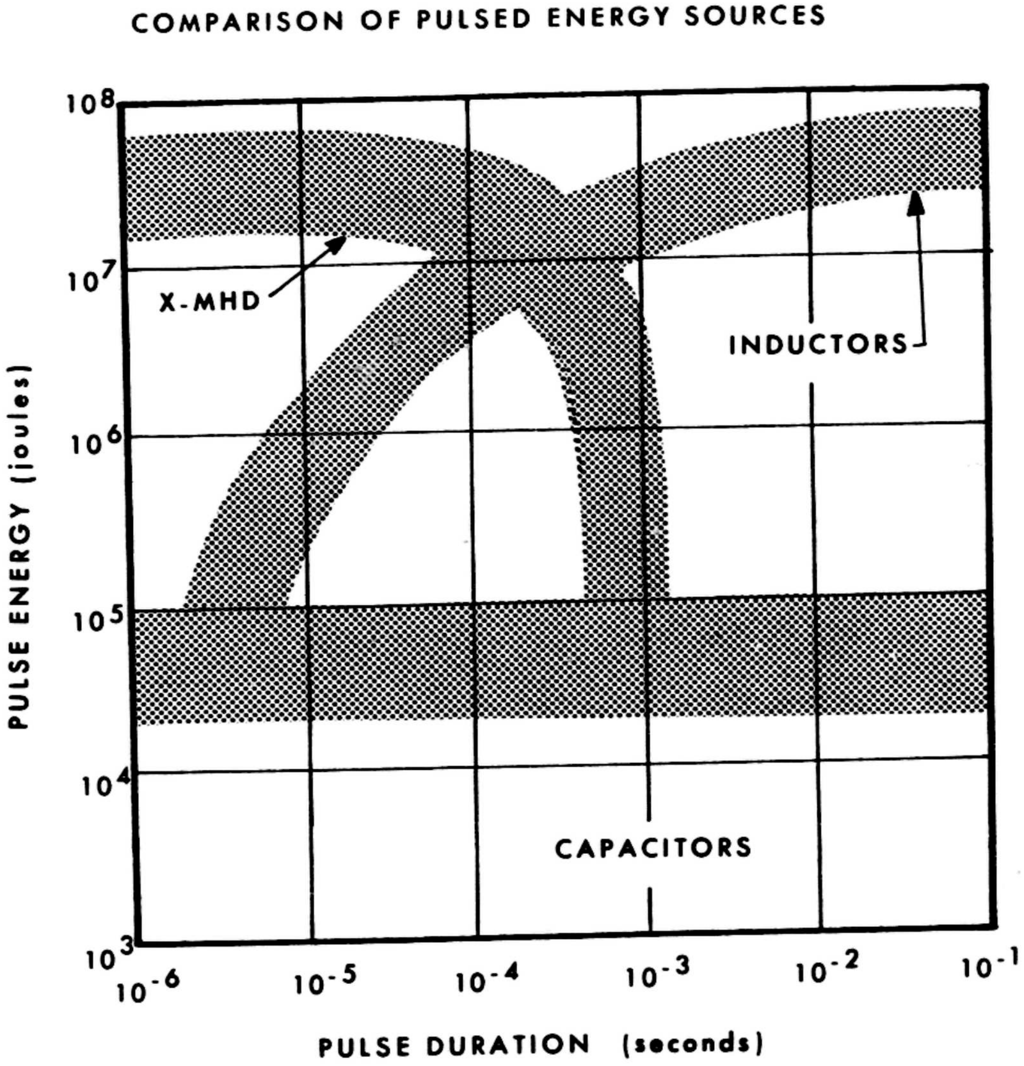

Figure 4. Comparison of Pulsed Energy Sources, MHD, Inductors, Capacitors. Pulse Energy versus Pulse Duration.

DEMAGNETIZING EFFECTS

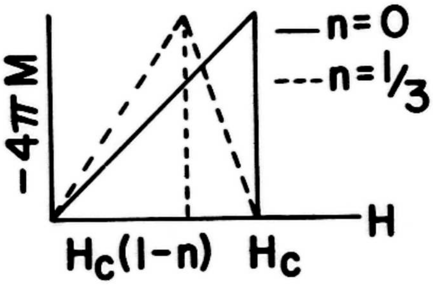

$$-4\pi M_I = \frac{H}{1-n}$$

$$\int^{H_c} 4\pi M dH = \frac{H^2}{8\pi}$$

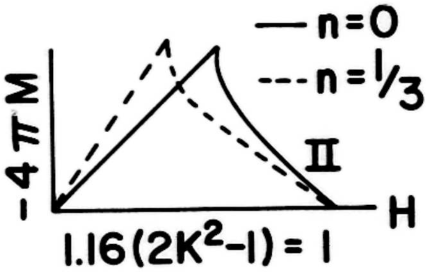

$$-4\pi M_{II} = \frac{H_{c2}-H}{1.16(2K_2^2-1)+n}$$

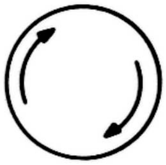

$$\frac{-4\pi M}{H^*} = \frac{1}{3} \; ; \; H^* = \frac{4\pi J_c R}{10}$$

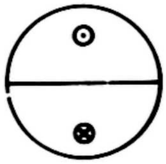

$$\frac{-4\pi M}{H^*} = 1 - \frac{1}{\pi}$$

$$\frac{4\pi M_\perp}{4\pi M_\parallel} = 2.045$$

$$\frac{Q_\parallel}{Q_\perp} = 1.021 \text{ (NbTi} - 7\mu - 18\text{kOe)}$$

Figure 5. Demagnetizing Effects for Ideal Type I and II Superconductors and for an Ideally Irreversible Superconductor for J_c = C.

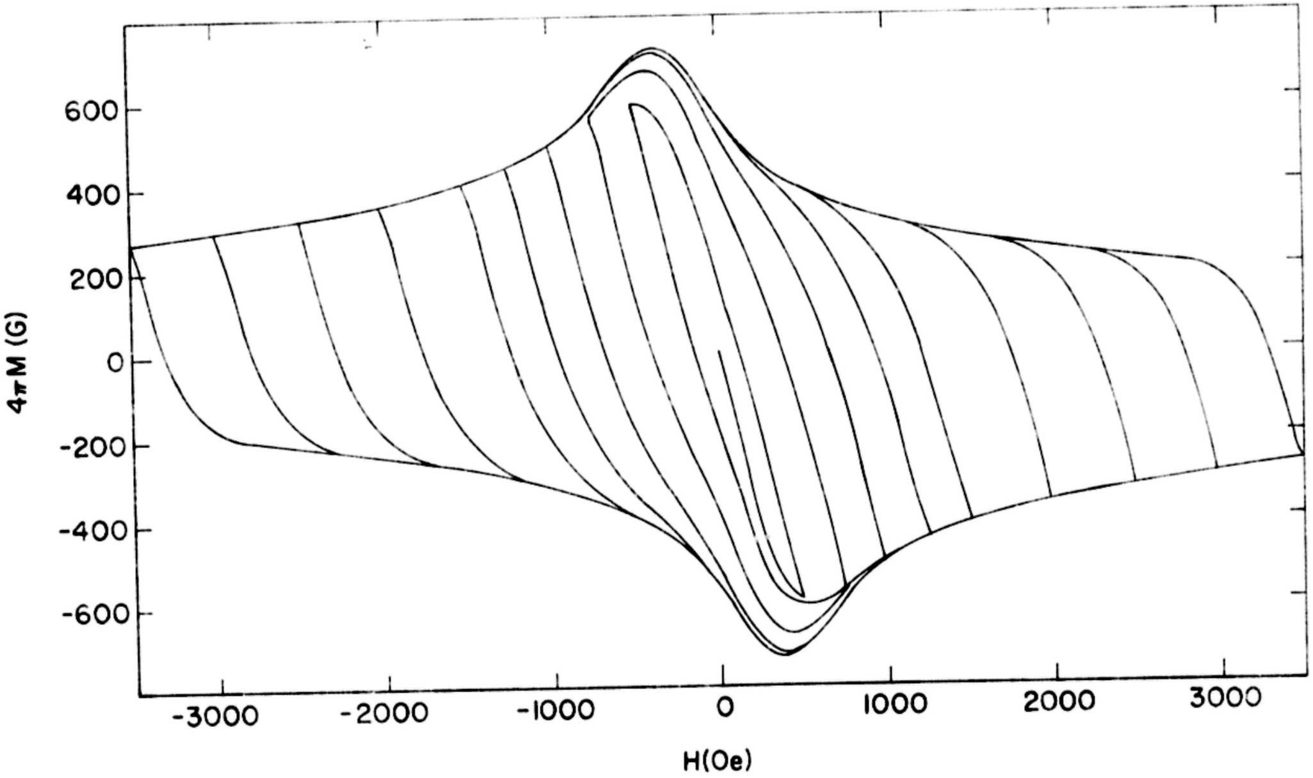

Figure 6. Series of Full Cycle Hysteresis Loops for Filamentary NbTi Wire (Supercon 241E-13) for Partial and Full Penetration. Magnetization vs Magnetic Field.

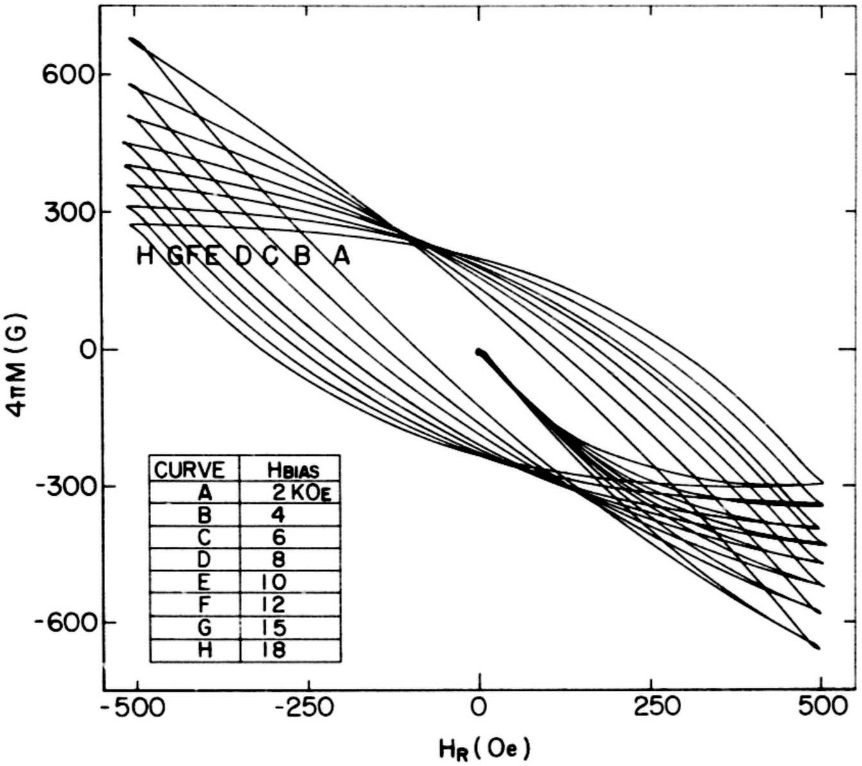

Figure 7. Minor Hysteresis Loop $h_m = 500$ G for Various Bias Fields for NbTi Wire (Supercon 241E-13).

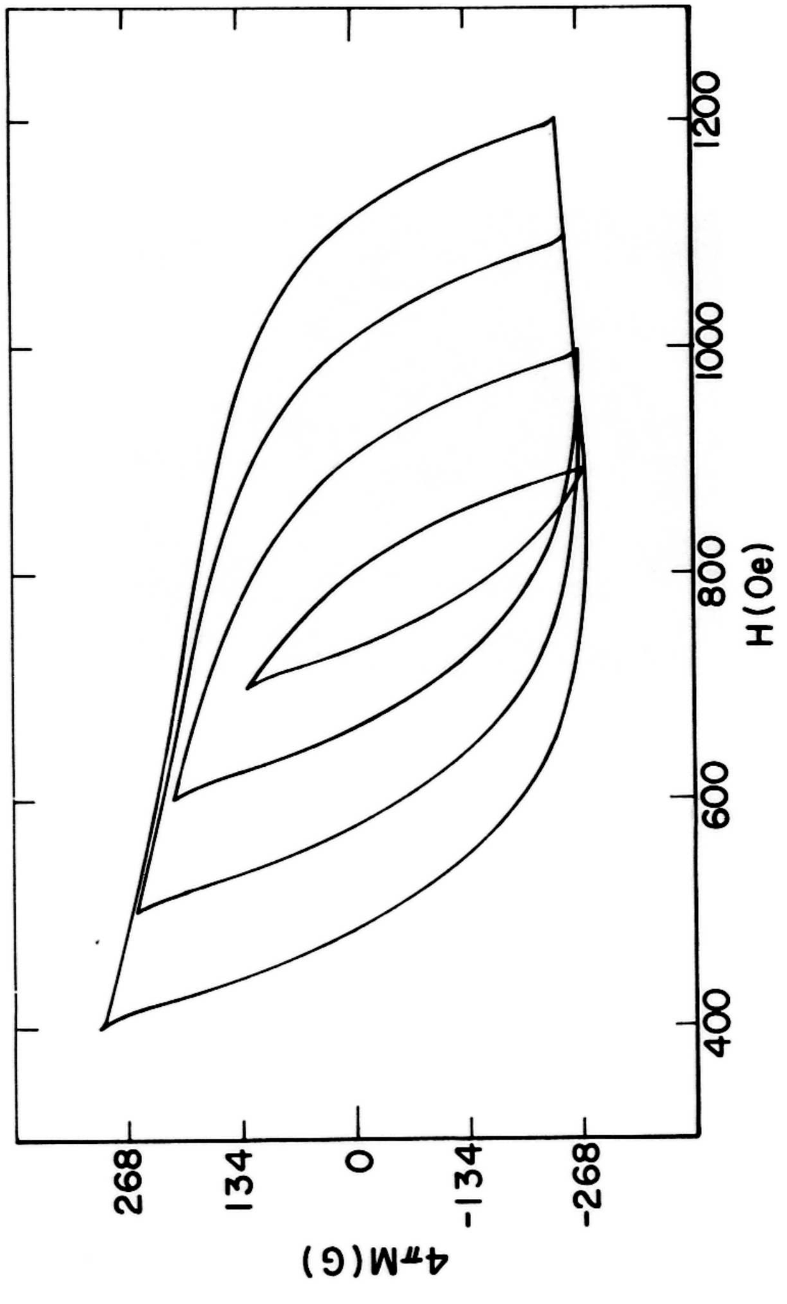

Figure 8. Typical Set of Hysteresis Loops for a Fixed Bias Field for Several Ripple Fields.

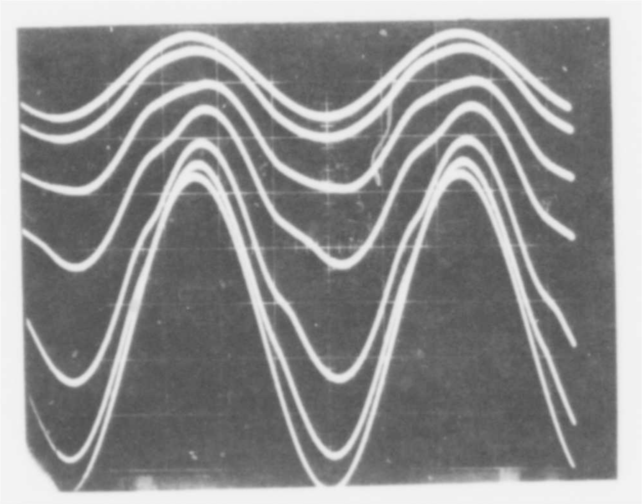

Figure 9. Typical Voltage Waveform Showing the Nonlinear Response of a Superconductor to an Alternating Field.

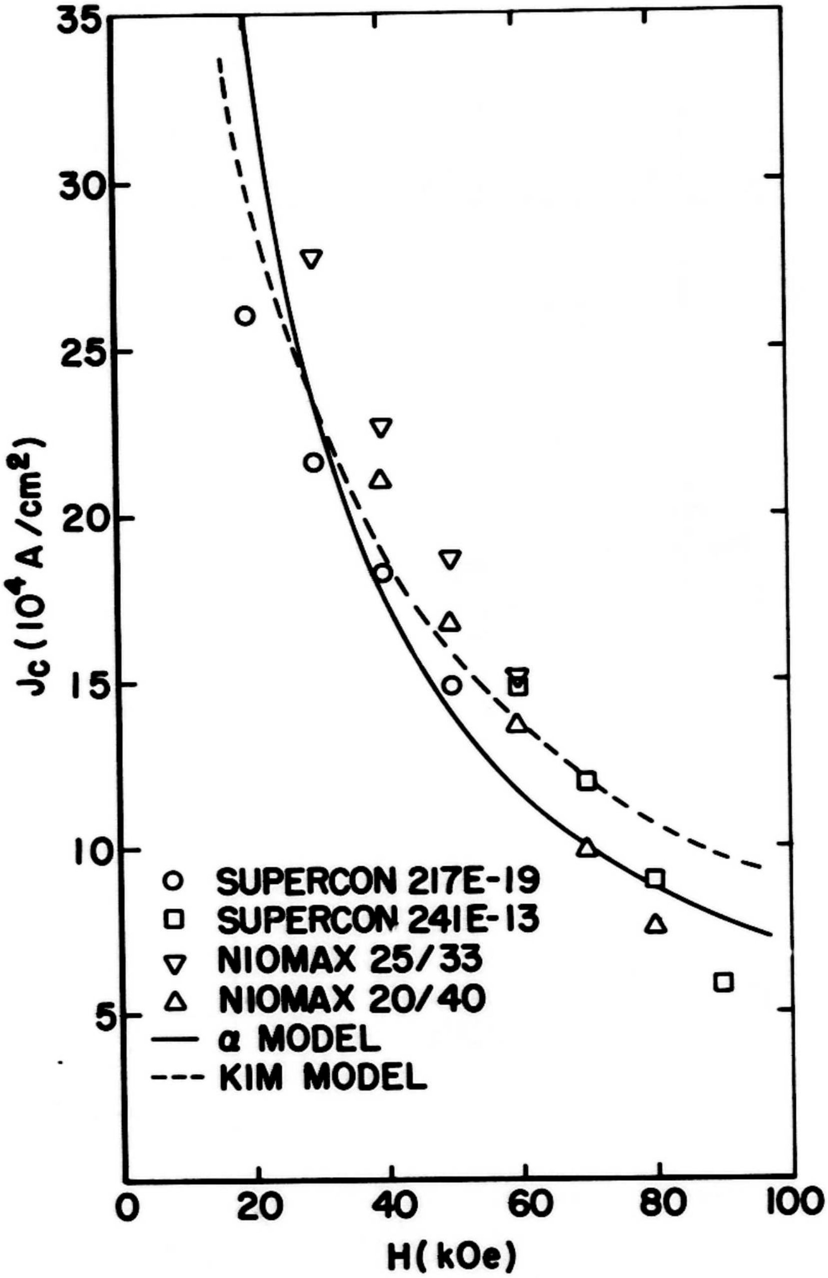

Figure 10. Critical Current Density vs Magnetic Field for Various NbTi Wires. "Universal Critical Current Curve." A LSF of the Alpha Model Yields a Parameter $\alpha = 7.0 \times 10^9$ A-G/cm^2 and a LSF of the Kim Model Yields $J_o = 7.9 \times 10^5$ A/cm^2 and H_o = 12.55kOe.

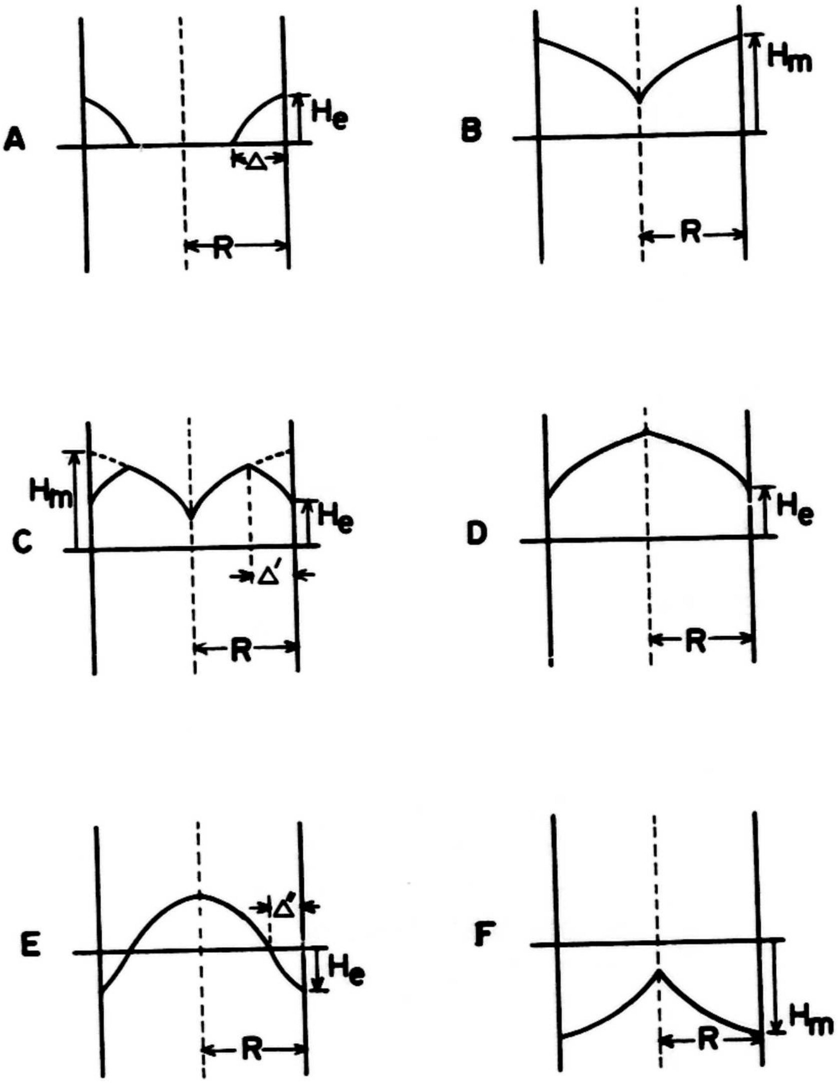

Figure 11. Schematic Diagram of the Field Profiles Across the Cross Section of a Long Cylindrical Sample of Radius R for Large Field Sweeps. a) Field Profile After the Applied Field is Raised From Zero to H_e. b) After the Applied Field Reaches Its Maximum H_m. c) As the Applied Field is Reduced From H_m to $(H^2-2H*^2)^{1/2}$. d) As the Applied Field is Reduced From $(H^2-2H*^2)^{1/2}$ to Zero. e) As the Applied Field is Reduced From 0 to -H*. f) As the Applied Field is Reduced From -H* to $-H_m$.

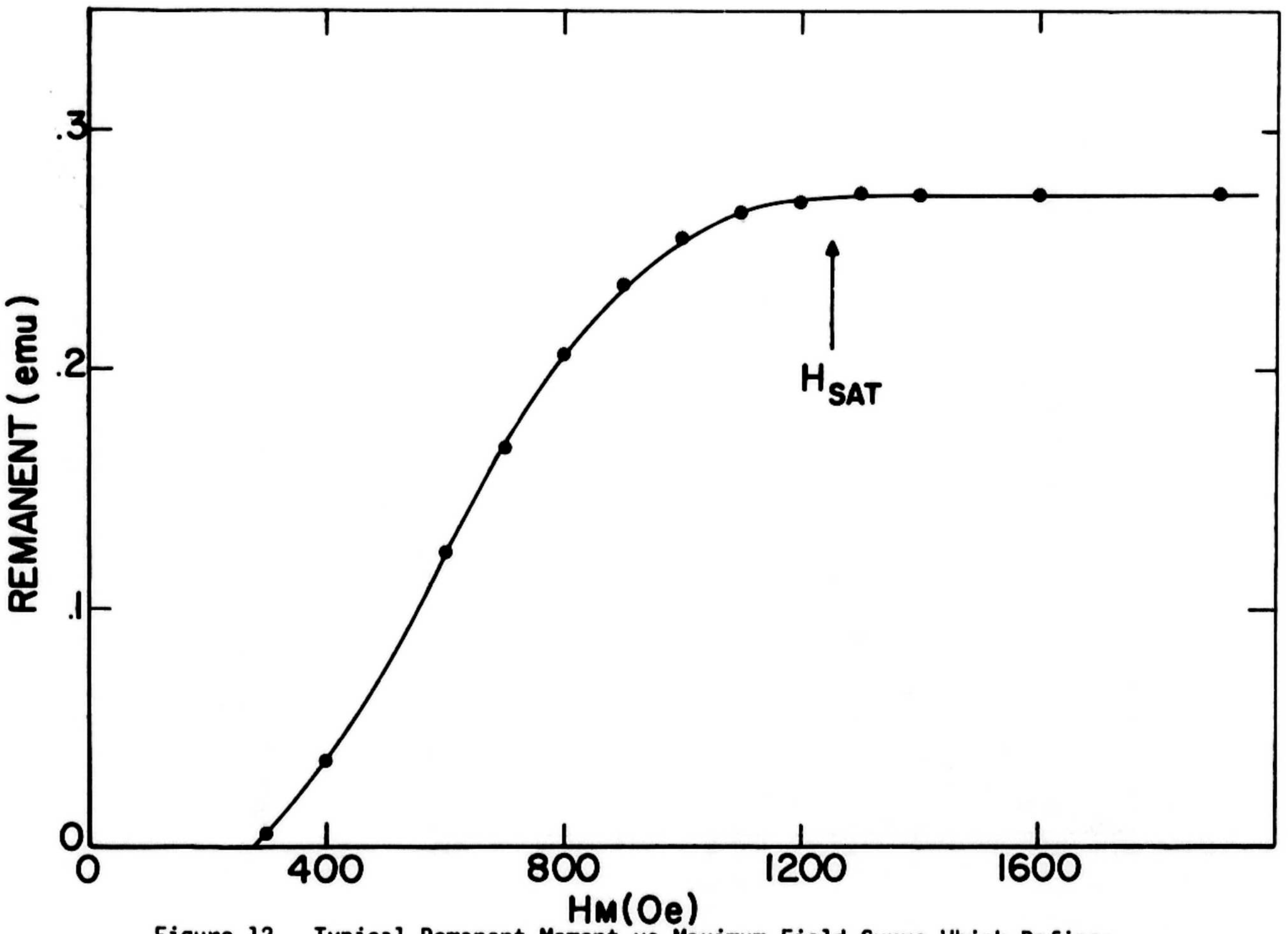

Figure 12. Typical Remanent Moment vs Maximum Field Curve Which Defines H_{SAT}.

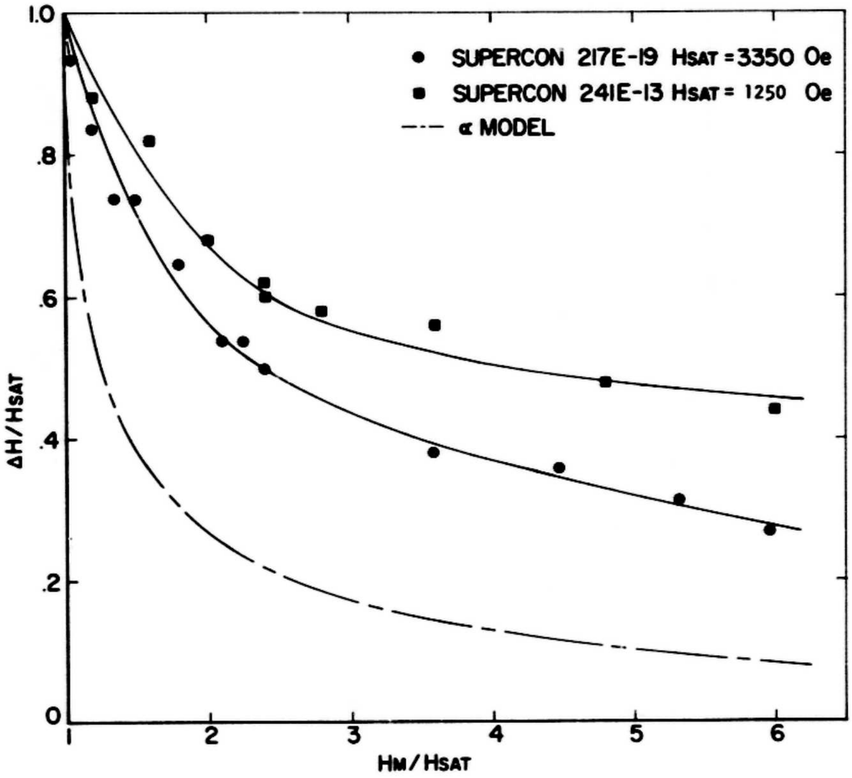

Figure 13. Reduced ΔH vs H_m Curve for Two NbTi Wires with Respectively 5 Micron (241E-13) and 18 Micron (217E-19) Superconducting Filament Diameters.

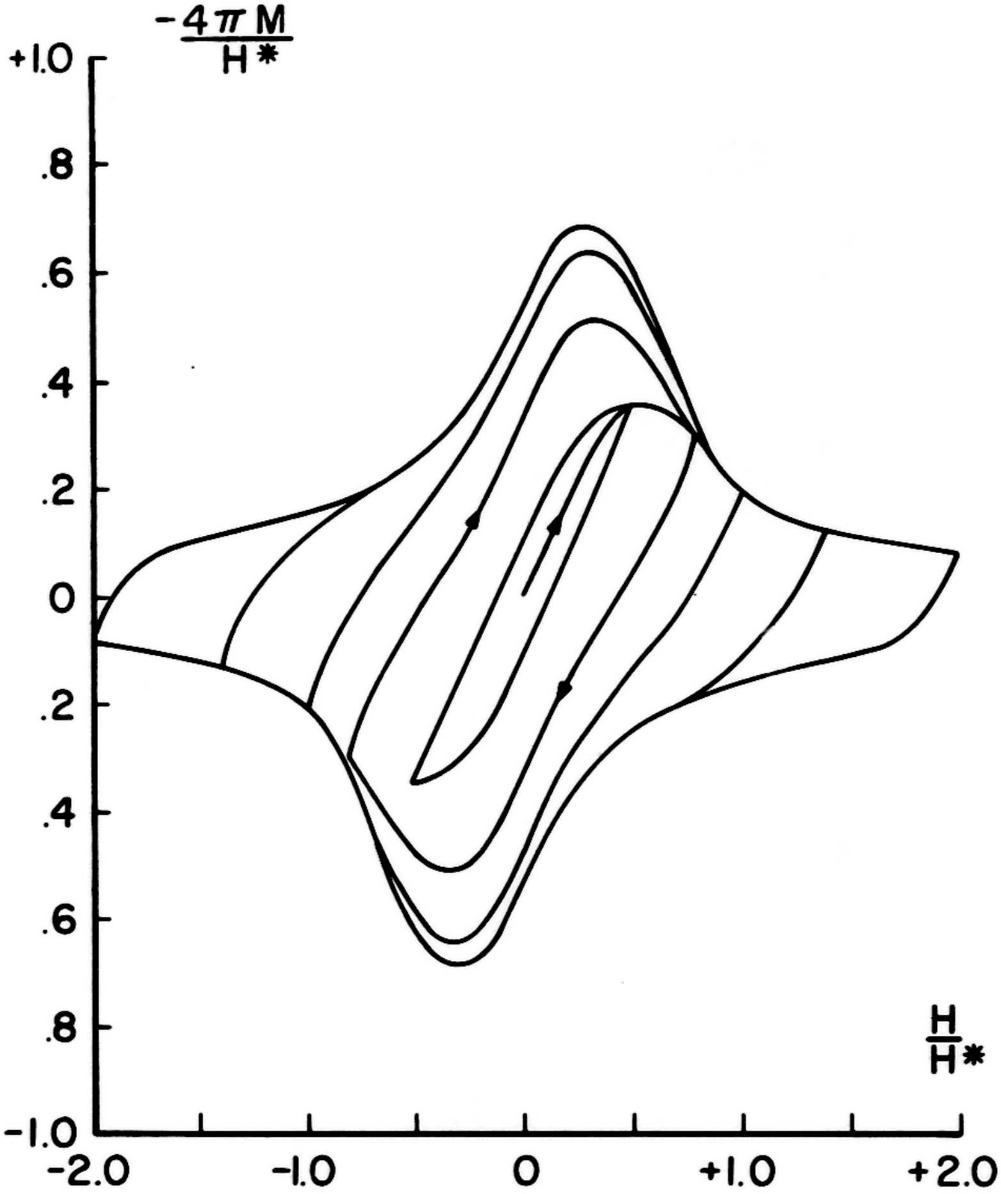

Figure 14. Full Cycle Hysteresis Loops for h_m = .5, .8, 1.4 and 2.0 Respectively-Reduced Magnetization vs Reduced Magnetic Field for the Alpha Model.

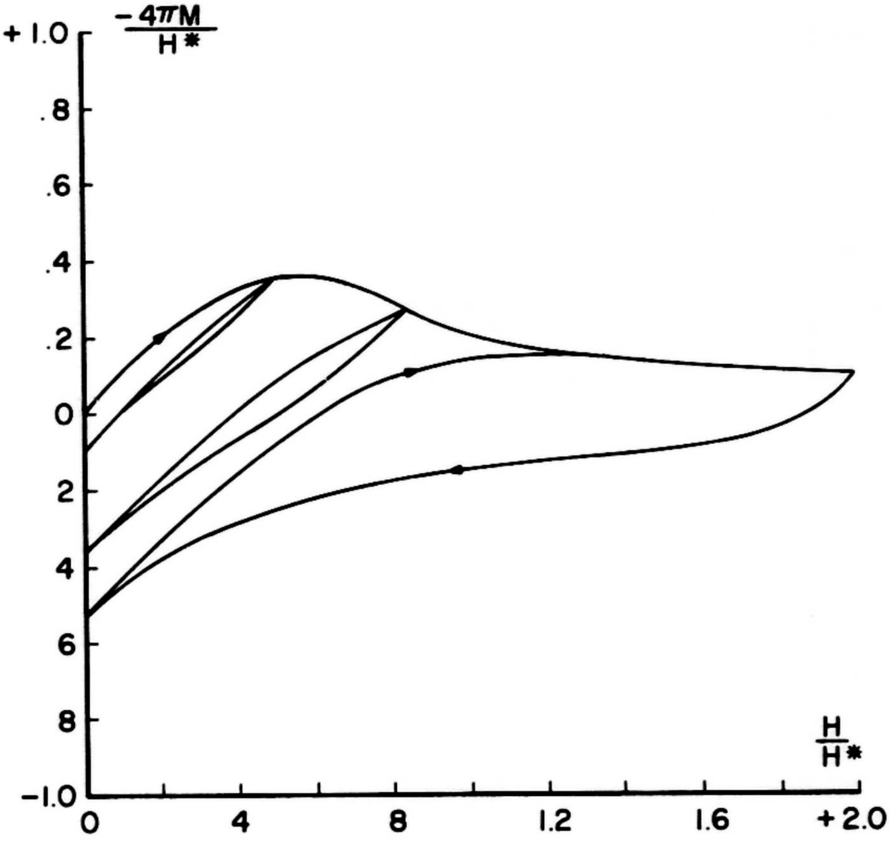

Figure 15. Half Cycle Hysteresis Loops for h_m = .5, .85 and 2 Respectively-Reduced Magnetization vs Reduced Magnetic Field for the Alpha Model.

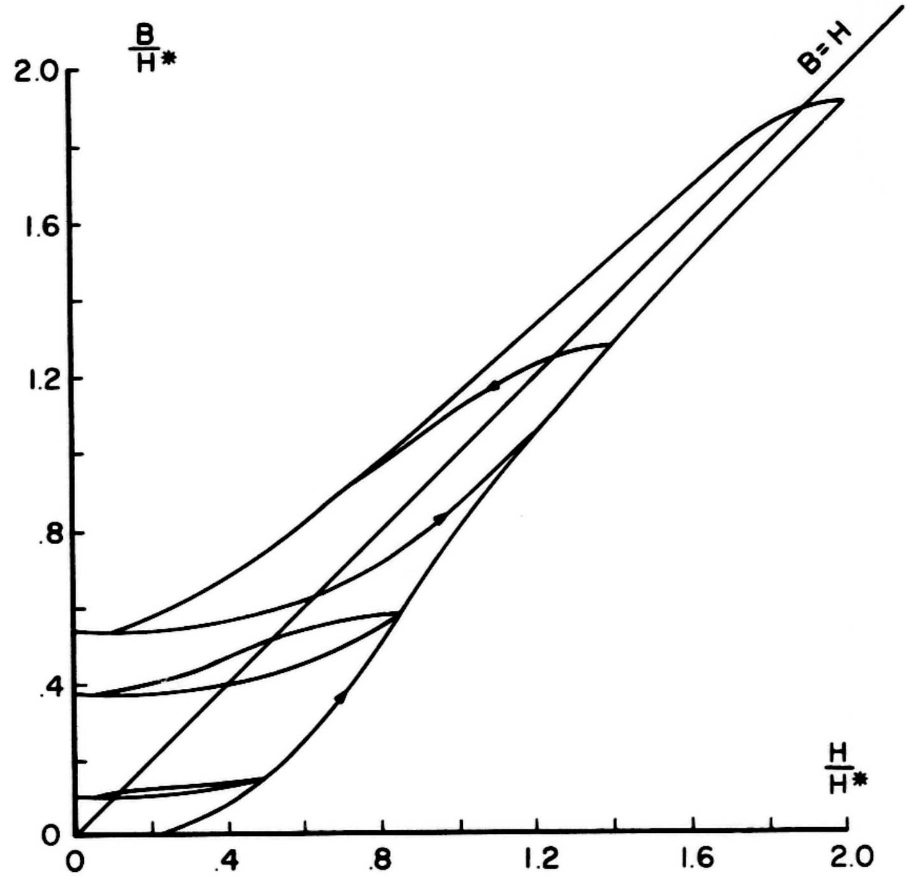

Figure 16. Half Cycle Hysteresis Loops for h_m = .5, .85, 1.4 and 2 Respectively-Reduced Magnetic Induction vs Magnetic Field for the Alpha Model.

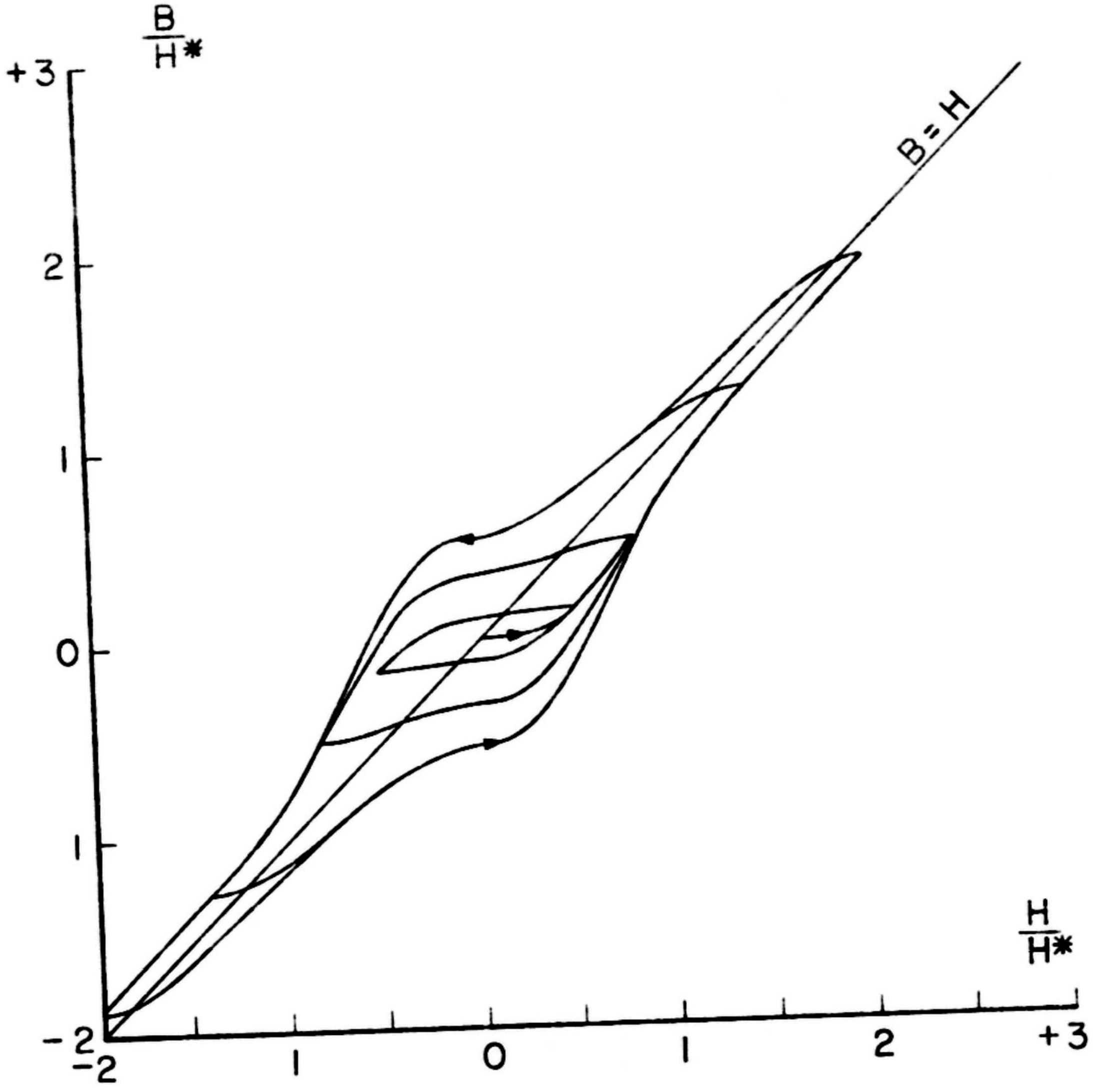

Figure 17. Full Cycle Hysteresis Loops for h_m = .5, .8, 1.4 and 2.0 Respectively-Reduced Magnetic Induction vs Magnetic Field for the Alpha Model.

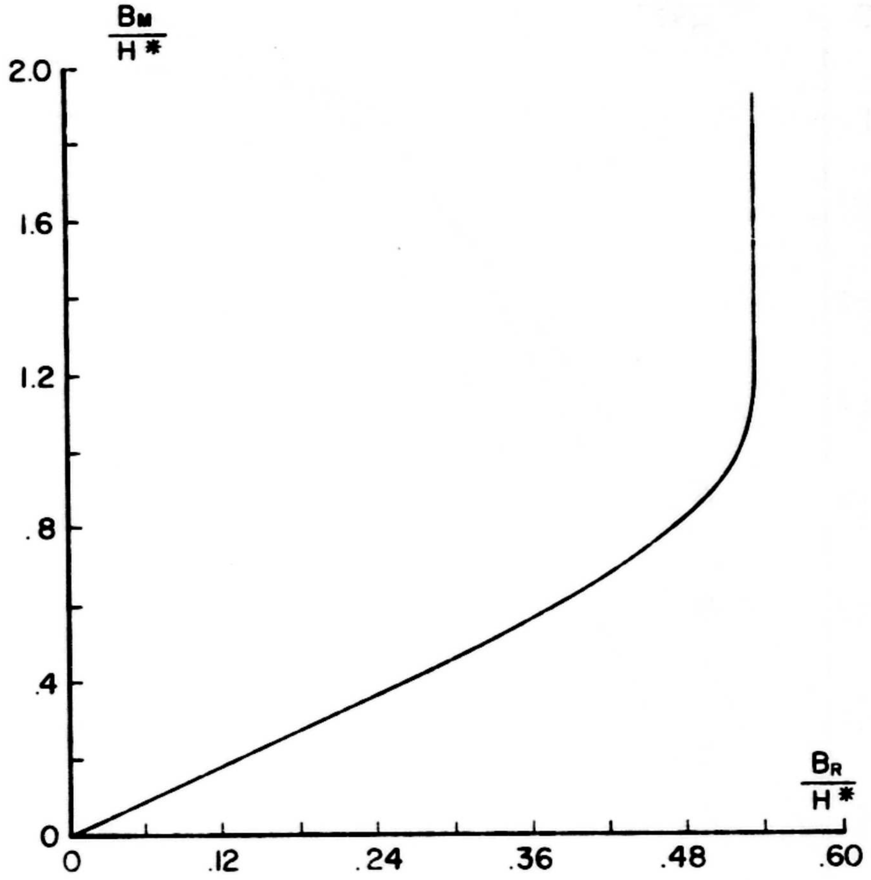

Figure 18. Reduced Magnetic Induction at Maximum External Magnetic Field vs Reduced Remanent Moment for an Initially Unmagnetized Sample Submitted to Successively Higher External Magnetic Fields for the Alpha Model.

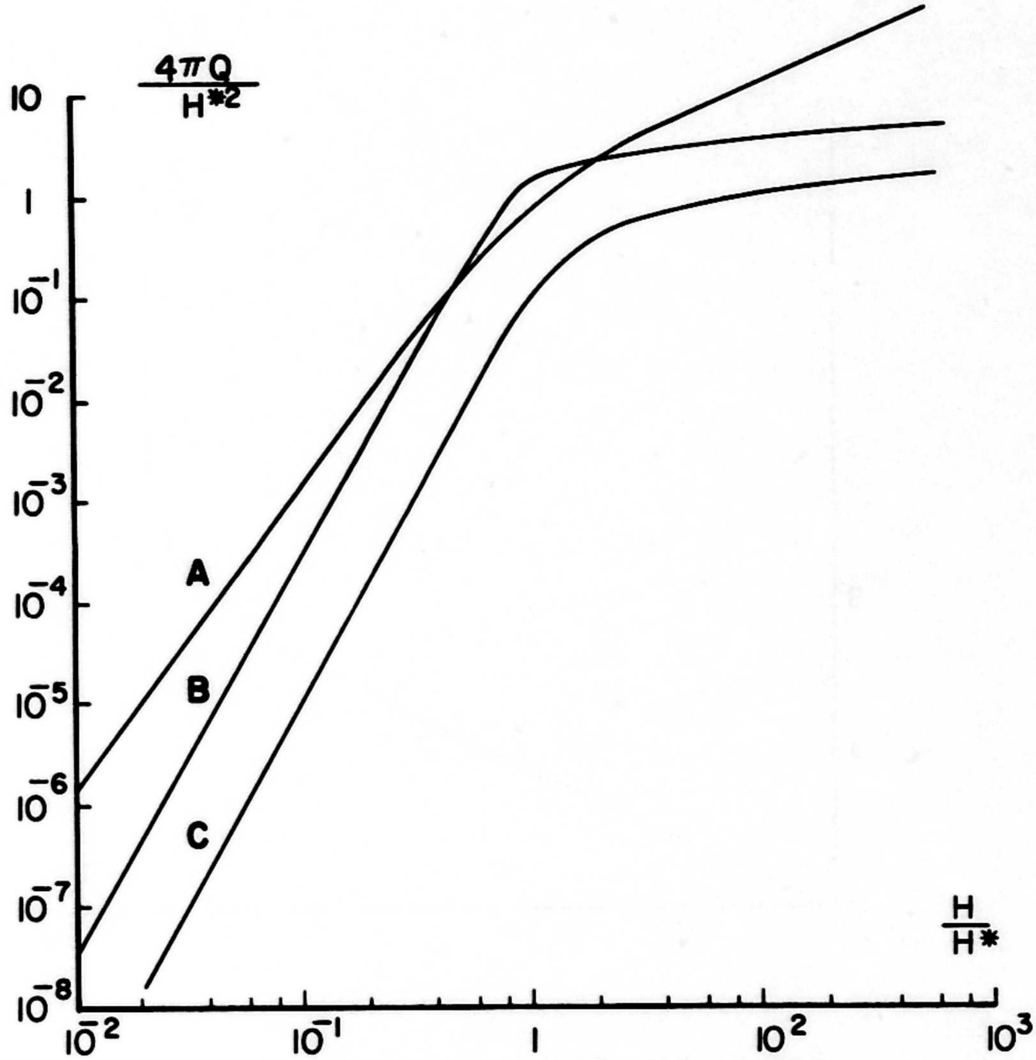

Figure 19. Reduced Hysteretic Energy Loss vs Reduced Magnetic Field. Curve A is Full Cycle Bean-London Model Loss, Curve B and C are Respectively Full Cycle and Half Cycle Loss for the Field Dependent Model.

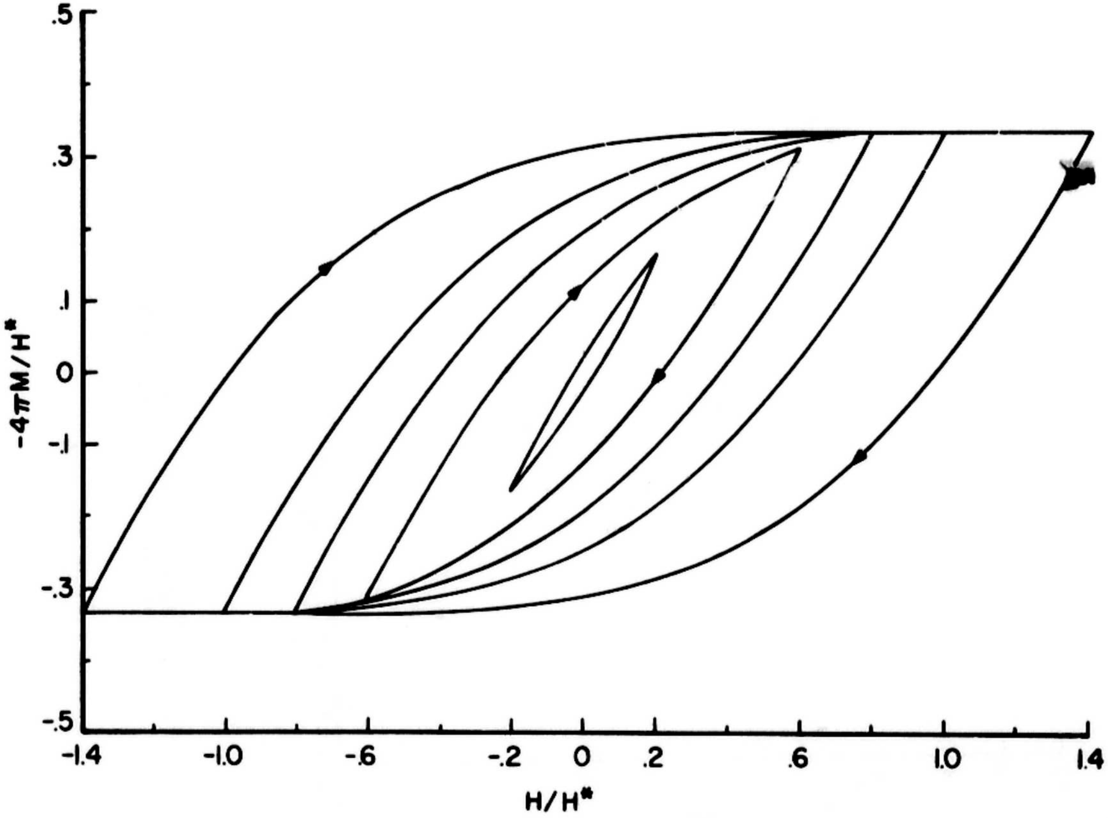

Figure 20. Reduced Magnetization vs Reduced Field for the Bean Model for Several Reduced Fields.

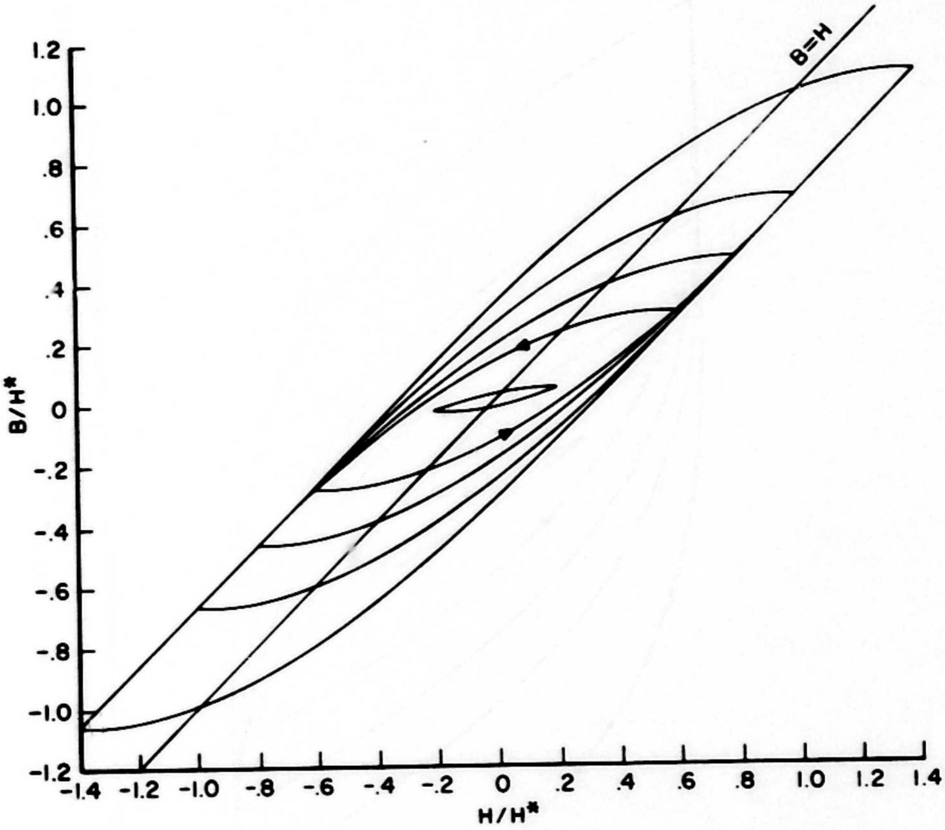

Figure 21. Reduced Magnetic Induction vs Reduced Field for Several Reduced Fields for the Bean Model.

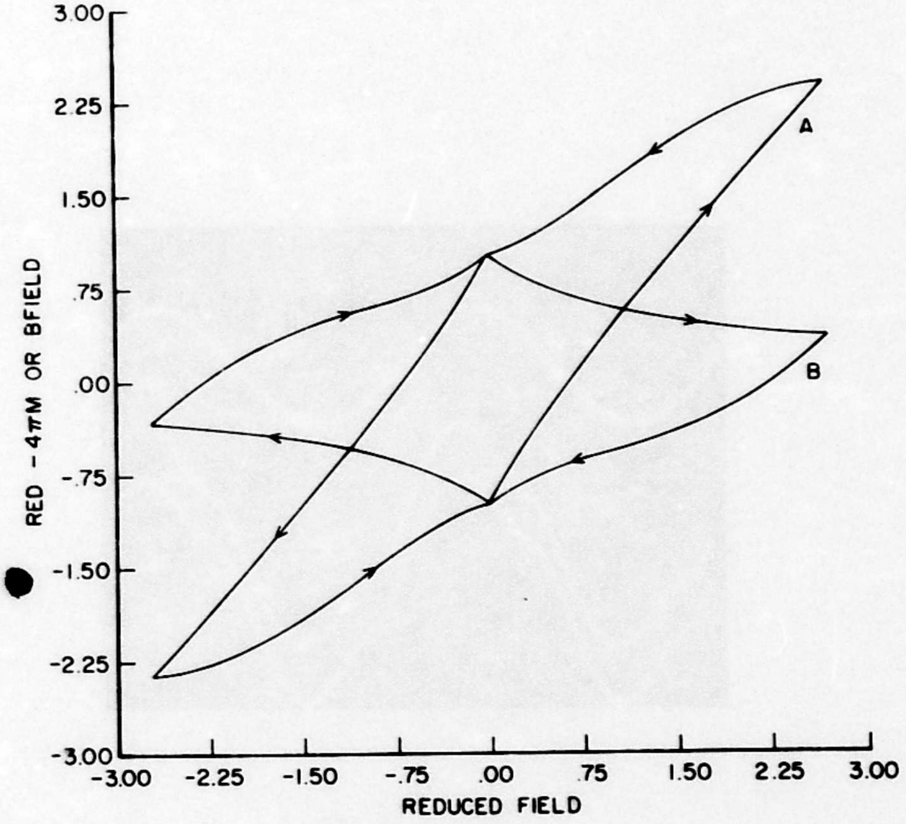

Figure 22. Reduced Magnetic Induction or Magnetization vs Reduced Field for the "Kim" Model. Curve B for Magnetization and Curve A for Induction. Full Penetration Only.

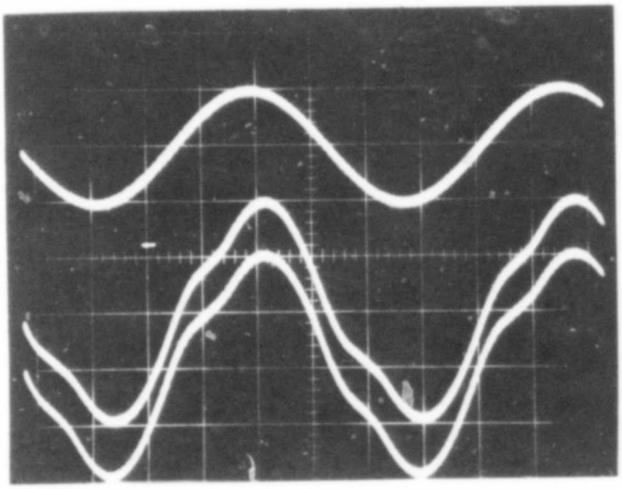

Figure 23. Experimental Total Voltage Waveforms, Inductive, and Loss Components.

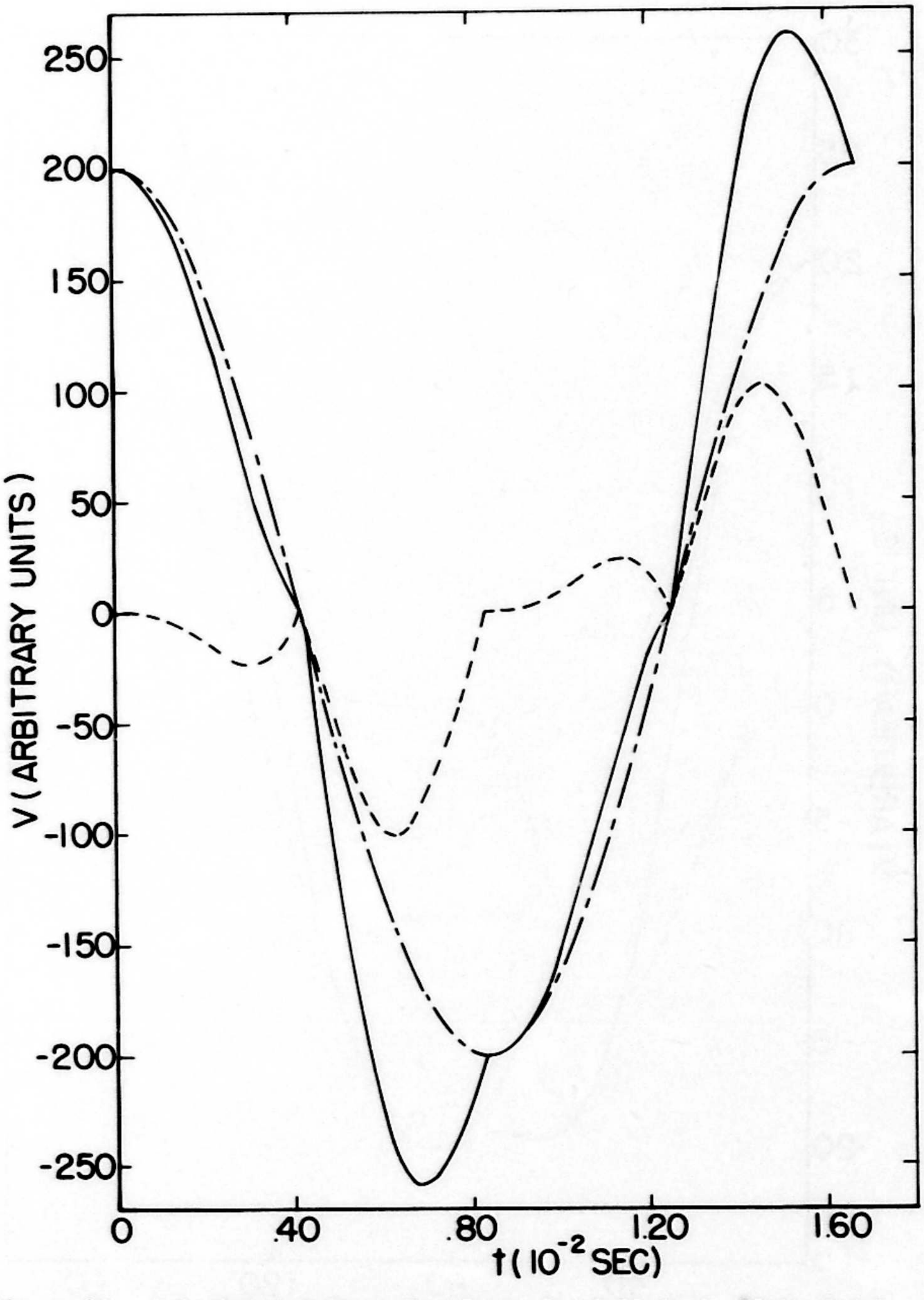

Figure 24. Calculated Voltage Waveforms for Full Cycle Alpha Model. The Dashed Line Represents the Superconductor Voltage, the Barred Line an Inductive Voltage, and the Solid Line the Sum of the Two.

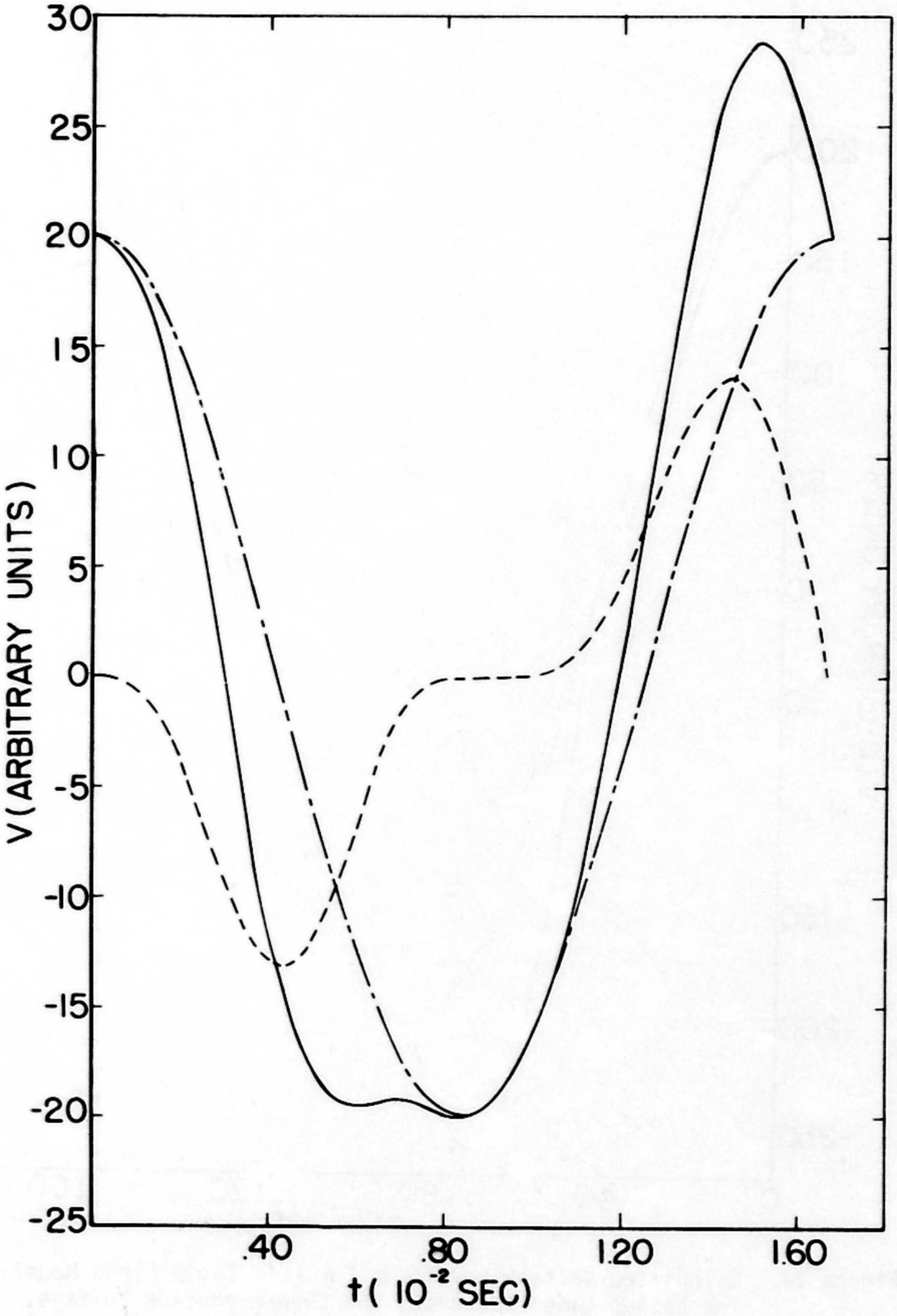

Figure 25. Calculated Voltage Waveforms for Half Cycle Alpha Model. The Dashed Line Represents the Superconductor Voltage, the Barred Line an Inductive Voltage, and the Solid Line the Sum of the Two.

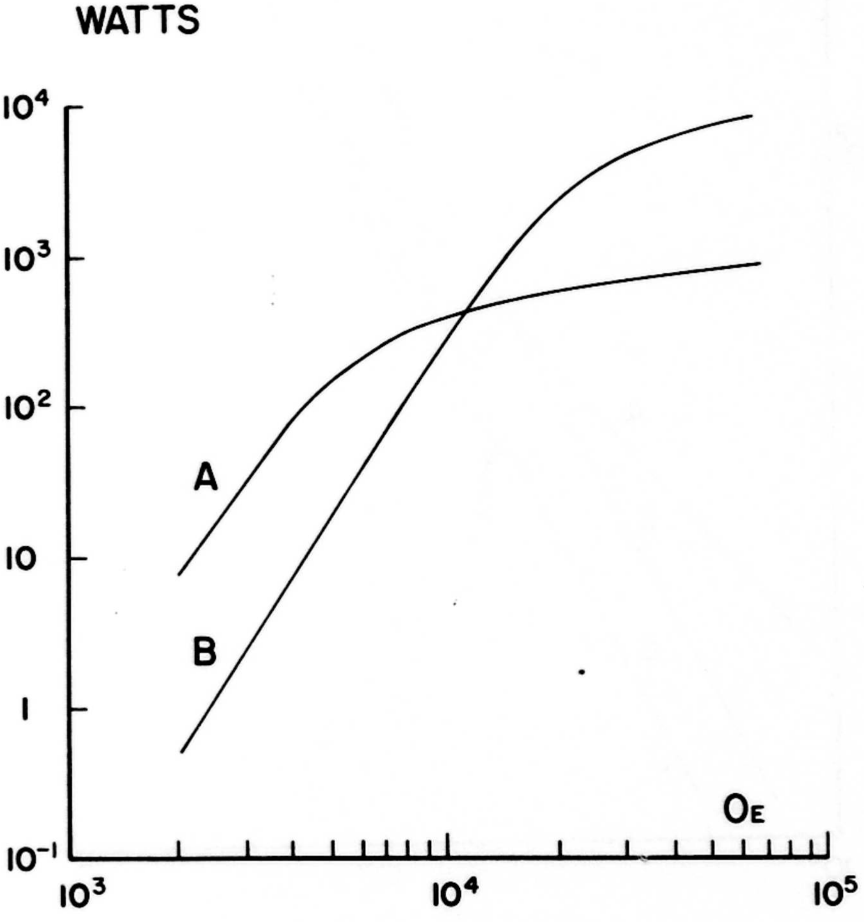

Figure 26. Power Dissipation in Watts vs Maximum Magnetic Field for a Frequency of 9.9 Hz, Haller's Coil Geometry, and an α of 5.7 X10^9 A-Oe/cm^2. Curve A Represents the Loss for a "Decoupled" Multistrand Wire With a Superconductor Radius of 27.6 Microns and 64 Filaments. Curve B Represents the Loss for Haller's Wire.

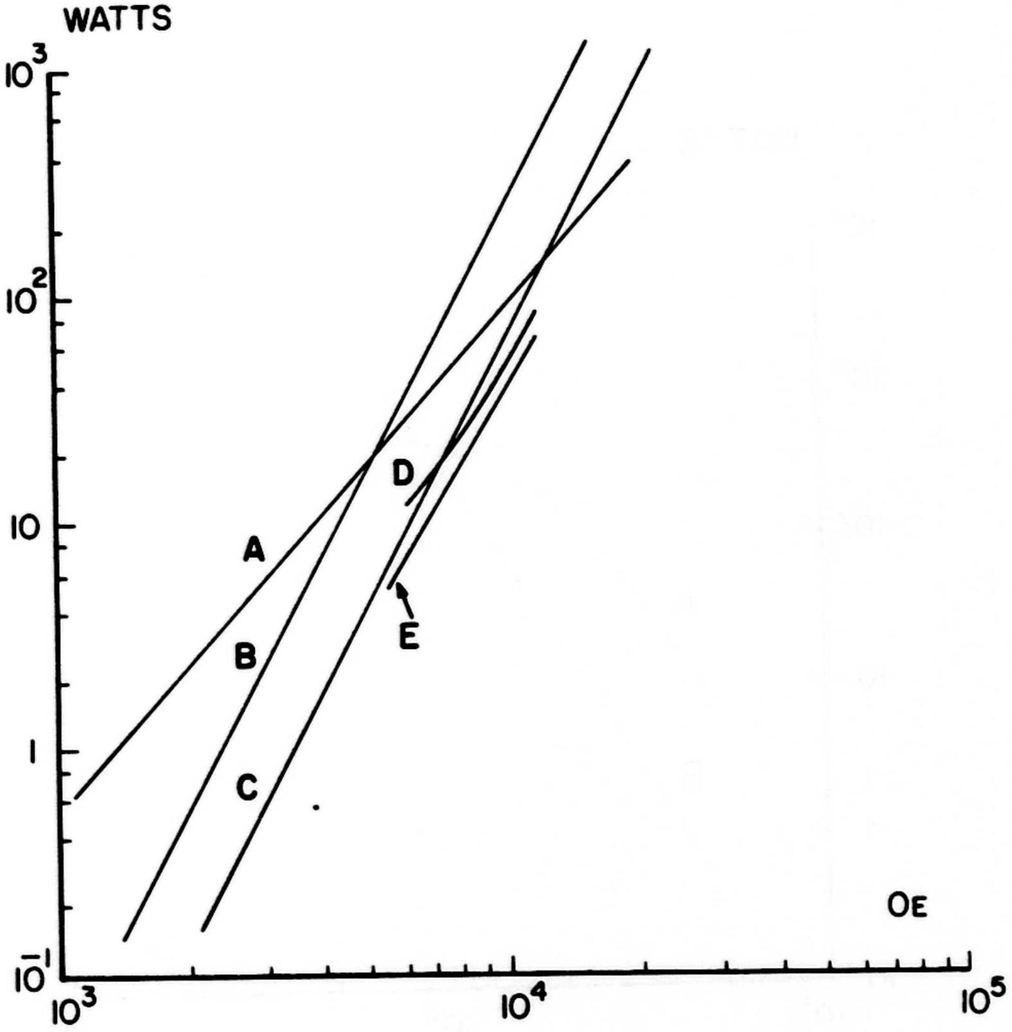

Figure 27. Power Dissipation in Watts vs Maximum Magnetic Field for Haller's Coil and a Frequency of 9.9Hz. Curve A Represents the Experimental Results, Curve B Obtained From Haller's Values of J and H ($\alpha = 5.7 \times 10^9$ A-Oe/cm^2), Curve C is Obtained by Varying α (2.42×10^{10} A-Oe/cm2) to Minimized Standard Deviation, Curve D Consists of Eddy Current Loss Plus Bean-London Hysteresis Loss, and Curve E Represents Only the Bean-London Hysteresis Loss (D and E Were Taken From Haller).

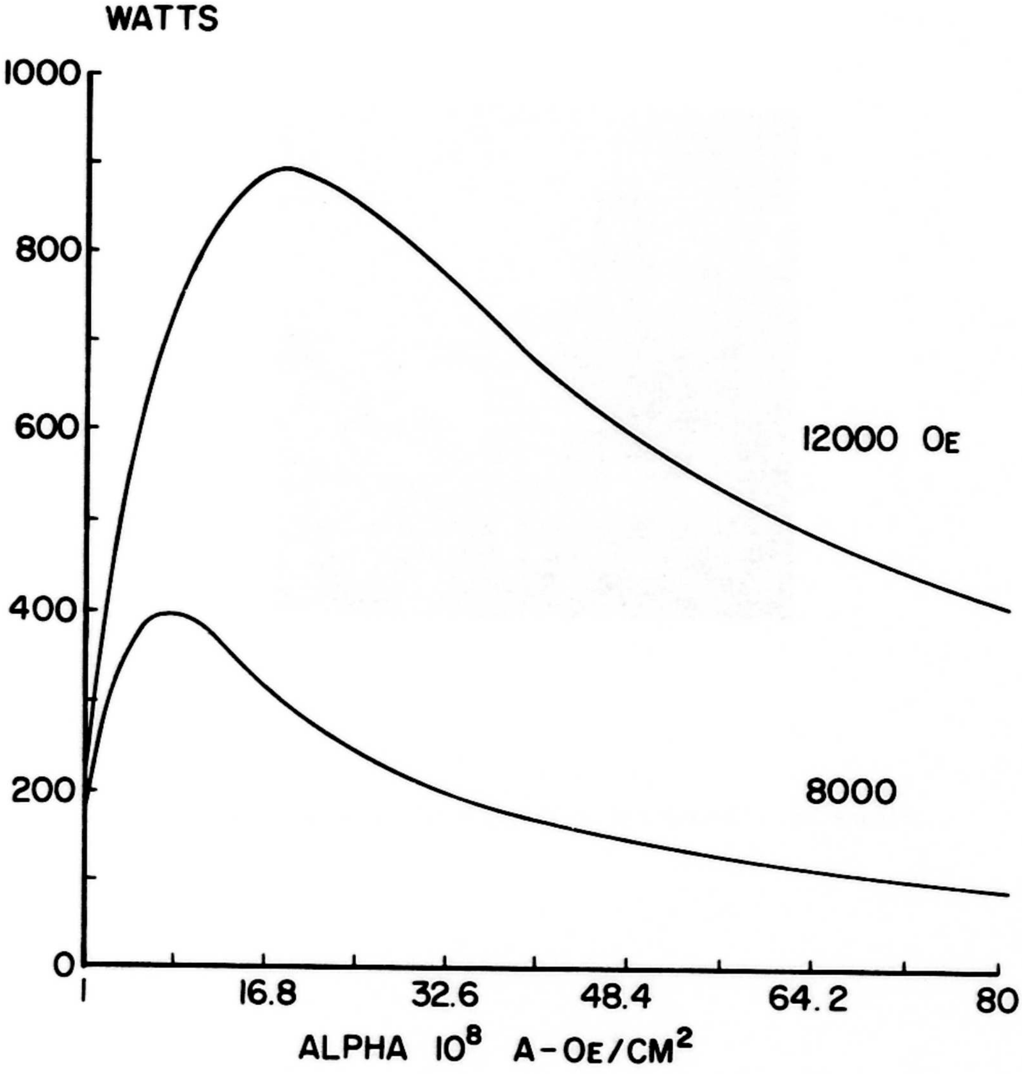

Figure 28. Power Dissipation in Watts vs Alpha for Two Different Maximum Magnetic Fields for Haller's Coil Geometry and a Frequency of 9.9 Hz.

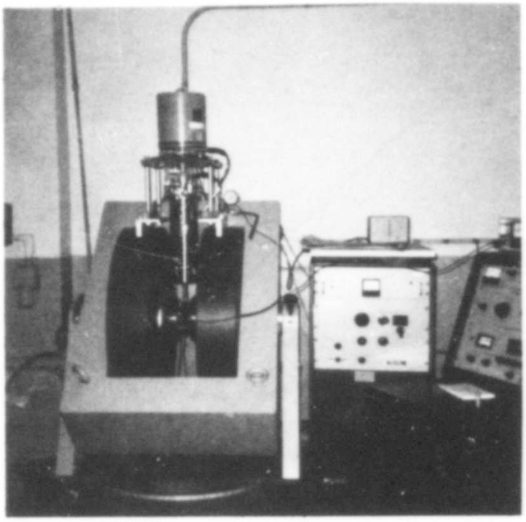

Figure 29. Photograph of Vibrating Sample Magnetometer.

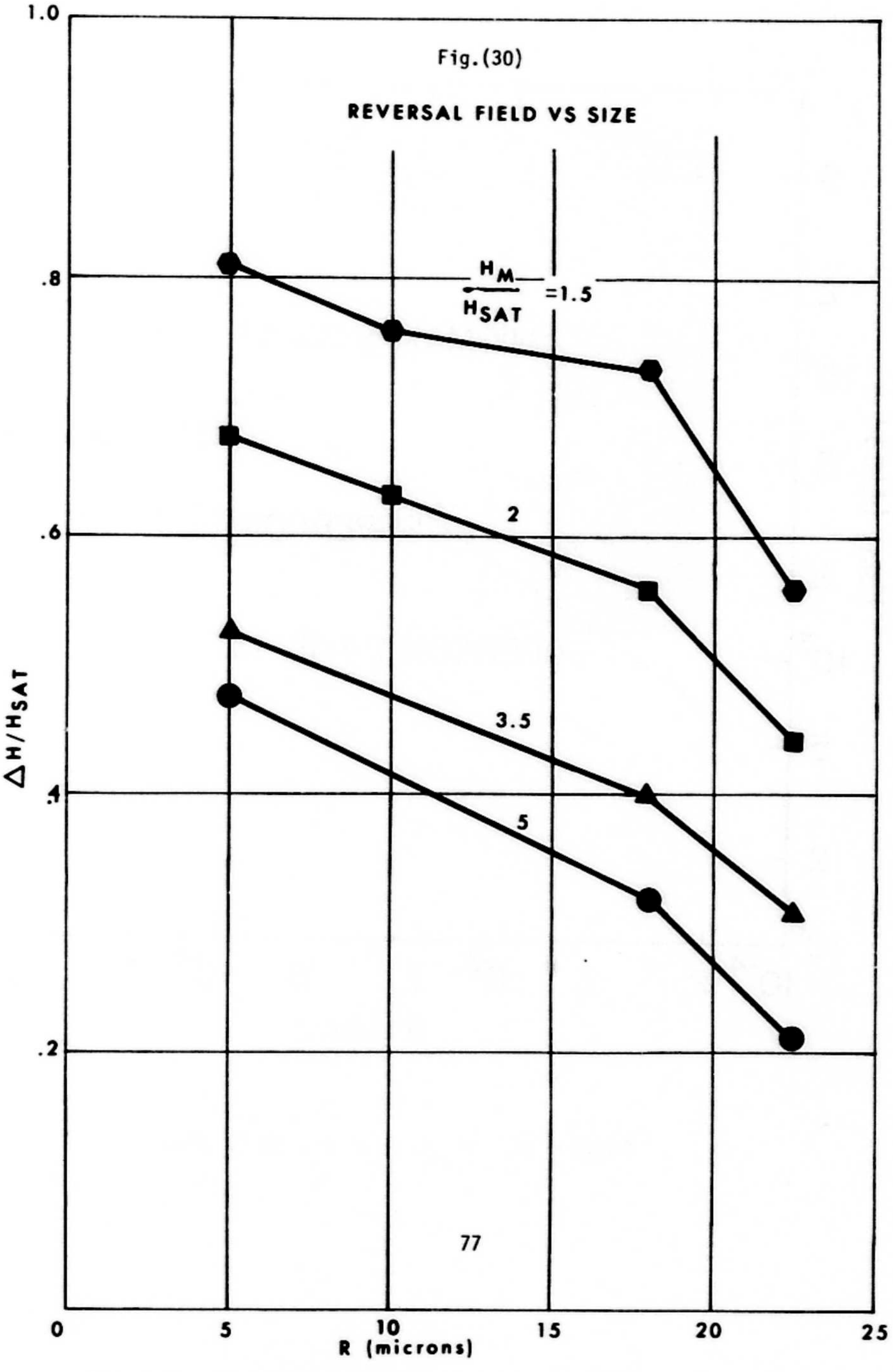

Figure 30. Plot of Reduced ΔH vs R for Constant Reduced Bias for NbTi Filamentary Wire.

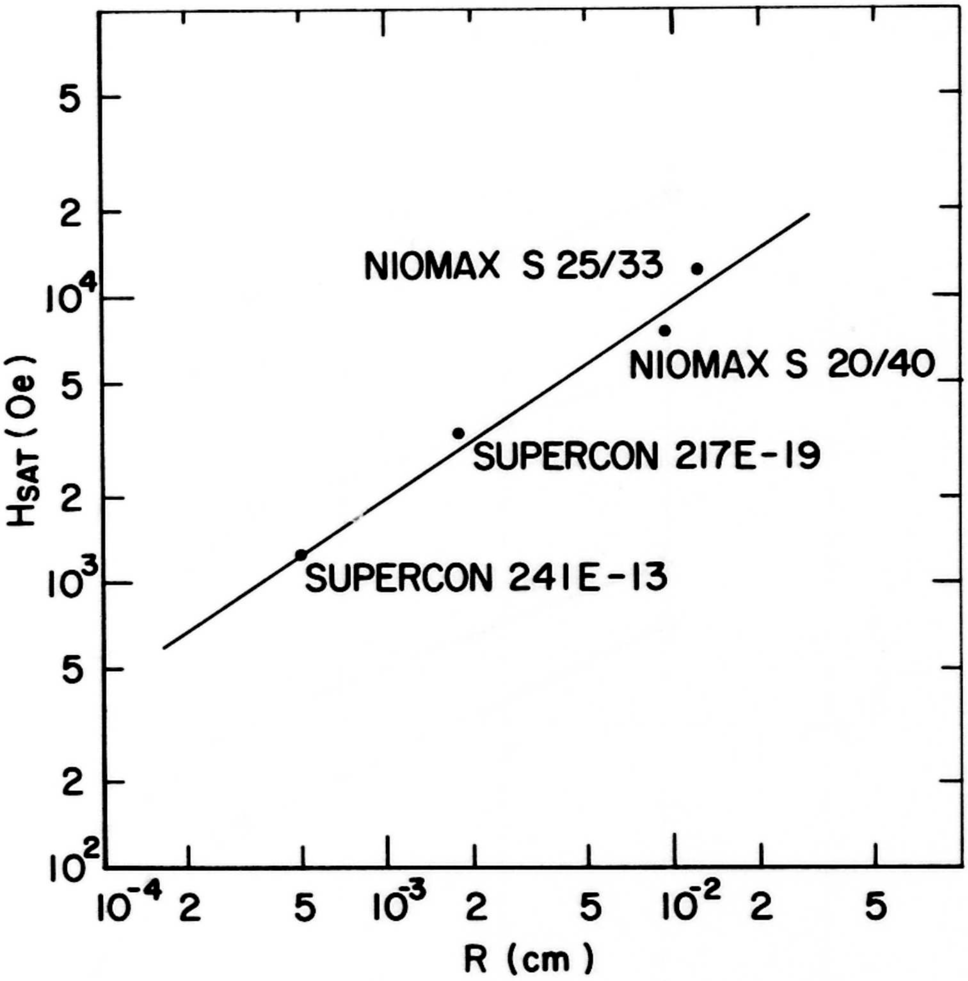

Figure 31. H_{SAT} vs R for NbTi Wire.

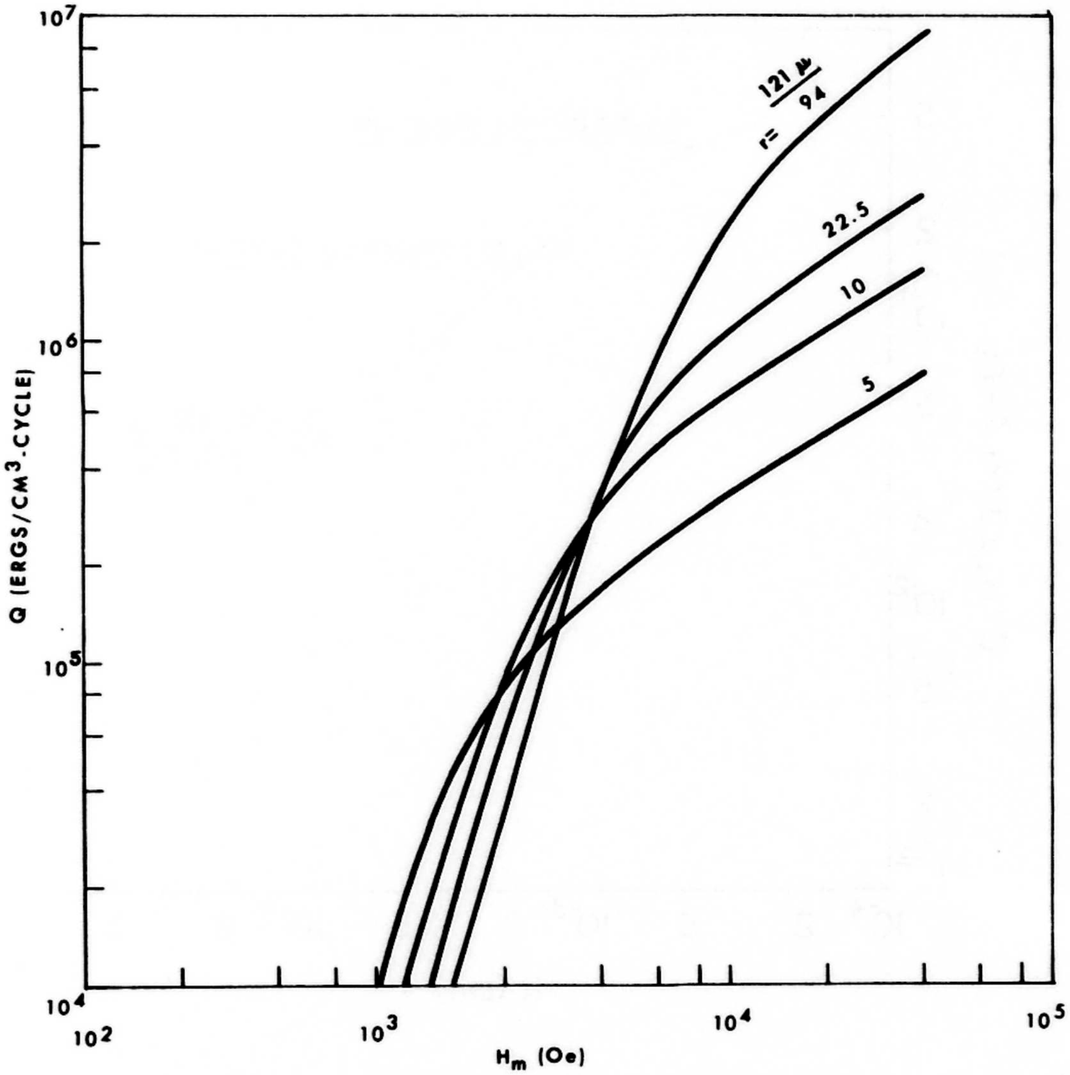

Figure 32. Half Cycle Experimental Hysteretic Loss for NbTi Wire for Filament Radii of 5, 10 (MCA Rotor Wire), 22.5 (Supercon Rotor Wire), 94, and 121 Microns.

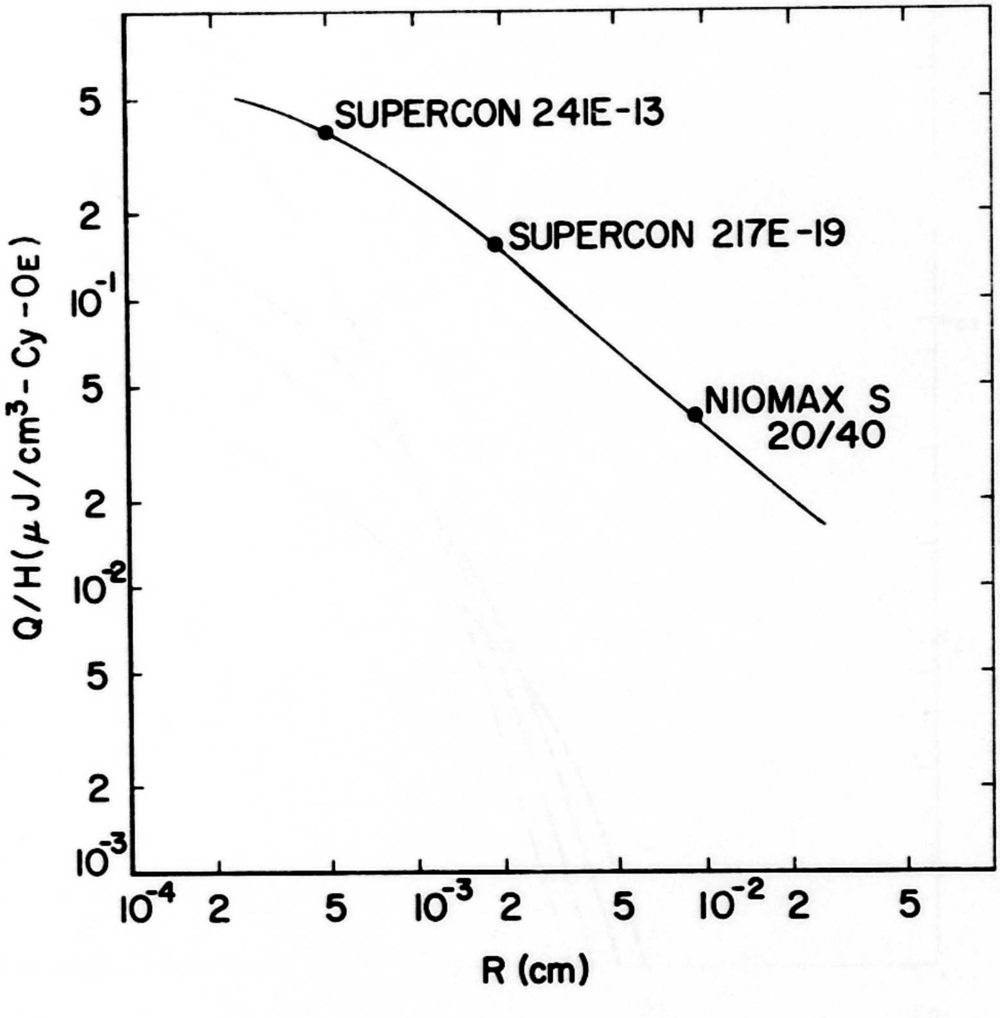

Figure 33. Half Cycle Hysteretic Loss for an H_m of 500G vs R Depicting Partial Penetration Loss Dependence on size.

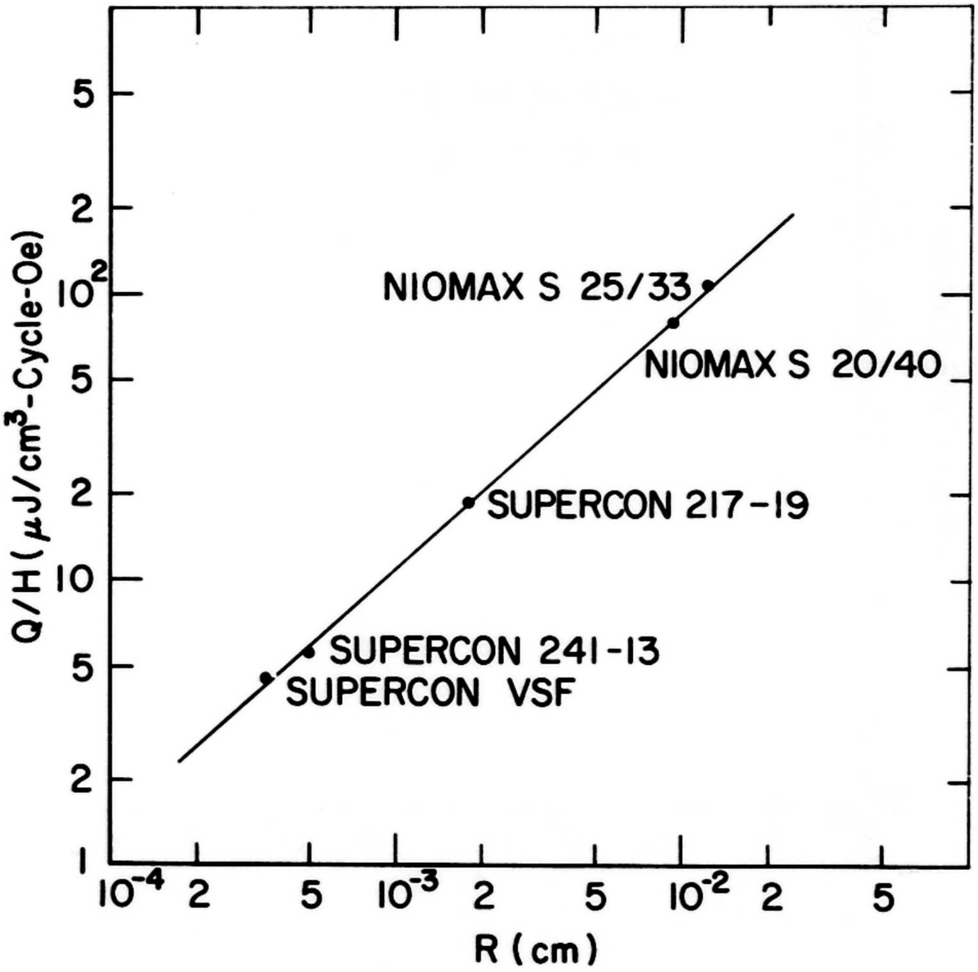

Figure 34. Half Cycle Hysteretic Loss for an H_m of 18kOe vs R Depicting Full Penetration Loss Dependence on Size.

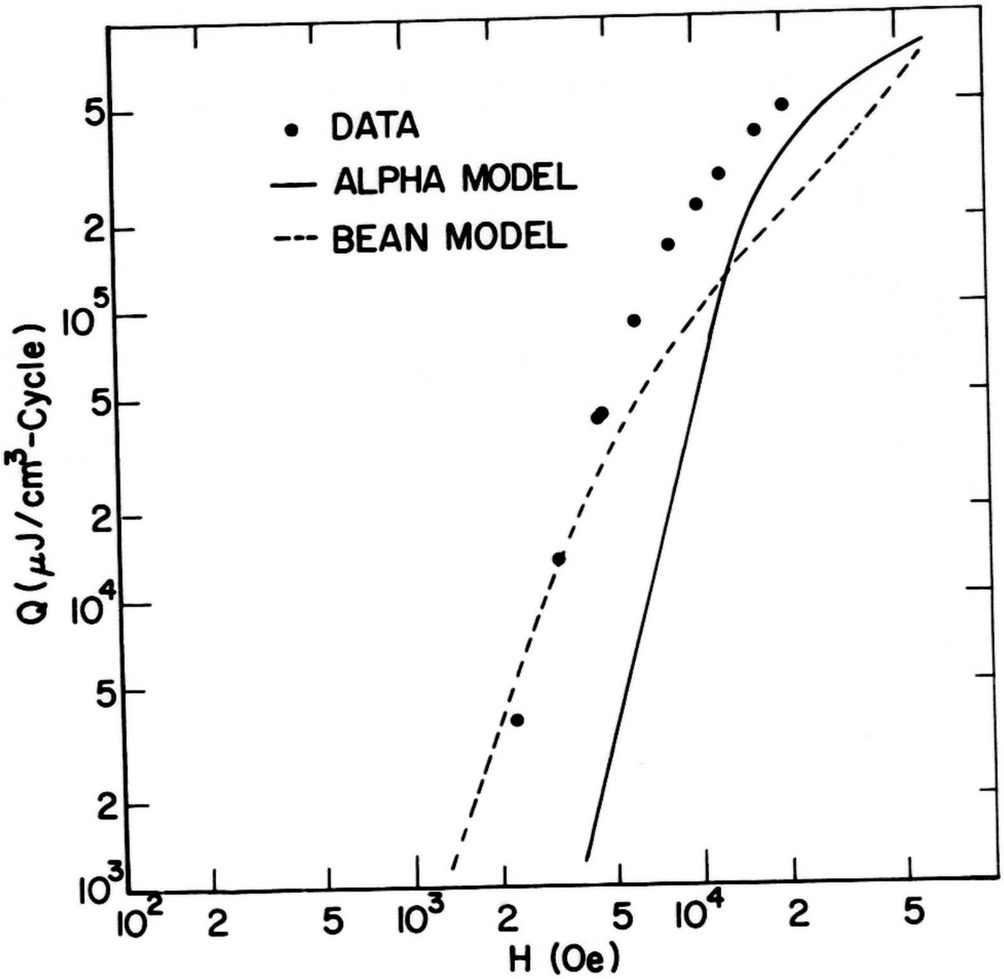

Figure 35. Half Cycle Hysteretic Loss for Niomax S 20/40. The Bean and Alpha Model Curves Were Obtained by a LSF of Short Sample Critical Current Data. (R = 94 Microns).

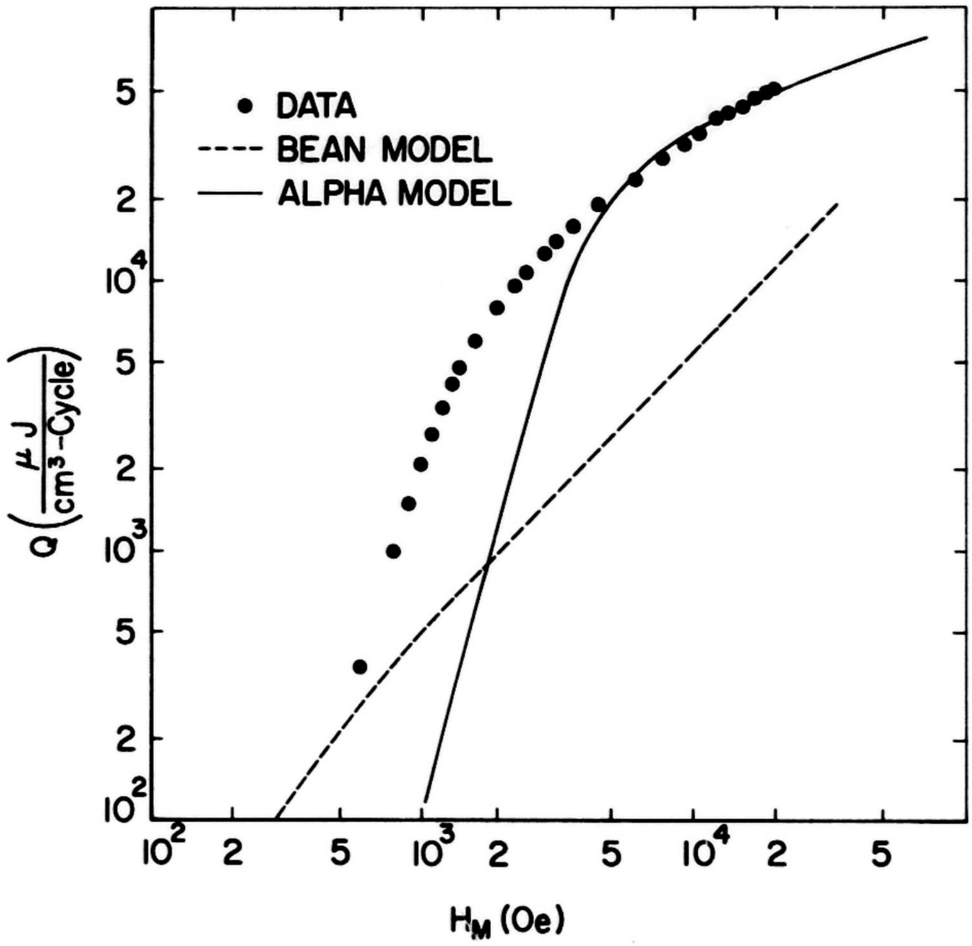

Figure 36. Half Cycle Hysteretic Loss for Supercon 241E-13 and Corresponding Bean and Alpha Model Curves. (R = 5 Microns)

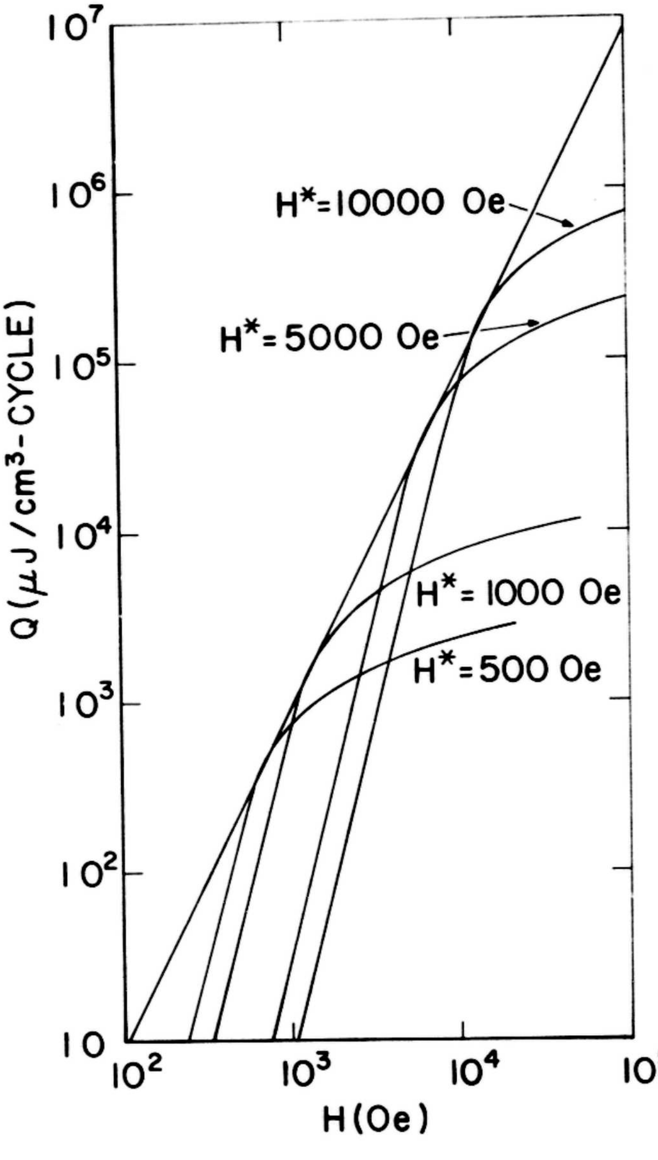

Figure 37. Theoretical Hysteretic Loss for Alpha Model for Various Penetration Fields for Half Cycle. Limiting Line Indicates Unphysical Region.

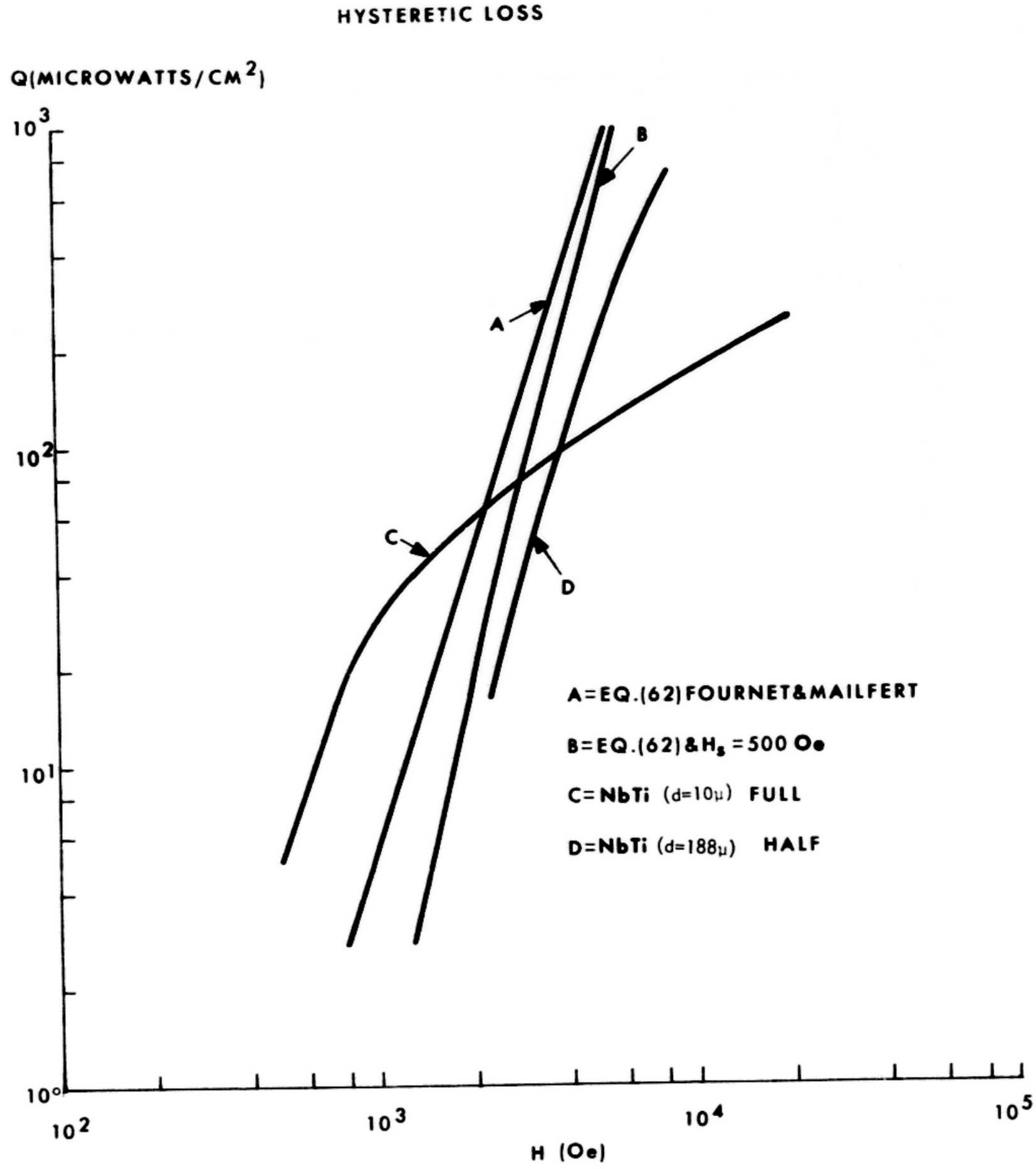

Figure 38. Fournet and Mailfert Theoretical Hysteretic Loss for the Universal J_c Curve Parameters $J_oH_o = 9.91 \times 10^6$ A-kG/cm^2 and H_o = 12.5kOe for Partial Penetration for the Kim Model Full Cycle is Represented by Curve A. Curve B Corresponds to Fournet and Mailfert Loss Including a 500G Surface Field. Curve C is the Full Cycle Loss for 10μ Diameter NbTi Wire (241E-13). Curve D is Half Cycle Loss Data for 188μ NbTi Wire (20-40).

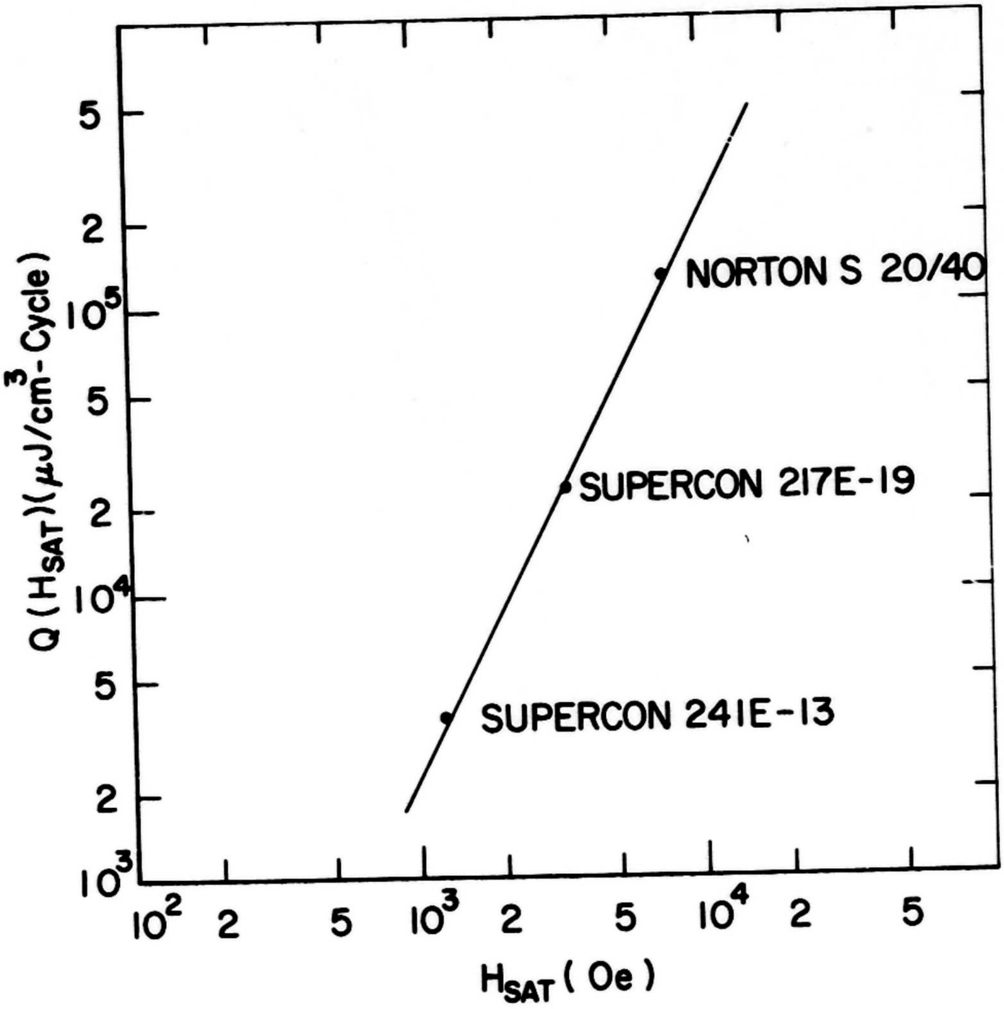

Figure 39. Plot of Q (H_{SAT}) vs H_{SAT} Used to Denormalize Universal Loss Curve for Half Cycle.

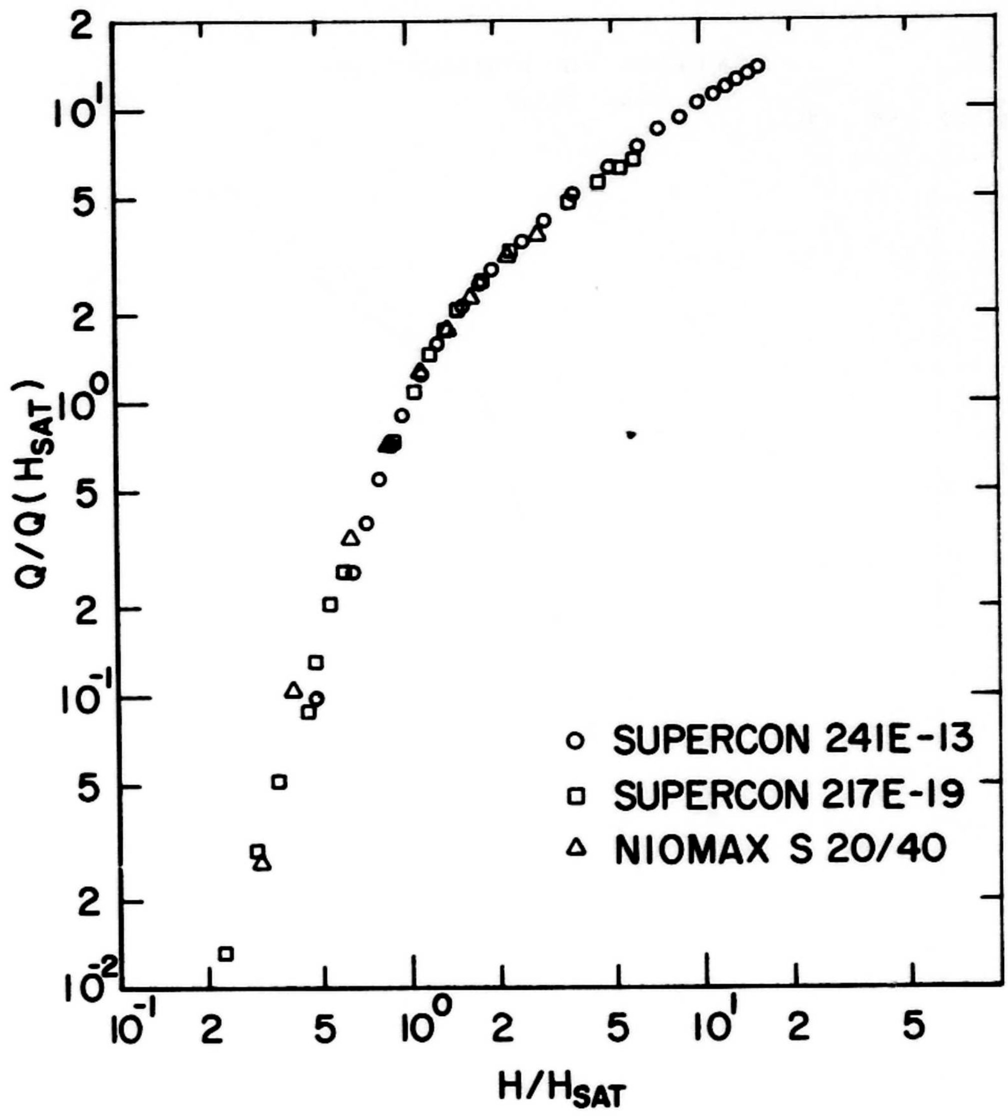

Figure 40. Universal Reduced Loss Curve, Reduced Q vs Reduced H for Half Cycle.

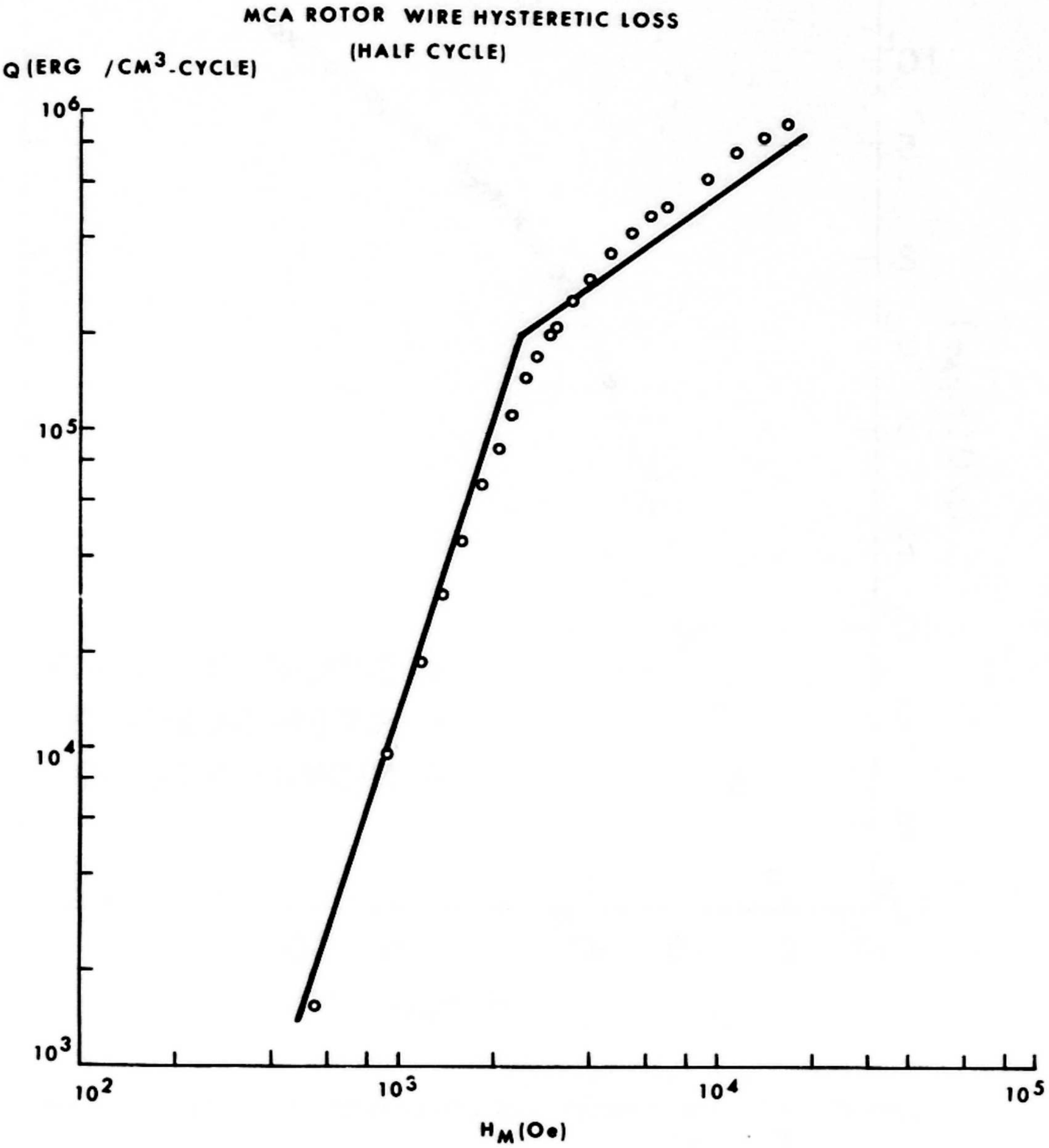

Figure 41. Hysteretic Loss of MCA Rotor Wire (20μ Diameter) Compared to Predicted Loss From Universal Loss Curve. Data Points Experimental Half Cycle.

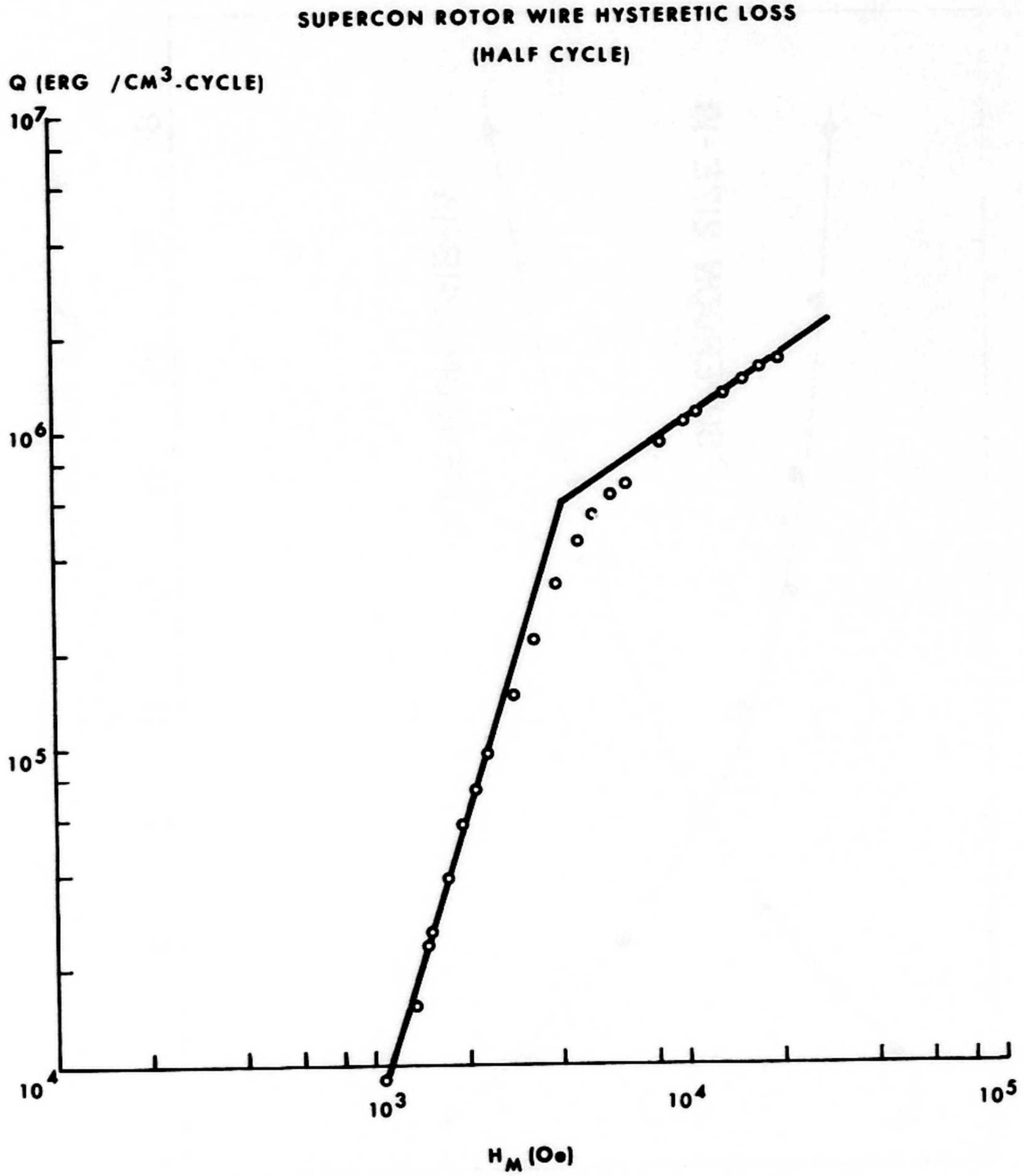

Figure 42. Hysteretic Loss of Supercon Rotor Wire (45μ Diameter) Compared to Predicted Loss From Universal Loss Curve. Data Points Experimental Half Cycle.

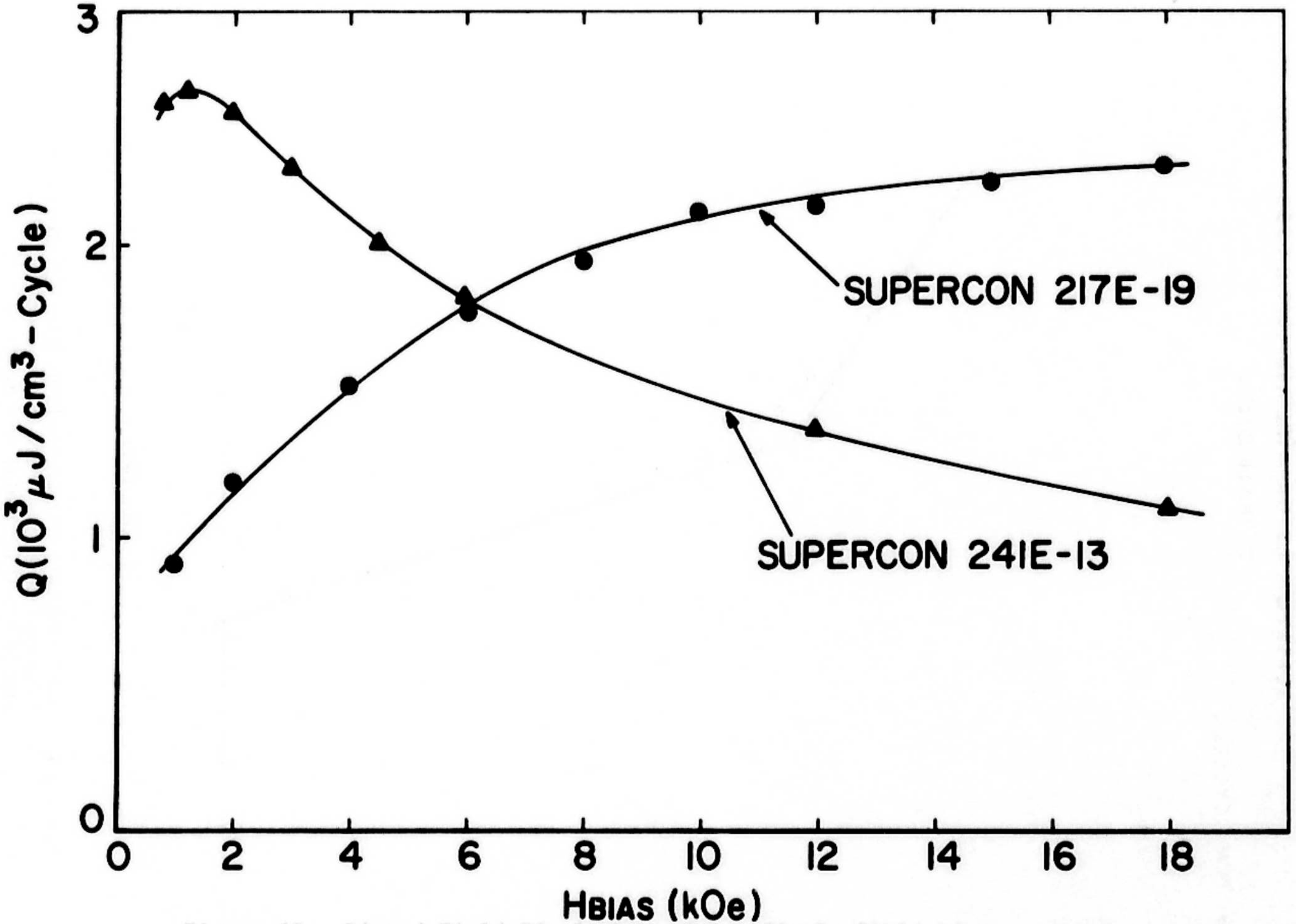

Figure 43. Biased Field Ripple Loss for a Ripple Field of H_m = 500 Oe. Q vs H_{BIAS} for Supercon 217E-19 and Supercon 241E-13.

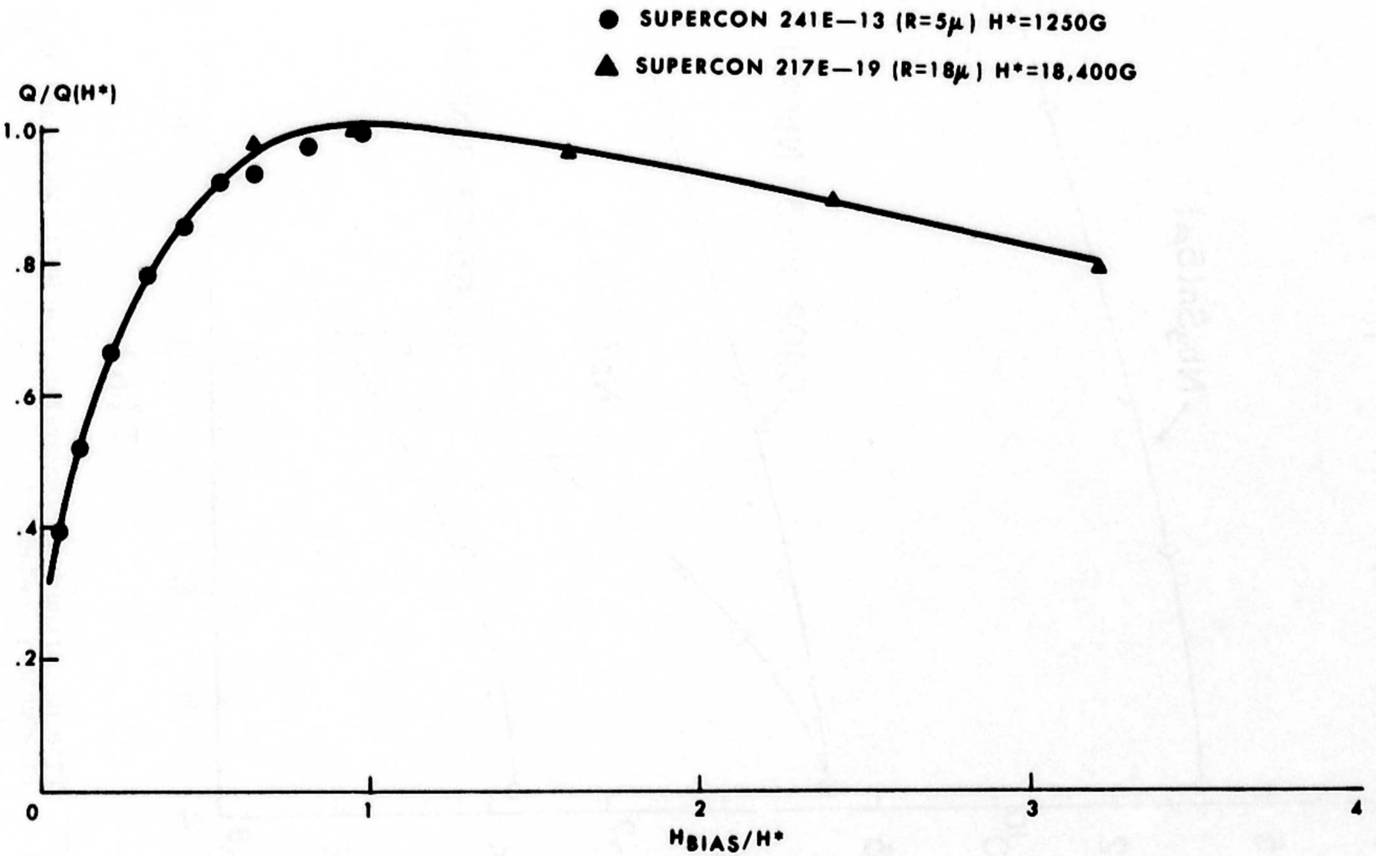

Figure 44. Plot of Reduced Q vs Reduced H for Bias Case. Q and H Are Reduced Respectively by the Hysteretic Loss at $H_{RIPPLE}=H^*_{EFFECTIVE}$ and $H^*_{EFFECTIVE}$ Corresponds to Theoretical Curve Where Pinning Strength Or Size is Varied For Fixed Field Change.

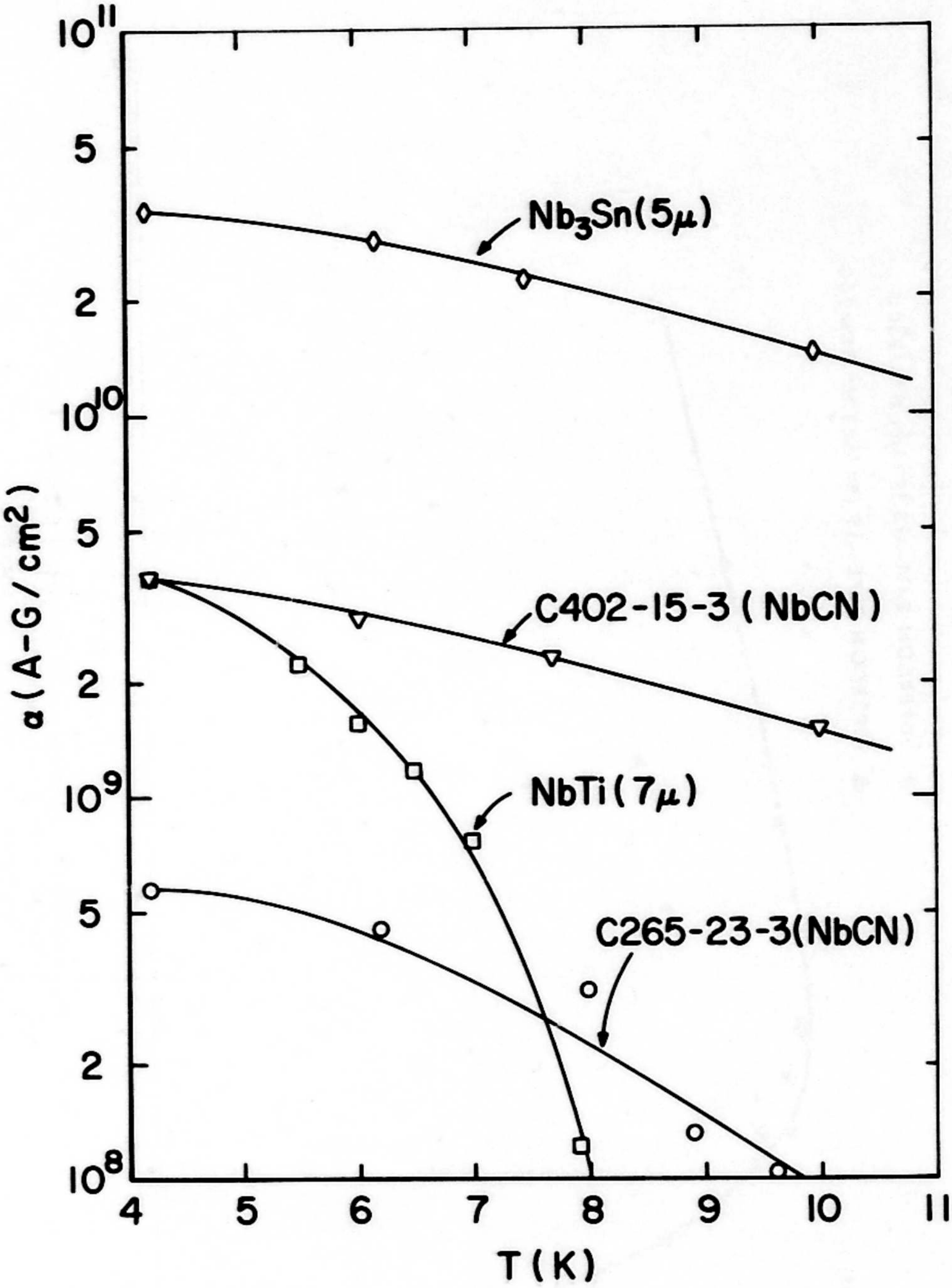

Figure 45. Pinning Strength vs Temperature For NbTi, NbCN, and Nb_3Sn Filamentary Conductors.

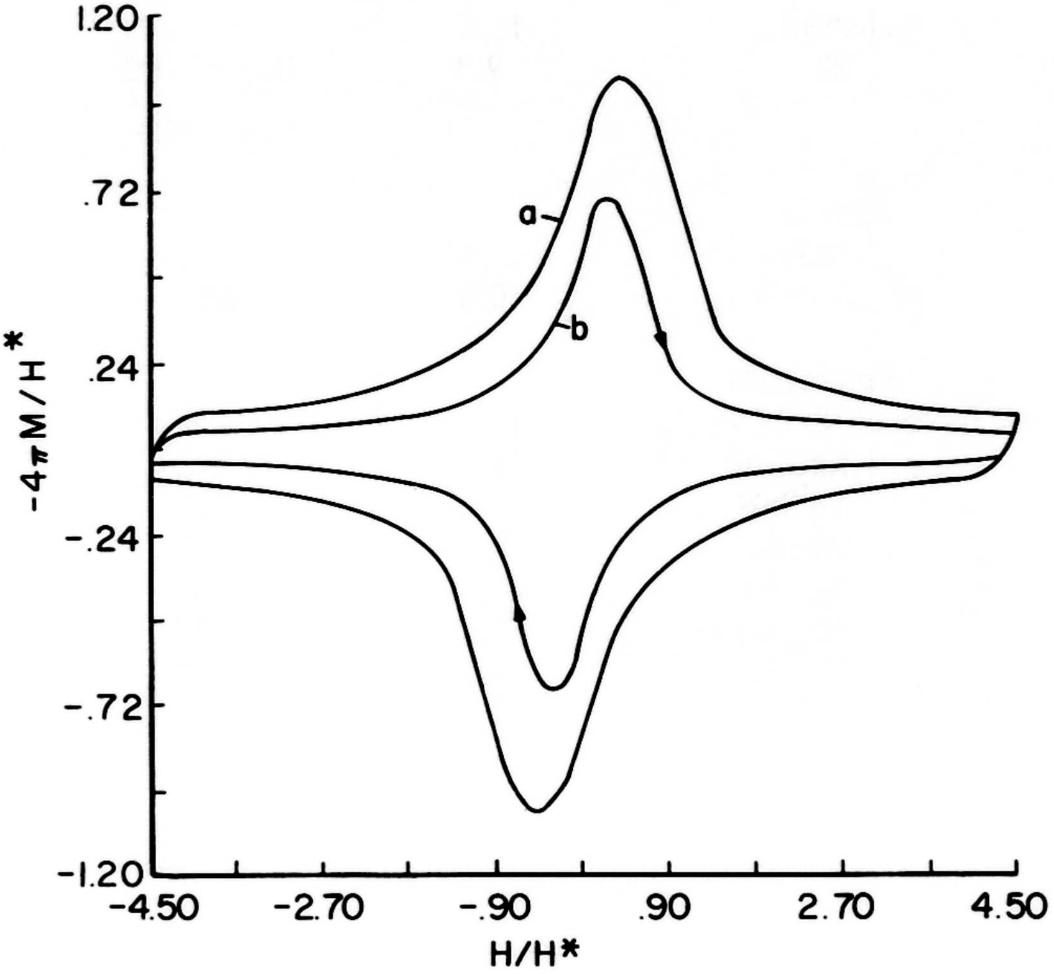

Figure 46. Hysteresis Loops for Multifilamentary Superconducting Wire. Curve a Is Obtained by Sweeping the External Magnetic Field. Curve b is Obtained From Static Field Measurements (Theoretical Model Curves Obtained From Effective Change in Size).

TABLE 1

SUPERCONDUCTING TRANSITION TEMPERATURE AND UPPER CRITICAL FIELD FOR SEVERAL USEFUL MATERIALS

Element	Tc, K	
Nb	9.3	$H_{c1}\sim 1400G$
		H_{c2}, kOe
Alloy		
NbZr	10.8	90
NbTi *	10.0	120
Compounds		
$Nb\,C_x\,N_{1-x}$	18	120
$Nb_3\,Sn$*	18	230
$V_3\,Ga$*	17	220
$Nb_3\,Al$	19.3	360
$Nb_3\,Ga$	20.3	340
$Nb_3\,Al_x\,Ge_{1-x}$	20.7	410
$Nb_3\,Ge$	23.2	440

TABLE 2

CHARACTERISTICS OF INDUCTIVE ENERGY STORAGE COILS CONSTRUCTED BY MCA AND AVCO

STAGE I - DEMONSTRATION COILS

	AVCO	MCA
ENERGY	20.8kJ (15.2)*	1kJ
HIGH VOLTAGE OUTPUT	13.5kV (~60kV)	14kV
INDUCTANCE	4.45mH	30mH
CURRENT	9350A	430A
FIELD	18kG	25kG
DIAMETER	.24m (MEAN)	.117m (OD)
LENGTH	.24m	.0875m (FORMER)
CONDUCTOR WEIGHT	1.87kg (4.1 LBS)	
COIL VOLUME	$.011m^3$ ($0.383\ FT^3$)	
REPETITION RATE	3 Hz	5Hz (.155, .2ms, 55ms)
PULSE TRAIN	Indefinite	200 (40 SEC)
CONDUCTOR	D = .0047 IN	D = .0045 IN
	192 FILAMENTS/WIRE	SINGLE FILAMENT
	.2mm PITCH	
	66 STRANDS/BRAID	48 STRANDS/BRAID
	6 BRAIDS/CABLE	
	SOLDER COATED	Polybondex
	c/s = 1.1 / 1.0	c/s = 1.4 / 1.0
	D_F = 6 μ	D_F = 97 μ

STAGE II - CONSTRUCTION OF 100kJ COIL AT 5Hz BY MCA

TABLE 3

CHARACTERISTICS OF MULTIFILAMENTARY WIRE USED BY WESTINGHOUSE IN THE CONSTRUCTION OF A SUPERCONDUCTING ROTOR WINDING

PROPERTY	MCA	NORTON
MATERIAL	NbTi + Cu	NbTi + Cu
COPPER/SUPER C	2:1	2:1
FILAMENTS	1350	300 (CENTER BARE)
FILAMENT DIA	20 μ	45 μ
WIRE DIA	.047"	.047"
ASPECT RATIO	1.5	1.5
POUNDS/COIL	20 LBS	22.7 LBS
TWIST	2/IN	2/IN
LENGTH	3000 FT	3000 FT
I_c @ 40 kOe	680 A	595 A
SUPER C AREA	4.2×10^{-3} cm^2	4.77×10^{-3} cm^2
OPERATING CURR	250 A	250 A
I_c @ 40 kOe & 6 K	475 A	416 A
Jc-WINDING	1.7×10^{4} A/cm^2	1.7×10^{4} A/cm^2
PACKING FACTOR	.75	—
TURNS/COIL	1200	1200
INSULATED	✓	✓
CHARGE TIME	1 MIN TO 40 kOe	1 MIN TO 40 kOe

TABLE 4

CHARACTERISTICS OF WIRE USED BY FERRANTI-PACKARD AND MCA TO CONSTRUCT LIGHTWEIGHT SUPERCONDUCTING MHD MAGNETS

PROPERTY	F-P DESIGN	MCA DESIGN
MATERIAL	NbTi + Cu	NbTi + Cu
COPPER / SUPER C	1.25:1	1.8:1
RESISTIVITY RATIO	200	—
FILAMENTS	211	180 (NONE CENTER)
FILAMENT DIA	50 μ	75 μ
TWIST	.5 /IN	1 /IN
WIRE DIM	.078" x .078"	.064" x .064"
MASS: WT	145 KG; 320 LBS	249 KG; 548 LBS
% SYSTEM WT	32%	44.4%
SYSTEM WT	990 LBS	1240 LBS
WIRE VOL	19,100 CM^3; 1160 IN^3	31,700 CM^3; 1935 IN^3
SUPER C VOL	8500 CM^3	11,350 CM^3
CHARGE TIME	—	10.6 MIN
WIRE LENGTH	4775 M; 15,700 FT	12,000 M; 39,400 FT
Jc-WINDING	"4.13×10^4 A/CM^2"	1.2×10^4 A/CM^2
OPERATING CUR	"2200 A"	380A @ 39 KOe

TABLE 5

LIST OF THE OPERATING RANGE OF VARIOUS PARAMETERS BEING CONSIDERED BY MAXWELL IN A PULSE FORMING NETWORK (PFN) STUDY.

OPERATING PARAMETER	OPERATING RANGE
AVERAGE POWER	3 MW-10 MW
ENERGY/PULSE	3KJ-100 KJ
PULSE RATE	100 PPS-1,000 PPS
OUTPUT VOLTAGE	40 KV-60 KV
PULSE SHAPE	TRAPEZOIDAL
PULSE WIDTH	20 μS-40 μS
PULSE RISETIME	2 μS
PULSE FALLTIME	4 μS
OPERATING TIME	1 MINUTE
LOADS	3 Ω -5 Ω

TABLE 6

OUTLINE OF CALCULATIONAL APPROACH FOR CRITICAL STATE MODELS

CRITICAL STATE THEORIES

A. BEAN MODEL B. α MODEL

BASIC ASSUMPTIONS

J_c = CONSTANT $J_c = \frac{\alpha}{H}$

$$\vec{\nabla} \times \vec{H} = \frac{4\pi \vec{J}}{10}, \text{ Oe A/cm}^2\text{, VOLTS}$$

$$\vec{B} = \frac{\int \vec{H} dv}{\int dv}$$

$$4\pi \vec{M} = \vec{B} - \vec{H}$$

RESULTS FOR CYLINDER IN AXIAL FIELD

PENETRATION DEPTH

$$\Delta = \frac{10H}{4\pi J_c} \qquad \Delta = \frac{5H^2}{4\pi\alpha}$$

TABLE 7

LIST OF ASSUMPTIONS OF THE CRITICAL STATE MODEL AND OF SOME ANALYTICAL EXPRESSIONS FOR J_c.

CRITICAL STATE MODEL ASSUMPTIONS

1) THERE IS A LIMITING MICROSCOPIC SUPERCURRENT $J_c(H)$ THAT A HARD SUPERCONDUCTOR CAN CARRY.

2) ANY ELECTROMOTIVE FORCE, HOWEVER SMALL, WILL INDUCE THIS FULL CURRENT TO FLOW LOCALLY.

3) CHOICE OF AN ANALYTICAL EXPRESSION FOR $J_c(H)$.

a)	$J_c(H) = J_B$	BEAN
b)	$J_c(H) = \frac{\alpha}{H^n}$	ALPHA (n=1)
c)	$J_c(H) = \frac{J_0 H_0}{H + H_0}$	KIM
d)	$J_c(H) = J_0 - \frac{J_0 H}{H_0}$	WATSON
e)	$J_c(H) = J_0 e^{-H/H_0}$	KARASIK

TABLE 8

EXPRESSIONS FOR THE PENETRATION FIELD (H^*) AND THE REVERSAL FIELD (H_R) FOR VARIOUS MODELS

VARIOUS EXPRESSIONS FOR H^*

①	$H^* = \left[\frac{4\pi}{10}(n+1)\alpha R\right]^{1/(n+1)}$	$n=0$ $n=1$	BEAN ALPHA
②	$H^* = (8\pi J_0 H_0 R/10 + H_0^2)^{1/2} - H_0$		KIM
③	$H^* = H_0 \ln\left\{\frac{4\pi J_0 R}{10 H_0} + 1\right\}$		KARASIK
④	$H^* = H_0 - H_0 e^{-4\pi J_0 R/10 H_0}$		WATSON
⑤	$H_R = 2H^*$		BEAN
⑥	$H_R = (H_m^2 - 2H^{*2})^{1/2}$		ALPHA
⑦	$H_R = \left\{(H_m + H_0)^2 - 2H^{*2} - 4H_0H^*\right\}^{1/2} - H_0$		KIM

TABLE 9

COMPARISON OF THE PREDICTIONS OF THE VARIOUS MODELS FOR H* AND H_{SAT} FOR NIOMAX-S 20-40 CALCULATED FROM SHORT SAMPLE J_c VS H DATA. THESE CAN BE COMPARED TO H* OBTAINED FROM EXPERIMENTAL HYSTERETIC LOSS AND SATURATION FIELD IN TABLE 10.

Model	Parameters	H*	H_{SAT}
Bean	J_c=18.6X10^4 A/cm^2	2100G	4200G
Watson	J_o=32.1X10^4 A/cm^2, H_o=95000G	3722	
Indirect Kim	J_o=63.6X10^4 A/cm^2, H_o=15000G	6229	
Direct Kim	J_o=52.9X10^4 A/cm^2, H_o=19800G	5475	9960
Karasik	J_o=37.6X10^4 A/cm^2, H_o=54200G	4271	
Alpha	α=6.06X10^9 A-G/cm^2	11700	16500

H_{SAT} (experimental) = 7375G

H* (Q_{EX}) = 9966 (from Alpha model and full cycle hysteretic loss)

α (Q_{EX}) = 4.2X10^9 A-G/cm^2 (from Alpha model and full cycle hysteretic loss)

TABLE 10

COMPARISON OF H* AND THE PINNING PARAMETER TO VALUES OBTAINED FROM HYSTERETIC FULL PENETRATION LOSS AND MODEL RELATIONSHIPS. COMPARISON OF H_{SAT}. RESULTS FOR NIOMAX-S 20-40, SUPERCON 241E-13, AND 217E-19 ARE PRESENTED

Sample	H_{SAT} (J vs H)			H_{SAT}	(J vs H)		*Alpha (18KG)		*Bean (18KG)	
	Alpha	Kim	Bean		α	J_c	$\alpha(Q)$	H*(Q)	$J_c(Q)$	H*(Q)
	Gauss	Gauss	Gauss	Gauss	A-G/cm^2	A/cm^2	A-G/cm^2	Gauss	A/cm^2	Gauss
Niomax-S 20/40	16500	9960	4200	7375	6.1×10^9	1.9×10^5	4.2×10^9	9966		
Supercon 241E-13	4414		130	1250	7.8×10^9	10^5	3.6×10^9	2125	1.7×10^6	1075
Supercon 217E-19	8473	5910	620	3350	8×10^9	1.4×10^5	3.9×10^9	4231	8.2×10^5	1858

* Parameters calculated from model expressions and experimental loss.

TABLE 11

FOURIER ANALYSIS OF FULL CYCLE ALPHA MODEL WAVEFORM FOR h_m = .3 AND OF HALF CYCLE ALPHA MODEL FOR h_m = .1, .5, 1.0

Alpha model harmonic content

1) Full cycle $h_m = .3$, 60Hz

Harmonic	C_i	S_i	V_i	V_i/V_3
DC	-6.7×10^{-8}			
1	7.92	-11.63	14	1.93
2	-.291	.046	.294	.04
3	-4.59	-5.64	7.27	1.00
4	-.0449	.374	.377	.052
5	-2.25	2.74	2.78	.384
6	.079	-.0514	.094	.013
7	-.347	-.574	.671	.092
8	.018	.127	.128	.018
9	-.317	.682	.759	.104

TABLE 11 (CONTINUED)

FOURIER ANALYSIS OF FULL CYCLE ALPHA MODEL WAVEFORM FOR $h_m = .3$ AND OF HALF CYCLE ALPHA MODEL FOR $h_m = .1, .5, 1.0$

2) Half cycle h_m=.1, .5, 1.0 respectively and $60H_z$

Harmonic	C_i	S_i	V_i	C_i	S_i	V_i	C_i	S_i	V_i
DC	-2.9×10^{-6}			-3.4×10^{-4}			-2.14×10^{-3}		
1	.0240	-.076	.080	2.82	-9.18	9.6	18.2	-64.7	67.2
2	.0183	-.026	.032	2.14	-3.17	3.82	13.3	-22.3	26.0
3	-.0152	6.84×10^{-3}	.0167	-1.80	.866	2.00	-11.8	7.20	13.8
4	-.0104	-8.02×10^{-4}	.0104	-1.20	-.052	1.20	-7.31	.803	7.35
5	-2.93×10^{-3}	1.32×10^{-4}	2.93×10^{-3}	-.339	.0273	.340	-2.04	.487	2.10
6	-2.70×10^{-3}	6.12×10^{-5}	2.7×10^{-3}	-.317	6.71×10^{-3}	.317	-2.04	.030	2.04
7	-1.5×10^{-3}	1.54×10^{-6}	1.50×10^{-3}	-.175	4.54×10^{-4}	.175	-1.08	.010	1.08
8	-1.3×10^{-3}	2.25×10^{-5}	1.30×10^{-3}	-.152	2.79×10^{-3}	.152	-.96	.022	.960
9	-8.96×10^{-4}	1.97×10^{-6}	8.96×10^{-4}	-.105	2.78×10^{-4}	.105	-.65	3.12×10^{-3}	.650

$V_i=(S_i^{\,2} + C_i^{\,2})^{1/2}$

$P_i=\tan^{-1}(S_i/C_i)$

TABLE 12

AMPLITUDE OF HARMONIC CONTENT NORMALIZED TO THIRD HARMONIC FROM FOURIER ANALYSIS OF EQUATION 5 OF BEAN WITH CUBIC TERM IGNORED, OF EQUATION 5 OF BEAN FOR h_m = .3 AND AND .8, OF HALF CYCLE ALPHA FOR h_m = .1, .5, 1, AND OF FULL CYCLE ALPHA FOR h_m = .3. DEPICTS VARIATION OF RATIO WITH AMPLITUDE OF h_m

h_m	I	II	h_m=.3	h_m=.8	h_m=.1	h_m=.5	h_m=1	h_m=.3
Harmonic	Bean's Cal.	Fourier Analysis	Fourier Total Bean	Fourier Total Bean	Alpha Half	Alpha Half	Alpha Half	Alpha Full
1	1.088	4.34	4.57	5.02	4.79	4.80	4.87	1.93
3	1.00	1.00	1.00	1.00	1.00	1.00	1.00	1.00
5	.238	.240	.241	.243	.175	.170	.152	.384
7	.111	.112	.113	.114	.09	.09	.08	.092
9		.0655	.0658	.067	.054	.053	.047	.104

Total Bean includes cubic terms of Bean's Eg.(5).

$|V_3/V_i|$ = 4.266 recalculated from Eq.(5) dropping cubic term

TABLE 13

DESCRIPTION OF VARIOUS NbTi MULTIFILAMENTARY WIRE. LISTING OF FIELD DEPENDENCE OF HALF CYCLE LOSS

1) Sample Parameters

Sample	Radius Wire	Radius Fil	# Fil	C/S	H_{SAT}^{**}	α J vs H A-G/cm^2	H*(α)	I_c(40kG)
Supercon 241E-13	232μ	5μ	1028	1.13	1250G	7.8X10^9	3122	138
Supercon 217E-19	732	18	54	2.12	3350	7.93X10^9	5991	89
Niomax-S 20/40	182	94	1	2.7	7375	6.1X10^9	11700	50
Niomax-S 25/33	156	122	1	.67	12000			105
Supercon VSF	188	3.5	360	1		4X10^9	1865	
MCA Rotor Wire	586	10	1350	2	2300			670
Norton Rotor Wire	586	22.5	300	2	3400			580

**experimental

2) Slope of half cycle hysteretic loss

Sample	Slope $<H_{BR}$	Slope $>H_{BR}$	H_{BR}
241E-13	3.42	.66	1600G
217E-19	3.13	.64	4100
20-40	3.32	.83	7400
Composite Curve	3.15	.65	1.0

TABLE 14

DIGITAL LISTING OF UNIVERSAL HALF CYCLE HYSTERETIC LOSS FOR HALF CYCLE SWEEPS FOR NbTi WIRE

$Q/Q(H_{SAT})$	H/H_{SAT}
.017	.25
.030	.30
.076	.40
.152	.50
.275	.60
.40	.70
.58	.80
.75	.90
.95	1.00
1.20	1.10
1.50	1.20
1.70	1.30
1.90	1.40
2.00	1.50
2.40	1.70
2.70	1.90
3.20	2.20
3.40	2.40
3.80	2.70
4.40	3.20
5.00	3.60
6.00	4.60
7.00	5.60
8.00	7.0
9.80	9.0
11.0	11.0
12.0	13.0
13.0	15.0
15.0	18.0

TABLE 15

SHORT SAMPLE CRITICAL CURRENT DATA FOR ROTOR WIRES OBTAINED BY CSCC

H kG	MCA WIRE A	SUPERCON WIRE A
40	670	580
50	615	530
60	550	470
70	490	400
80	355	300

APPENDIX

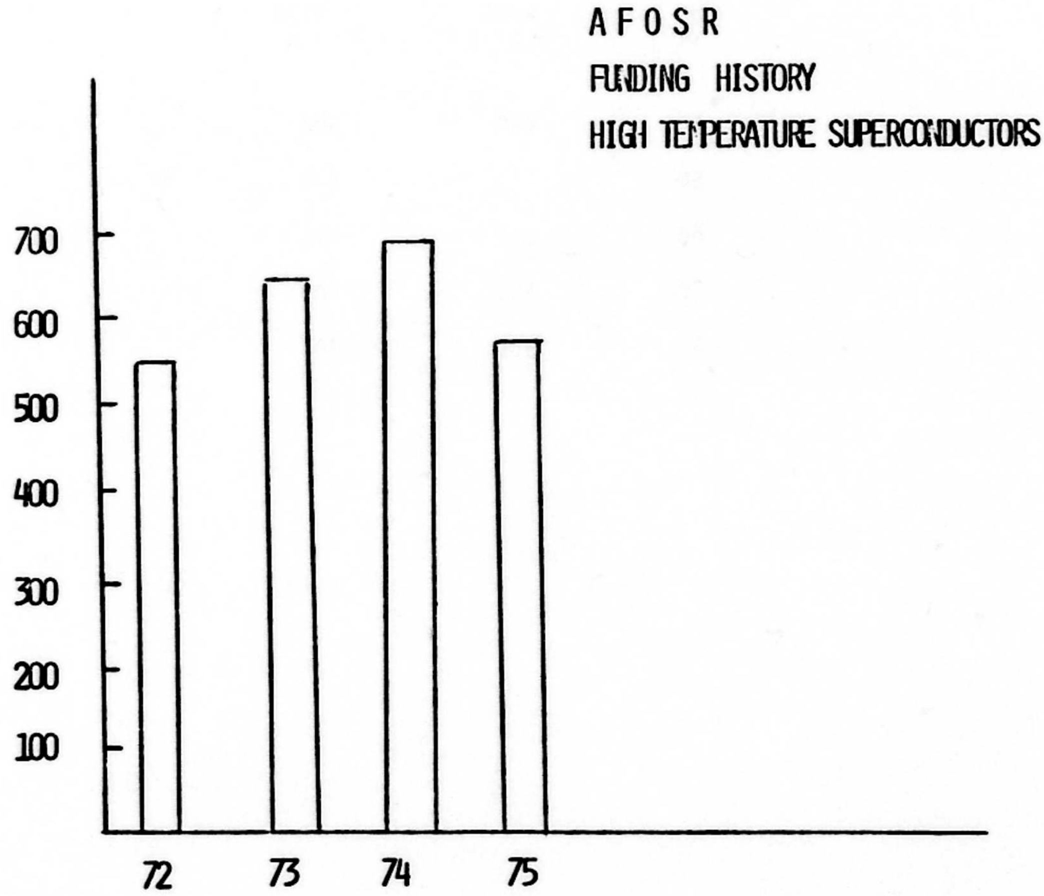

AFOSR
FUNDING HISTORY
HIGH TEMPERATURE SUPERCONDUCTORS

RECENT AFML FUNDING OF SUPERCONDUCTIVITY

#	FY71	FY72	FY73	FY74	FY75
1	50				
2			50*	50	
3			25	33	19.5
4			15**	15**	15**
TOTAL	50		90	98	34.5

*10K AFWL; **15K MATCHING FUNDS CDRB

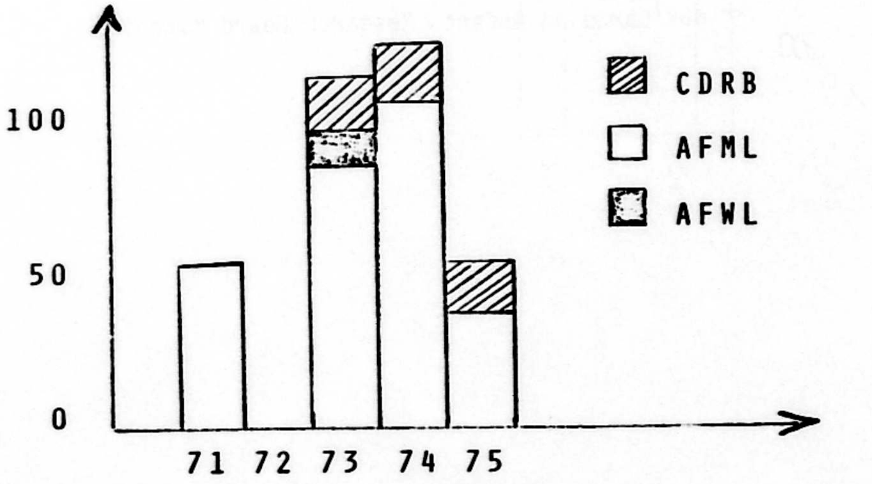

RECENT AFML FUNDING OF SUPERCONDUCTIVITY

Funds

1. The Carborundum Company 50K
   F33615-71-C-1709; AD751545
   Superconducting yarn
   12 months (7/1/72) end
   73710324

2. The Carborundum Company 100K*
   F33615-73-C-5110
   Superconducting Yarn
   12 months (4/1/74)
   73710324

3. University of Oklahoma
   F33615-73-C-5049 77.5
   Research on Relationship between Surface Properties
   and Superconducting Properties
   24 months (3/1/75)
   73670309

4. Canadian Superconductor and Cryogenic 45**
   Company Ltd.
   F33615-73-C-5163
   AC Loss Measurement in Superconductors
   18 months (12/31/74)
   73710229

* 10K AFWL
** 45K Canadian Defense Research Board Matching

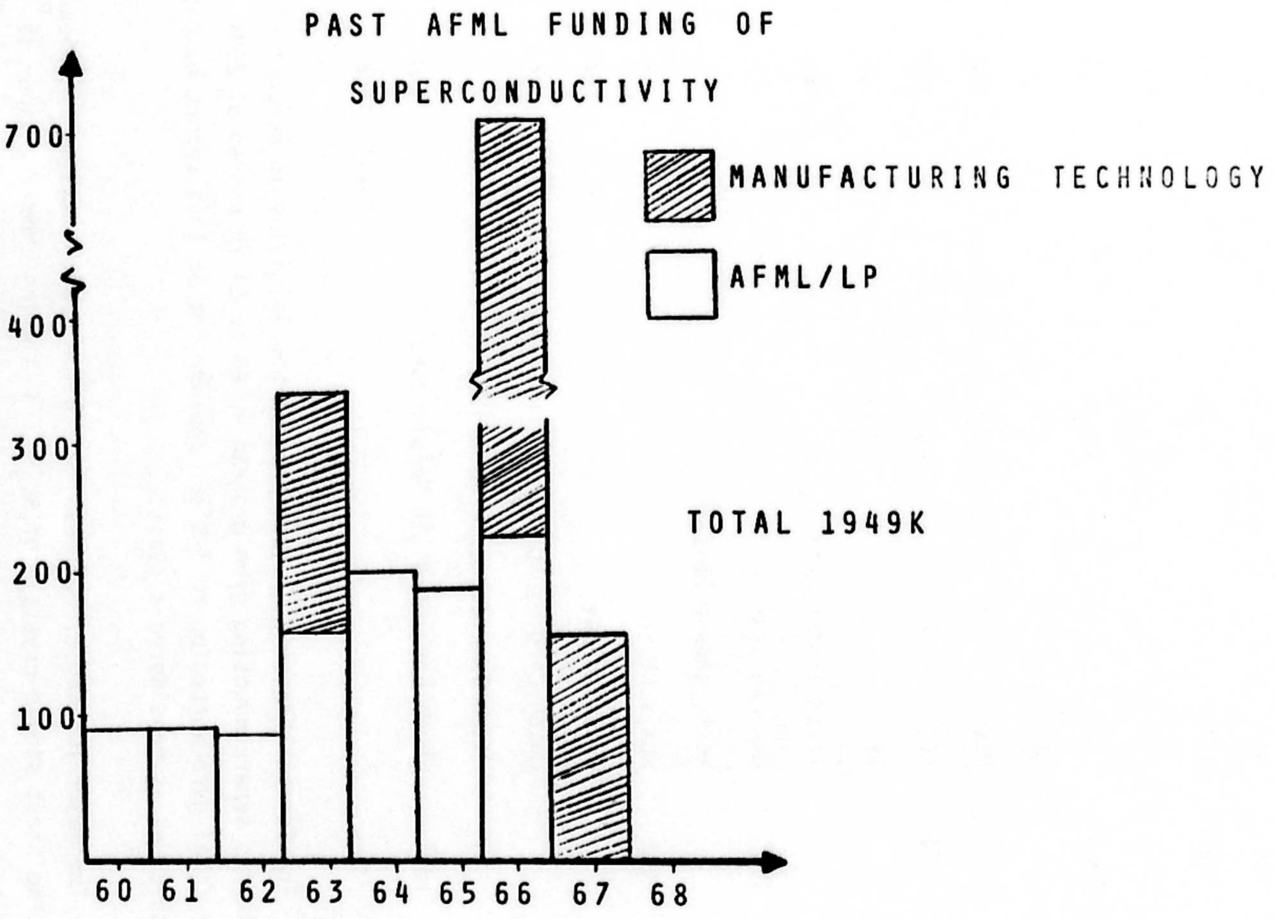
PAST AFML FUNDING OF
SUPERCONDUCTIVITY
▨ MANUFACTURING TECHNOLOGY
☐ AFML/LP
TOTAL 1949K
700
400
300
200
100
60
61
62
63
64
65
66
67
68

PAST AFML FUNDING OF SUPERCONDUCTIVITY

FY			Funds (1000's)
1960	RCA	Nb_3Sn	100
1961	RCA	Nb_3Sn	100
1962	RCA	Nb_3Sn	99
1963	RCA	Nb_3Sn	130
	GE	AC Loss	70
	MRC	Nb_3Sn Manufacture	150
1964	RCA	Nb_3Sn	100
	GE	AC Loss	75
	Texas Instruments		40
1965	GE - AC Loss		95
	Westinghouse Nb-C-N		100
1966	RCA - Nb_3Sn		90
	Westinghouse		95
	Union Carbide AC Loss		60
	Union Carbide Nb_3Sn Manufacture		~ 580
1967	Union Carbide Nb_3Sn Manufacture		170
		Total	2054

The General Electric ac loss program was initially in support of an Avionics superconducting gyro program in 63 or 64 in excess of 200K. The final gyro worked up to 3 G's. However the ac loss report by Charles Bean et al is considered a classic.

The major funding of RCA resulted in the growth and characterization of the first single crystals of Nb_3Sn. RCA using chemical vapor deposition produced long lengths of superconducting Nb_3Sn tape and patents were granted. The MRC manufacturing methods program on Nb_3Sn was terminated because of performance problems.

Union Carbide's ac loss study produced another classic paper. The niobium results are the basis for their large scale efforts in transmission lines. The manufacturing methods program for plasma sprayed Nb_3Sn magnets did not attain desired goals although magnets were produced.

Some of the investigators were Hume, Cody, Bean, Schmidt, Livingston, Walker, and Meyerhoff.

☆ U.S. GOVERNMENT PRINTING OFFICE: 1975 — 657-630/218